NASA TECHNICAL NOTE

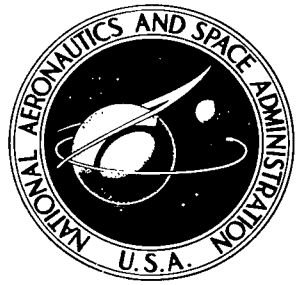

NASA TN D-6205

AN EXPERIMENTAL INVESTIGATION OF THE AIRFLOW OVER A CAVITY WITH ANTIRESONANCE DEVICES

by Donald A. Buell

Ames Research Center

Moffett Field, Calif. 94035

NATIONAL AERONAUTICS AND SPACE ADMINISTRATION • WASHINGTON, D. C. • MARCH 1971

1. Report No.	2. Government Accession No.	3. Recipient's Catalog No.
NASA TN D-6205		

4. Title and Subtitle	5. Report Date
AN EXPERIMENTAL INVESTIGATION OF THE AIRFLOW OVER A CAVITY WITH ANTIRESONANCE DEVICES	March 1971
	6. Performing Organization Code
7. Author(s)	8. Performing Organization Report No.
Donald A. Buell	A–3691
9. Performing Organization Name and Address	10. Work Unit No.
NASA Ames Research Center Moffett Field, Calif., 94035	188–48–01–01–00–21
	11. Contract or Grant No.
	13. Type of Report and Period Covered
12. Sponsoring Agency Name and Address	Technical Note
National Aeronautics and Space Administration Washington, D.C. 20546	14. Sponsoring Agency Code

15. Supplementary Notes

16. Abstract

Airflow over deep cavities was investigated in a wind tunnel and in flight at high subsonic speeds at equivalent or actual altitudes of 7 to 12 km. The cavities were large, with opening dimensions on the order of 1 m. Pressures were measured in and near the cavities with and without externally mounted devices intended to suppress resonance in the cavities. Some of the devices reduced the pressure fluctuations from as much as 50 to 2 or 3 times the amplitude occurring in a normal attached boundary layer. The pressure data were analyzed for spectral content, coherence, phase, shear-layer thickness, and shear-layer location.

17. Key Words (Suggested by Author(s))	18. Distribution Statement
Cavity flow Antiresonance device Resonance Spoiler	Unclassified – Unlimited

19. Security Classif. (of this report)	20. Security Classif. (of this page)	21. No. of Pages	22. Price*
Unclassified	Unclassified	73	$3.00

*For sale by the National Technical Information Service, Springfield, Virginia 22151

TABLE OF CONTENTS

NOTATION

C_p pressure coefficient, $\frac{\bar{p} - p_\infty}{q}$

f frequency of oscillation, Hz

G spectral density of pressure, $(N/m^2)^2/Hz$

H height of wraparound spoiler (fig. 5 and table 1), cm

h height of inlet to cambered-plate diffuser (fig. 5 and table 1), cm

L maximum streamwise dimension of cavity opening, m

l span of antiresonance device (fig. 3 and table 1), m

M Mach number

m index of acoustical normal mode approximately tangent to cavity walls in plane parallel to opening

m_ν index of vortex shedding mode

n index of acoustical normal mode along radii of cavity in plane parallel to opening

n_Z index of acoustical normal mode perpendicular to cavity opening

p_∞ free-stream static pressure, N/m^2

$\bar{p}$ mean value of measured pressure, N/m^2

$\sqrt{\overline{p^2}}$ rms of measured pressure fluctuation about mean value, N/m^2

q free-stream dynamic pressure, $\frac{1}{2}\rho V^2$, N/m^2

U velocity computed from rake measurements, m/s

V free-stream velocity, m/s

x,y,z coordinates for pressure measuring locations (fig. 11), m

γ coherence between pressure fluctuations,
square of modulus of cross spectrum between pressures a and b
$G_a G_b$

δ boundary-layer thickness on wind-tunnel wall with no cavity, 0.13 m

θ mean phase angle between pressure fluctuations (positive when pressures at the first mentioned location lead), deg

ρ free-stream density, kg/m^3

AN EXPERIMENTAL INVESTIGATION OF THE AIRFLOW OVER A CAVITY WITH ANTIRESONANCE DEVICES

Donald A. Buell

Ames Research Center

SUMMARY

Airflow over deep cavities was investigated in a wind tunnel and in flight at high subsonic speeds at equivalent or actual altitudes of 7 to 12 km. The cavities were large, with opening dimensions on the order of 1 m. Pressures were measured in and near the cavities with and without externally mounted devices intended to suppress resonance in the cavities. Some of the devices reduced the pressure fluctuations from as much as 50 to 2 or 3 times the amplitude occurring in a normal attached boundary layer. The pressure data were analyzed for spectral content, coherence, phase, shear-layer thickness, and shear-layer location.

INTRODUCTION

The investigation reported herein was initiated in support of plans to install an infrared telescope in an airplane in order to carry it above the infrared-absorbing troposphere. Since windows pass only a small portion of the infrared spectrum, it is desirable to have the telescope enclosure open to the airstream; thus the goal of the investigation was to examine the airflow over and in a cavity representative of a telescope enclosure, and to develop devices that would minimize pressure and light disturbances within the enclosure. The same goal with respect to pressure disturbances usually applies to any type of cavity on an airplane; therefore the configurations of the cavities used in the investigation were kept simple and as general as possible so that the results of the investigation would have wide applicability. The tests were limited to deep cavities (depth greater than width) and to high subsonic speeds.

The airflow over cavities has been studied extensively in the past, especially at low speeds. The mechanism that produces "organ piping" has been of particular interest. Blokhintsev (ref. 1) showed that airflow over a deep cavity causes vortices to form at the mouth and to be shed at a given reduced frequency or multiples thereof. Dunham (ref. 2) photographed the formation of the vortices and noted that the fundamental reduced frequency is obtained when one vortex at a time is in the cavity opening. The first overtone occurs when two vortices are present, etc. These vortices move downstream and strike the rear of the cavity opening, exciting one of the natural acoustic modes of the cavity if the shedding frequency coincides with the acoustic frequency. Rossiter (ref. 3) observed flow at both subsonic and supersonic speeds over a variety of cavity shapes and proposed an empirical equation for the frequency of vortex shedding.

The response of the acoustic modes depends on the impedance of the air in the cavity opening as well as on the impedance of the cavity walls. Harrington (ref. 4) noted an interaction between

shedding frequency and cavity response frequency which he ascribed to vorticity effects on the impedance at the cavity opening. Plumblee, Gibson, and Lassiter (ref. 5) examined the effect of the moving airstream on the impedance at the opening and set forth a method for computing the acoustical response characteristics of a cavity. Response frequencies computed according to the method of Plumblee and excitation frequencies computed with the aid of Rossiter's equation were further checked by East (ref. 6) in low-speed experiments. Unfortunately, neither method of computation establishes the mode to be expected, and some of the factors in the equations, such as the velocity of the shed vortices, are not precisely defined for the general case. Nevertheless, the resonance phenomenon seems to be reasonably well understood, at least in a practical sense.

Many investigations have also been directed toward suppressing resonance. For example, Rossiter used small spoilers upstream of the cavity to reduce periodic pressure fluctuations. Certain adaptations of flow deflectors in the upstream position may accomplish the same purpose, although the primary function of deflectors is usually to reduce steady-state air velocity in the cavity (e.g., ref. 7). Many other schemes have been proposed and tested, but none lent themselves as readily to the present application as those mentioned. It appears that very few investigators have concerned themselves with the goal of the present investigation – simultaneous suppression of resonance and minimization of the associated random pressure fluctuations.

The present investigation consisted basically of measuring pressures in cavities with and without various antiresonance devices. To obtain full-scale Reynolds numbers the cavities were large, with an opening greater than 1 meter. Moreover, the relationship between the tunnel boundary-layer thickness and the size of the opening was representative of what would be expected on an airplane. A few pressure measurements were also made in a Boeing KC–135 airplane in which an open telescope enclosure had been installed. The latter measurements were made with the cooperation of MIT Lincoln Laboratories and the U.S. Air Force, which operated the airplane.

It might be mentioned that air injection was tried in the cavities installed in the wind tunnel and found unsatisfactory as a resonance suppressor, but the crudeness of the injection system rendered the results inconclusive. Another goal of the wind-tunnel tests was the minimization of light disturbances, and optical measurements were made for this purpose; however, problems due to vibration of the optical system were not satisfactorily resolved, and the results can only be considered qualitative.

APPARATUS

Wind Tunnel and Cavities

The majority of the tests were performed in the Ames 6- by 6-Foot Supersonic Wind Tunnel. The test section of this facility is square in cross section and has slots in the floor and ceiling to permit transonic testing.

The cavities were formed by removing a window in the side of the wind-tunnel test section and attaching large welded steel tubing of circular cross section as illustrated in figure 1; the wall thickness of the tubing was 6.4 mm. The "shallow" cavity was formed by installing the wind-tunnel window at the end of the first section of tubing, at which point the tubing was supported from the

tunnel framework. The deeper cavity was formed by moving the window to the end of two additional sections of tubing cantilevered from the first section. Figure 2 is a photograph of the deep cavity structure.

Antiresonance Devices

The devices employed to suppress resonance were modifications of two basic configurations. One configuration was the high-aspect ratio "diffuser" illustrated in figure 3; the device was constructed so as to allow air to pass beneath a ramp, through the diverging channel formed by the ramp and the wall, through a porous surface, and over the cavity opening. It was intended that this diffusion process would cover the opening with a thick blanket of low-energy air. The porous surface consisted of an expanded-metal gridwork normally covered with perforated steel sheet to provide the desired porosity. The height of the diffuser was approximately equal to the thickness of the boundary layer on the wind-tunnel wall. Table 1 gives the geometric details of this and the other antiresonance devices. A porous spoiler (figs. 3 and 4) was derived from the diffuser configuration by cutting away the ramp between ribs, and a second variation was obtained by substituting a perforated steel sheet for the 45° ramp and omitting the covering on the expanded-metal framework.

The second basic configuration was a long diffuser wrapped around the cavity opening as shown in figures 5 and 6. It consisted of a cambered plate with a streamlined cross section mounted on a porous support. A "wraparound" spoiler (fig. 7) was created by removing the plate. The various heights and porosities tested are given in table 1.

Airplane

The airplane in which measurements were made was a Boeing KC–135 operated by the U.S. Air Force under the project name "Press." The airplane contained a telescope in a cavity that was open to the airstream. The airplane and the rectangular opening to the cavity are shown in figure 8. The telescope was mounted parallel to the axis of the airplane, and objects to the side of the airplane were viewed by means of a dynamically stabilized flat mirror. Figure 9 indicates the location of the larger objects in the cavity: the mirror, gimbals, torque motors, and the front end of the telescope tube.

The cavity was protected by a permanently mounted 45° diffuser of the same general shape and height as the 45° diffuser tested in the wind tunnel. This configuration was, in fact, originally developed for the airplane from work described in reference 7. Although the diffuser was no longer than the actual cutout in the side of the fuselage, a sliding door partially covered the cutout at the top leaving the diffuser extended, in effect, about 30 cm beyond the upper side of the opening.

Instrumentation

The primary instrumentation for the tests was a number of differential-pressure transducers each 3.2 mm in diameter. The transducers were basically 1.2 mm circular diaphragms connected to semiconductor strain gages of approximately 2500 Ω and installed so that the diaphragms were

flush with the mounting surface. The transducers were connected to individual direct-current power supplies and amplifiers; the signals were recorded on a frequency-modulated magnetic-tape recorder. The frequency response of a complete system was limited primarily by the speed of the recorder. The response was flat from 0 to 2500 Hz in the wind-tunnel system and was flat from 0.5 to 10,000 Hz in the airplane. The connection from the transducers to the reference pressure was closed while data were recorded to eliminate low-frequency fluctuations of the reference pressure. The transducers were mounted in the walls of the wind tunnel and cavity at the locations shown in figure 10. In addition, in both the airplane and the wind tunnel, tranducers were mounted in aluminum channels stretched across the cavities (see figs. 9 and 10(b)).

The static pressures or, more precisely, the time-averaged pressures on the walls of the wind-tunnel cavities and of the wind tunnel were transmitted through 1.6 mm orifices to scanivalves and slow-response transducers outside the wind tunnel. The orifice locations are shown in figure 10. The inside diameter of the connecting tubing ranged from 1.1 to 3.2 mm, and the length was approximately 6 m.

In a few tests, a total-pressure rake was installed in the cavity opening, and a second rake was installed in the wake downstream of the cavity. The rakes are shown in figures 7 and 4, respectively. The rake in the cavity could be moved in a streamwise direction from a remote station. The cables, which extended to the tip of the rake, were added after a particularly adverse test condition caused one of the cables near the base to break. The inside diameter of the tubes in the movable rake was 0.8 mm, and in the wake rake, 1.8 mm. The rake tubes were connected to recording equipment in the same manner as the static pressure tubing.

No attempt was made to determine the static pressures in the highly disturbed region of the cavity opening except at the walls. In order to compute velocities from the movable-rake measurements, the static pressure was assumed to be that measured on the cavity wall most remote from the airstream. A static pressure was measured at the tip of the wake rake and was assumed to apply to the entire region of the rake.

Light scattering was measured with a wind-tunnel schlieren system in which the camera had been replaced by a photomultiplier tube. The light beam was passed through the cavity and the wind tunnel. An electrical indication of the knife-edge position was correlated with the photomultiplier output to indicate the width of the light-source image at best focus. Unfortunately, the light source vibrated erratically and this difficulty was not identified and eliminated early enough to ensure accurate results.

TESTS

Wind Tunnel

The wind-tunnel pressure was adjusted such that the unit Reynolds number was within 10 percent of that of an airplane flying at 12.2 km in a standard atmosphere. The wind-tunnel static temperature was approximately 40°C warmer than that of a standard atmosphere. Some configurations were also tested at Reynolds numbers which were 50 percent higher, corresponding approximately to a 9.1 km altitude. Most of the test Mach numbers were between 0.6 to 0.9. In this

speed range, resonance of the cavity was clearly audible, and care was taken to note changes in the resonance condition as the airspeed was varied so that test conditions could be selected judiciously. A few tests were conducted at lower speeds.

Pressure fluctuations in the cavities were recorded continuously for 4 minutes at each test condition. During this interval, optical measurements were made, and, in most cases, 5 or more readings were taken of the static pressures for later averaging. In separate tests, the cavity rake was moved across the opening and the rake pressures were recorded once for each of 5 positions. Sufficient measurements were made without the rakes and transducer channels to ensure that these items did not affect the airflow in and around the cavity.

Airplane

Flights were made at altitudes from 6.7 to 11.3 km and Mach numbers from 0.6 to 0.8. Air conditioning normally vented into the cavity for temperature control was turned off. Pressure fluctuations were recorded for 5 minutes at each test condition.

CORRECTIONS

The large blockage (up to 6.5 percent) of the antiresonance devices in the wind tunnel posed special problems of data correction. Pressures were measured on the wall opposite the cavity for every configuration. The pressures near the cavity centerline reflected the effects of both solid and wake blockage while those at the farthest downstream station, 2.2 m from the cavity centerline, were affected primarily by wake blockage. Hensel's method (ref. 8) was used to derive the blockage corrections. Data were discarded if the local Mach numbers corresponding to the measured pressures exceeded unity at any station.

The wake blockage was assumed to be half the velocity increment caused by the cavity and attachments at the downstream pressure-measuring station; the pressure gradient was usually zero this far downstream. It was further assumed that the wall containing the cavity was a reflection plane in the center of a wind tunnel. The height of the wind tunnel was assumed to be greater than the actual height to account for the plenum chambers behind the slots. Thus, the tunnel section on which the solid-blockage corrections were based was effectively a solid-wall section 3.7 m square. With these assumptions and following the procedures of reference 8, the maximum blockage correction by which the velocity was increased was 12 percent. The static pressures and parameters depending on velocity were correspondingly corrected. An effect of the tunnel walls on the cavity-resonance phenomenon presumably remains and will be further considered as the results are presented.

SPECTRAL ANALYSIS

Power and cross-power spectra of the pressure fluctuations were obtained by passing the recorded transducer outputs through synthesized band-pass filters and averaging an appropriate

combination of the signals. The analyses were performed by means of a combined analog and digital computing process described in reference 9. Additional operating parameters of the system are given in reference 10. The only important revision to the procedure outlined in these references was to analyze the data at eight times the recorded speed to facilitate analysis of the low-frequency data.

The averaging of the filtered signals was accomplished by true integration at a fixed frequency. As the real-time frequencies were varied from 1.25 to 2500 Hz, the real-time bandwidth was changed from 0.25 to 100 Hz in five finite steps. The corresponding integration times were changed from 160 to 16 seconds.

RESULTS AND DISCUSSION

The results are presented first in terms of the root-mean-square pressure fluctuation and the associated static pressures in the cavity. The resonance phenomenon is analyzed by the presentation of frequencies and phase angles of the predominant modes. Typical spectral characteristics of the various configurations are presented, and the effect on the shear layer is shown by velocity profiles. The discussion is concluded with some comments on the observed light scattering.

The coordinate system used to identify the measuring locations is given in figure 11. The data presented are from measurements at $y = 0$ (approximately), except as noted. Only the lower Reynolds number data are presented since the Reynolds number effect was so small (see next section).

Root-Mean-Square Pressure Fluctuations

Figure 12 is the first of a series of figures showing the variation with Mach number of the averaged pressure fluctuations in dimensionless form. The cavity pressures presented in this section were measured on a transducer at $x = 1.1L$ and $z = 0.4L$ (the downstream transducer in fig. 10(a)). The fluctuations at this location were always as large as the measured fluctuations elsewhere in the cavity or larger. The results in this form do not differentiate between modes of resonance. As will be shown subsequently, the cavity with the plain opening had a different mode of acoustical oscillation at a Mach number of 0.6 than at higher Mach numbers. A still different mode of oscillation was excited at Mach numbers below 0.6, but this speed regime was not investigated in any detail.

In comparison with the resonance condition, the amplitude of the fluctuations in the normal wind-tunnel-wall boundary layer (no cavity) and in the cavity with the porous spoiler were small. These rms values are from 2 to 3 times as large as the value normally quoted, 0.006, for an attached boundary layer on a subsonic airplane. The fluctuations in the resonating cavity were as much as 50 times as large as those in the airplane boundary layer.

When the configurations of figure 12 were tested at a 50-percent higher Reynolds number, the amplitudes of the fluctuations were within 20 percent (mostly within 5 percent) of the values

shown in the figure. This difference was considered negligible in view of the sensitivity of the response to other factors.

The effect of spoiler porosity on pressure fluctuations is shown in figure 13. The solid spoiler was clearly inferior to the other configurations tested in suppressing cavity resonance, indicating that some minimum amount of flow through the porous surface is required for the spoiler to be effective. The results shown in this figure were obtained with a "square" cavity opening (see fig. 1), but a comparison with data for a round opening (fig. 12) shows that the shape of the opening was unimportant.

The effect of span of a porous spoiler on pressure fluctuations is shown in figure 14. Also shown is a comparison with data for a porous ramp configuration. The differences in the results are too small to be of significance.

The amplitudes of fluctuation in the cavities with 45° diffusers are shown in figure 15 for both the wind-tunnel and the airplane tests. The amplitudes for the airplane were quite close to those presented previously for the porous spoiler. However, the wide disparity between these values and the other results in figure 15 requires explanation. The pressures in the airplane were measured near the upper side of the cavity, where the diffuser extended some distance past the opening. This overhang and the diffuser height were approximately the same as that of the long-span wind-tunnel diffuser, so the long diffuser was presumed to represent the flight article more closely than the short diffuser. The data at low speeds supported this presumption. The higher level of fluctuation for the short diffuser is attributed to vortices that had been shed from the tips and had entered the cavity.

The situation was complicated at high speeds by the development of a strong resonance in the wind-tunnel cavity with the long diffuser. In earlier tests on the airplane, an audible resonance had been obtained when the inlet to the diffuser was reduced in size. This result agrees with a conclusion drawn from the porous spoiler data – that some minimum amount of air must pass through the porous surface to suppress resonance. It is to be noted also that the diffuser would be expected to produce an adverse pressure gradient upstream of the diffuser inlet. It is possible that at higher speeds a condition peculiar to the wind tunnel aggravated the pressure gradient and triggered a flow separation that extensively blocked the flow of air into the diffuser.

Another pertinent factor is the action of the tip vortices. In reference 11 Obremski reported pronounced flow alterations from tip vortices shed from similarly configured diffusers on an airplane. He attributed part of his success in suppressing resonance to the favorable "downwash" from the tip vortices. In the present investigation this action was largely eliminated by the close proximity of the wind-tunnel walls to the tips of the long diffuser. There was no such interference with the short diffuser, and neither was there a pronounced resonance. In his tests (two narrow cavities in tandem), Obremski observed that at low speeds the 45° diffuser suppressed resonance which the porous spoiler did not. It is concluded that the 45° diffuser is an effective antiresonance device, but the span and the inlet size are critical factors.

A few wind-tunnel tests were conducted with the porosity on the 45° diffusers increased from 35 to 68 percent; the change in porosity had very little effect.

Figure 16 presents data for two porosities and two heights of the wraparound spoiler, originally intended to be part of the cambered-plate diffuser. Only the low spoiler with 27-percent

porosity permitted the cavity to resonate; the other combinations of porosity and height also produced fairly high levels of fluctuation, but of a random type. Observation of tufts in the cavity gave evidence of considerable three-dimensional air movement when the wraparound spoiler was attached. The results indicate that the wraparound spoiler behaved like a diffuser with large tip vortices.

Figure 16 shows that at low speeds the level of fluctuation was decreased by decreasing either the porosity or the height; that is, the best results were produced by minimizing the amount of air flowing through the spoiler surface. The resonance at higher speeds is evidence once again that the air through the porous surface should not be decreased without limit. The data in figure 16 actually apply to spoilers with only the upstream portion $\pm 45^\circ$ from the stream direction at the specified porosity. Other tests indicated that there was little effect from porosity changes in more downstream locations.

Data for three combinations of porosity and height of the cambered-plate diffuser are shown in figure 17. The lower two curves compare closely with the data for corresponding configurations in figure 16. It is concluded that adding the cambered plate to the wraparound spoiler did not materially affect the pressure fluctuations in the cavity. With zero porosity on the low diffuser (fig. 17), the resonance was more severe than with the plain opening.

Figure 18 is a plot of fluctuation amplitudes for the deep cavity with and without two antiresonance devices. The results are the same as those previously presented in that the plain opening caused resonance, the 45° diffuser did not suppress resonance at high speeds, and the porous spoiler suppressed resonance at all speeds in the test range. There is an effect of cavity depth, of course, since the cavity response in resonance is a function of cavity size and exciting frequency.

From the preceding data the 35-percent porous spoiler appears to be the most consistent of the devices in maintaining a low fluctuation level, but it is emphasized that such effectiveness has been shown only for a limited range of test conditions and cavity sizes. Obremski's experience and the unpublished results of other tests on cavities suggest that the porous spoiler as tested was not high enough to inhibit resonance at very low speeds.

Static Pressures

Figure 19 presents static-pressure coefficients at various locations in or near the cavities for most of the configurations discussed in the previous section. Pressures at the edge of the airstream were measured only with the round cavity opening. (The effect of opening shape was negligible.) The installation of the antiresonance devices naturally increased the upstream pressures on the tunnel wall. Pressures at all other locations were decreased by most of the devices. The pressures at the end of the cavity farthest from the airstream ($z/L = 1.6$) are not shown but were almost identical to those in the center of the cavity at $z/L = 0.4$.

The relationship between the pressures at the center and downstream locations in the cavity reflected the degree to which the airflow impinged upon the rear face of the cavity. There was a surprising lack of correlation between this air impingement and the existence of resonance in the cavity. For example, both the plain opening (fig. 19(a)) and the high wraparound spoiler with

52-percent porosity (fig. 19(c)) caused a difference in pressure coefficient of about 0.2 between the center and downstream cavity pressures. The first of these configurations resonated (fig. 12) while the second did not (fig. 16). Alternatively, neither the 35-percent porous spoiler (fig.19(b)) nor the long 45° diffuser (fig. 19(a)) caused much pressure difference between the center and downstream locations. However, the porous spoiler suppressed resonance (fig. 12) while the long 45° diffuser did not (fig. 15).

Frequency and Phase at Resonance

The behavior of the cavities in resonance is best explained by a comparison of the data with available theory. In terms of the present report, Rossiter's expression for frequency of vortex shedding (ref. 3) is

$$F = \frac{V}{L} \frac{(m_V - 0.25)}{(M + 1/H)}$$

where

m_V number of vortices in the opening

H ratio of vortex velocity to free-stream velocity

Rossiter's approximate value, 2/3, for H was used and the shedding frequencies were computed to be those shown by the solid lines in figure 20. Three vortex shedding modes are shown for the shallow cavity in the upper part of the figure, and one for the deep cavity is shown below. The figure also shows the frequencies for several normal acoustical modes (dashed lines) as computed by the method of reference 5. The application of the method to the present model is outlined in the appendix. The indices n_Z and m designate which harmonic is being excited in the depth mode and the tangential mode, respectively. The air movement in the depth mode is parallel to the axis of the cavity while that in the tangential mode is parallel to the plane of the cavity opening. The measured frequencies of the dominant fluctuation are denoted in figure 20 by the symbols, a filled symbol indicating a stronger response. The majority of the measurements lie close to the combined tangential and depth mode described by $m = 1$ and $n_Z = 2$.

The measured frequencies approach the normal mode frequency in the manner observed by Harrington (ref. 4); that is, when the vortex-shedding frequency was higher than the normal mode frequency, as in the deep cavity, the measured frequency coincided with the latter value. However, when the shedding frequency was less than the normal mode frequency, as in the shallow cavity, the measured frequency was approximately equal to the shedding frequency. The effect of the shed vortices on the impedance as suggested by Harrington is apparently missing from the response equations. As the shedding and normal mode frequencies moved farther apart, the response amplitude diminished, and finally a different mode emerged. Unfortunately, it is not readily apparent which mode will emerge when several are possible.

Figure 20 shows that three distinct mode shapes were excited at the various speeds, and figure 21 shows the corresponding phase angles. The measurements are from transducers in a channel across the cavity, and all are referenced to the phase at the most downstream location. The angles

are reasonably close to those predicted by the theory outlined in the appendix. Of course, the measuring technique cannot discern the cycle of fluctuation relative to another, so the values have been adjusted by 360° where it seemed appropriate.

Pressure Spectra

Samples of spectra of the pressure fluctuations in the cavities are presented in figures 22 to 31. The parameter G, which is a mean square pressure per hertz, was normalized with the square of the free-stream dynamic pressure, q, and with L/V to make it a dimensionless spectral power per unit of reduced frequency, fL/V. This spectral density varies over so many orders of magnitude that the scale has been shifted from plot to plot. A line in the left margin marks a value of 0.001 for purposes of comparison. The frequency scales are identical on all the plots.

The spectra of the pressures on the wind-tunnel wall are shown in figure 22. The peak near a reduced frequency of 4 accounted for about half the rms value noted in figure 12 and is attributed to an aerodynamic "noise" peculiar to the wind tunnel. The peak also appeared in data for the cavity with a cover over the opening (fig. 23), although the magnitudes of the peak and of most of the rest of the spectra were about one order of magnitude less than for the tunnel wall. The spectral densities in the reduced-frequency range from 0.04 to 2.0 in figure 23 are typical of the instrumentation noise level at which the data lose aerodynamic significance.

Spectra are shown in figure 24 for three locations in the open cavity with no antiresonance devices. The points have been loosely faired where there is reason to suspect meaningless results; for example, the string of constant spectral values near a reduced frequency of 1 represent a sort of minimum resolving power of the analyzer when it is adjusted to evaluate the large fluctuations at resonance. At frequencies on either side of this range, the analyzer components were adjusted to be more sensitive.

With the cavity in resonance, most of the energy lies in the peak near a reduced frequency of 0.75. The peak at twice this frequency is merely a reflection of distortion in the wave shape of the main fluctuation. The spectral densities for the front and center of the cavity are about the same as for the wind-tunnel wall (fig. 22) except that the periodic component has been added, along with some fluctuation at adjacent frequencies. The spectral densities for the downstream location were generally higher than for the more forward locations, and this is typical of most of the wind-tunnel configurations examined. Spectra of the pressures measured in the airstream just downstream of the opening (not shown) were almost as large as those in the cavity at the downstream face.

Figure 24 shows that energies in the main fluctuation were an order of magnitude less at the center than near the upstream or downstream face. This is typical of most of the resonating configurations. The theory outlined in the appendix would lead to an expectation of no periodic fluctuation in the center when the cavity is resonating in the combined depth and tangential modes. The amplitudes of fluctuation on the wind-tunnel wall opposite the cavity (data not shown) were similar to those at the cavity center.

Spectra of the pressures in the presence of the porous spoiler are given in figure 25. A comparison of figures 24 and 25 shows that the spoiler appreciably lowered the spectral densities at all reduced frequencies above 0.1, although vestiges of the resonance peak still remain. At the low

frequencies the effect of the spoiler was adverse but relatively small in terms of energy. The spectra for large and small extremes in spoiler porosity are shown in figures 26 and 27. In both cases there are spectral peaks near a reduced frequency of 0.8. The spectra for the spoiler with no porosity were much like those with no spoiler. This similarity also existed for other configurations that had a strong resonance, and such spectra will not be considered further.

The cavity with the long-span 45° diffuser did not resonate at low Mach numbers, and figure 28 presents spectra for this situation. The spectra were not greatly different from those for the porous spoiler (fig. 25). Shortening the diffuser (fig. 29) noticeably increased the fluctuation level at the downstream face of the cavity. These higher spectral densities are evidently the result of the additional vorticity from the tips of the diffuser. A similar result was produced by the wraparound spoiler (fig. 30). Resonance peaks are present in figures 29 and 30, but the amplitude is small.

Spectra of the pressures in the airplane cavity are shown in figure 31. At reduced frequencies above 0.1 the values are approximately the same as for the comparable configuration in the wind tunnel at lower Mach numbers (fig. 28). The spectral densities for the airplane are significantly lower at low frequencies, which suggests that the wind-tunnel flow characteristics or the blockage effects were responsible for some low-frequency fluctuation.

Cross-Spectral Characteristics

Cross spectra of the pressure fluctuations are presented in figures 32 to 35 in the form of coherence and phase angle between various locations in the cavities. A comprehensive presentation has not been attempted because of the difficulty in separating the many effects that are reflected in the cross spectra. As a result, few valid generalizations can be made. For example, coherence results when there is communication between the points of measurement, either through normal-mode pressure waves or through waves radiated from a common source in the shear layer or through convection of the turbulent air mass in the cavity. A few samples of coherence are presented to indicate qualitatively which effect predominated.

The coherence for various spacings of the pressure transducers in the wind-tunnel cavity is shown in figures 32 and 33. Figure 32 pertains to a configuration in resonance and figure 33 to a configuration without resonance. The data have been faired rather loosely, ignoring points at which the spectral values were questionable. Both configurations produced narrow bands of high coherence at frequencies which in many cases correspond to normal-mode frequencies of the cavity. The high coherence at low frequencies is assumed to be due to wind-tunnel inputs that are nonrepresentative of flight.

The coherence between pressures somewhat deeper in the cavity and closer to the cavity walls is presented in figure 34. Several configurations are included to show the effect of the antiresonance devices on coherence in the wind-tunnel cavity. The narrow-band peaks of coherence caused by the porous spoiler (fig. 34(a)) were typically quite pronounced at locations remote from the airstream. The long-span 45° diffuser (fig. 34(b)) caused similar peaks. In contrast, figure 34(a) shows much less coherence from the three-dimensional air movement associated with the wraparound spoiler. Tip vorticity from the short 45° diffuser also destroyed much of the coherence (fig. 34(b)). The lack of coherence indicates an advantage for the latter two devices in some situations.

Both coherence and phase angles are shown for the airplane cavity in figure 35. There were fewer peaks of coherence than had been observed in the wind tunnel. This result is attributed partly to the tip-vortex action of the diffuser and partly to the difference in normal-mode characteristics of the cavities. It should be remarked that more definite coherence peaks were obtained on instrumentation deep in the cavity, but these data have been omitted because of expected interference from the many large objects in the cavity.

The phase angles in figures 35(a) and (b) vary in a manner that might indicate an upstream convection at low and moderate frequencies. However, it is expected that the phase variation was actually caused by waves traveling upstream in an air mass that was moving downstream. The phase angles are too inaccurate to have meaning where the coherence is less than about 0.1. Thus, phase had little meaning in the wind-tunnel data except at the coherence peaks. (Examples of the phase angles at the resonant peak were given in fig. 21.)

Velocity Profiles

The total pressures measured on the rakes were converted to velocities and were normalized by the velocity at the tip of the rake that extended deepest into the wind-tunnel airstream. Some plots of these velocity ratios versus distance into the airstream are presented in figures 36 to 38. The distance scale is in terms of boundary-layer thickness with no cavity, which was 13 cm, based on a straight-line fairing of the velocity ratio to the seventh power.

The static pressures used in the velocity calculation were only approximate, for the reasons noted in the Instrumentation section. Even the total pressures were likely to be in error at the low-velocity boundary of the shear layer, where the angle of flow diverged excessively from that of the rake tubes. Consequently, the velocity profiles are only approximations, particularly where the velocity ratios approach zero. In addition, the data at $x/L = 1.40$ in figures 36(a) and 38 were recorded with the movable rake in place, and figure 38 includes the effect of support cables extending to the tip of the rake.

Configurations which caused a strong resonance are paired in the (a) and (b) parts of figures 36 to 38 with configurations having very little pressure fluctuation. The most noteworthy result is that resonance was associated with the growth of thick shear layers with a uniform variation of shear throughout the layer. In contrast, the nonresonating configurations had relatively thin layers of high shear behind the outer edge of the antiresonance device.

If the inaccurate low-velocity points are ignored, the shear layers develop approximately as described for a free-jet boundary in reference 12 following the equation:

$$\frac{U}{U \text{at tip}} = \frac{1}{2}\left[1 + \operatorname{erf}\left(\sigma \frac{\Delta z}{x}\right)\right]$$

where

σ an empirical constant

Δz distance outward from the point at which U/Uat tip $= 1/2$

The parameter Δz is somewhat arbitrarily defined because the location of the shear layer varied so much from one configuration to another.

It is indicated that the shear layers for the nonresonating configurations in figures 36(b) and 37(a) have a σ of about 12, which is close to the value, 13.5, quoted in the reference. The shear layers in resonance are best represented by a σ of about 6, or twice the thickness to be expected in the free-jet shear layer. This comparison and the fact that a wide variety of devices did not greatly thicken the shear layer unless resonance developed suggests that the thickening is a result rather than a cause of resonance.

Figure 37(b) also shows that, when the cavity was in resonance, the thick layer was not necessarily down in the cavity where it would impinge on the downstream wall. It is certain, however, that the usual vortices were forming close to the cavity opening and transmitting the necessary excitation to it. Evidently, the porous spoiler was successful in attenuating the regular vortex formation by injecting a welter of small high-frequency vortices into the shear layer.

The remarks on shear-layer thickness should not be construed as applying to the boundary layer downstream of the cavity. For example, although the shear layer behind the porous spoiler (fig. 36(b)) was thinner than that with no device (fig. 36(a)), it was displaced into the stream as compared to the latter. Thus, downstream of the cavity, the shear layer associated with the porous spoiler develops into a layer as thick as, but less stable than, the layer behind a plain opening, which is energized by resonance. In general, the absence of resonance was associated with incipient or developed separation downstream of the cavity opening (e.g., fig. 37(a), $x/L = 1.40$).

Light Scattering

As indicated previously, the light scattering was measured with a light beam that passed through the cavity and wind tunnel. To evaluate the light scattering in the shear layer, it was necessary to separate the effects of the wind-tunnel air stream, the boundary layer on the opposite wall of the wind tunnel, and the slowly moving air in the remainder of the light path. The total deflection from these sources was assumed to be the square root of the sum of the mean square of the individual components. Thus evaluated, the scattering in the shear layer behind the best antiresonance devices was from less than one to two times the scattering from one of the tunnel-wall boundary layers. The scattering from the thicker shear layers produced by strong cavity resonance was two to five times as great as that from the wall boundary layer. While there appeared to be differences in the effects of the various antiresonance devices, the data were not sufficiently dependable to be definitive.

CONCLUSIONS

Two cavities with and without antiresonance devices have been tested in a wind tunnel and one cavity with a diffusion device has been tested in an airplane. Analysis of the results leads to the following conclusions:

1. Resonance was suppressed by several different porous devices mounted upstream or around the cavity opening.

2. The more effective devices reduced the root-mean-square amplitude of the pressure fluctuations to a level two or three times as high as in the normal attached subsonic-airplane boundary layer.

3. In the speed range examined (M = 0.6 to 0.9), a 35-percent porous spoiler was the most consistent of the devices tested in the wind tunnel in maintaining a low level of pressure fluctuations.

4. Pressure fluctuations measured in the airplane cavity were of about the same magnitude as those in the best wind-tunnel configuration.

5. In the wind-tunnel tests, cavities with inadequate or no antiresonance devices resonated in a combined depth- and tangential-mode at high subsonic speeds.

6. In extreme cases, the root-mean-square amplitude of the cavity pressure fluctuations was as much as 50 times as great as in the normal attached boundary layer of a subsonic airplane.

7. The measured frequencies at resonance were approximately equal to the excitation frequencies predicted by Rossiter and the response frequencies predicted by a modification to the method of Plumblee, Gibson, and Lassiter.

8. The devices that suppressed resonance produced thinner shear layers and led to better light transmission than the resonating cavities.

9. Resonance was not suppressed merely by keeping the shear layer out of the cavity.

10. The suppression of resonance made the boundary layer downstream of the cavity more susceptible to separation.

Ames Research Center
National Aeronautics and Space Administration
Moffett Field, Calif., 94035, Aug. 31, 1970

APPENDIX

ACOUSTICAL NORMAL MODES OF THE WIND–TUNNEL CAVITY

Plumblee, Gibson, and Lassiter (ref. 5) derived an expression for the impedance of the air in the rectangular opening of a cavity radiating into a moving medium. They then developed expressions for the frequencies and amplifications with which a cavity having that opening and five rigid walls would respond to an excitation. The source of the excitation was not considered in any detail.

Since the present investigation concerned a cylindrical cavity, the equations were slightly revised following the method of Morse (ref. 13). When a normal mode is excited, the pressure in excess of the static pressure is

$$\tilde{p} = A \cosh\left(\frac{\pi g z'}{L_z}\right) \cos(m\phi)\, J_m\left(\frac{\pi \alpha_{mn} r}{a}\right) e^{-i\omega t}$$

where

A	amplitude of fluctuation
g	complex distribution parameter determined from $g \tanh(\pi g) = \frac{i\omega}{c} \frac{L_z}{(R + iX)}$
z'	coordinate in the z direction (fig. 11) but with origin at the closed end of the cavity
L_z	depth of cavity
ϕ,r	cylindrical coordinates in the cavity with the origin at the centerline and $\phi = 0$ in the free-stream direction
m,n	indices of tangential and radial waves
a	radius of the cavity
J	Bessel function
α_{mn}	solutions to the equation $dJ_m(\pi\alpha)/d\alpha = 0$ given in reference 13
ω	circular frequency of response $= 2\pi f = \pi c \sqrt{(\alpha_{mn}/a)^2 - (g/L_z)^2}$
c	speed of sound
R+iX	impedance at the cavity opening given in reference 5 as a function of Mach number, opening dimension, and frequency

The indices m and n identify modes of fluctuation in a plane perpendicular to the cavity axis. The frequency f and the distribution parameter g are interdependent, and there is a series of frequencies that will satisfy the equations for each combination of m and n. These various possible "depth" modes are identified by an index n_z.

The expansion by Plumblee et al. of the equation for determining g was adapted and programmed for digital computation. The same thing was done for their equations for a simplified method, which is applicable when m and n equal zero. Unfortunately, the two methods did not give the same result until the sign of the reactance X was reversed in the more comprehensive method. With this alteration, the methods gave identical frequencies for pure depth modes. Also, the computations agreed satisfactorily with measurements at low speed, where a pure depth mode actually existed. The more comprehensive method with the reactance alteration was used to compute all other modes. It should be pointed out that the significance of the alteration decreased as the various modes combined to give higher frequencies.

An obvious discrepancy in applying the impedance values from reference 5 to the present situation was that the cavity openings in the computation and experiment were not the same shape. Also, reference 5 did not provide for an opening smaller than the cavity. Rather than attempt to modify and repeat all the work of reference 5, the opening was assumed square but was varied in size from one entirely enclosed by the actual circular opening to one entirely enclosing the actual opening. The computed differences in frequency were negligible. The effects of Mach number were also found to be quite small for this particular cavity.

REFERENCES

1. Blokhintsev, D. I.: Acoustics of a Nonhomogeneous Moving Medium. NACA TM 1399, 1956, Article 27.

2. Dunham, William H.: Flow-Induced Cavity Resonance in Viscous Compressible and Incompressible Fluids. Fourth Symposium on Naval Hydrodynamics, Office of Naval Research, Department of the Navy, ACR-92, 1962, pp. 1057-1081.

3. Rossiter, J. E.: Wind-Tunnel Experiments on the Flow Over Rectangular Cavities at Subsonic and Transonic Speeds. R.&M. No. 3438, Aeronautical Research Council, 1966.

4. Harrington, Marshall C.: Excitation of Cavity Resonance by Air Flow. American Physical Society, Division of Fluid Dynamics, New York, January 30 to February 2, 1957.

5. Plumblee, H. E.; Gibson, J. S.; and Lassiter, L. W.: Theoretical and Experimental Investigation of The Acoustic Response of Cavities in an Aerodynamic Flow. Technical Rep. WADD TR-61-75, Air Force Systems Command, 1962.

6. East, L. F.: Aerodynamically Induced Resonance in Rectangular Cavities. J. Sound Vibration, vol. 3, no. 3, May 1966, pp. 277-287.

7. Wolford, R. D.: Skyscraper Airborne Radiation – Measuring System, Cavity Temperature and Air Flow Control Analysis. Rep. BSR-445, The Bendix Corp., 1961. Prepared for Geophysics Res. Directorate, Air Force Cambridge Research Center, ARDC, USAF, Bedford, Mass.

8. Hensel, Rudolph W.: Rectangular-Wind-Tunnel Blocking Corrections Using the Velocity-Ratio Method. NACA TN 2372, 1951.

9. Lim, Raymond S.; and Cameron, William D.: Power and Cross-Power Spectrum Analysis by Hybrid Computers. NASA TM X-1324, 1966.

10. Chyu, Wei J.; and Hanley, Richard D.: Power- and Cross-Spectra and Space-Time Correlations of Surface Fluctuating Pressures at Mach Numbers Between 1.6 and 2.5. NASA TN D-5440, 1969.

11. Obremski, H. J.; and Thomas, D. R.: TRAP–MATS Aircraft Modification Program Phase I R&D Test Report. Martin Marietta Corp. Rep. no. ER 14862, 1969.

12. Schlichting, Hermann: Boundary-Layer Theory. Fourth ed., McGraw-Hill Book Co., Inc., 1960, pp. 598-599.

13. Morse, Philip M.: Vibration and Sound. Second ed., McGraw-Hill Book Co., Inc., 1948, pp. 397-399.

TABLE 1.– GEOMETRIC DETAILS OF THE ANTIRESONANCE DEVICES

45° diffusers in wind tunnel	
Span l (fig. 3)	
Long	1.78 m
Short	1.07 m
Porosity	
Basic, expanded metal grid covered with perforated sheet, 3.56 mm holes, 4.76 mm spacing	35 percent
Expanded metal grid only	68 percent
45° diffuser on airplane	
Height	12.2 cm
Span	1.85 m
Porosity, aluminum angle frame covered with perforated sheet, 1.59 mm holes, 2.78 mm spacing	25 percent
Porous spoilers	
Span l (fig. 3)	
Basic	1.78 m
Shortened	1.42 m
Porosity	
Expanded metal grid	68 percent
Covered with perforated sheet	
3.56 mm holes, 4.76 mm spacing	35 percent
6.35 mm holes, 7.94 mm spacing	39 percent
Covered with wire mesh	
0.71 mm wire, 4.23 mm spacing	48 percent
Porous 45° ramp	
Span l (fig. 3)	1.78 m
Porosity of 45° ramp, framework covered with perforated sheet, 3.56 mm holes, 4.76 mm spacing	39 percent
Porosity of vertical surface, expanded metal grid	68 percent
Wraparound spoilers	
Height H (fig. 5)	
Low	10.2 cm
High	16.0 cm
Porosity	
Basic, 2.22 cm holes, 2.93 cm spacing	52 percent
Covered with perforated sheet, 3.56 mm holes, 4.76 mm spacing	27 percent
Cambered-plate diffusers	
Airfoil section	
Thickness distribution	Forward 40 percent of NACA 64-006
Mean line	Segment of ellipse with major and minor axes of 91.5 and 18.3 cm
Height at inlet, h (fig. 5)	
Low	7.4 cm
High	13.2 cm
Height at exit, H (fig. 5)	
Low	10.2 cm
High	16.0 cm

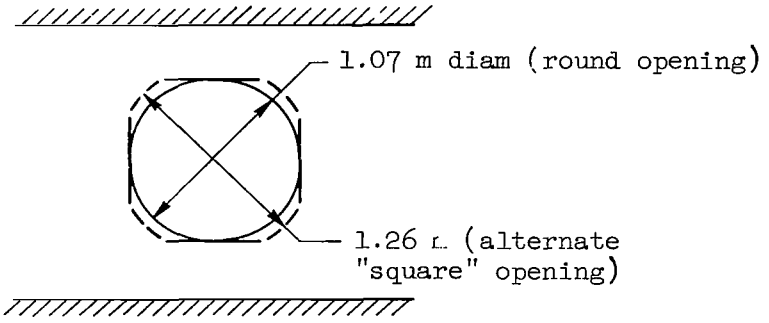

View A-A

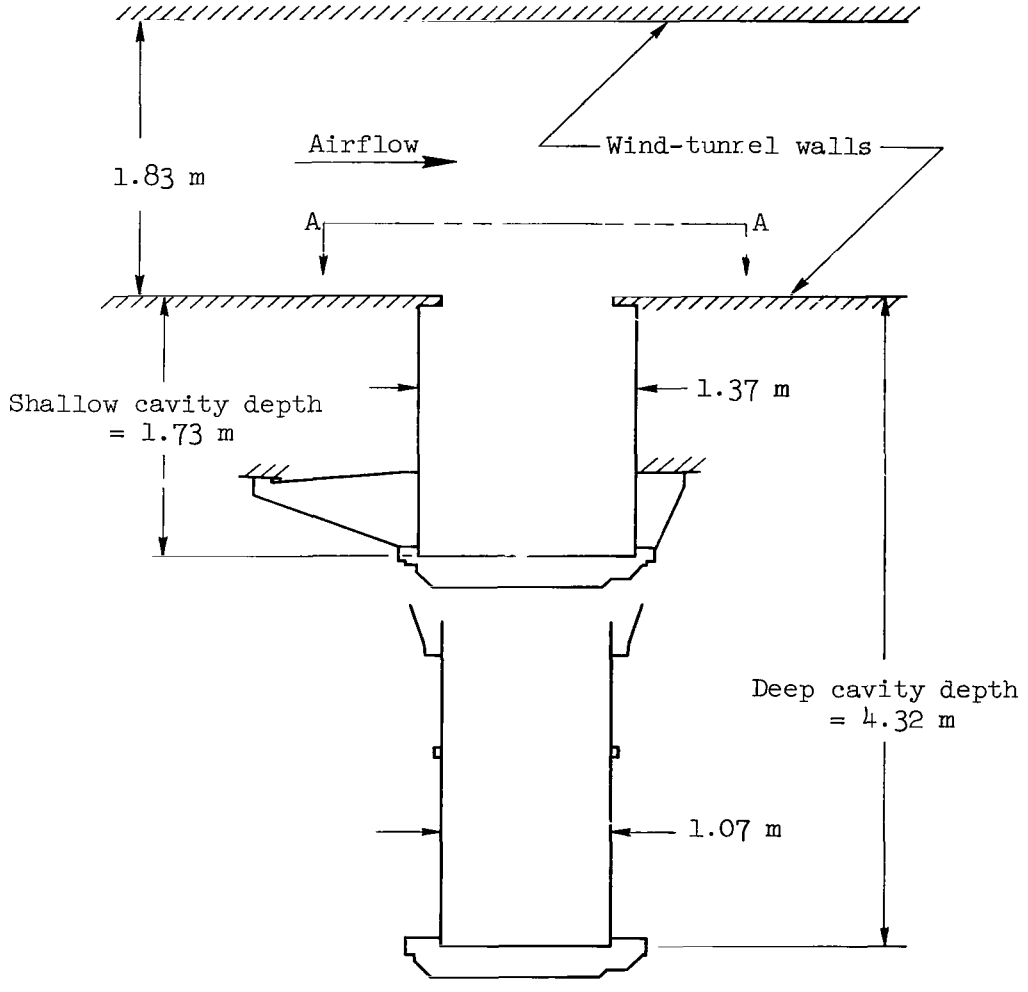

Figure 1.- Wind-tunnel test section and cavity dimensional data.

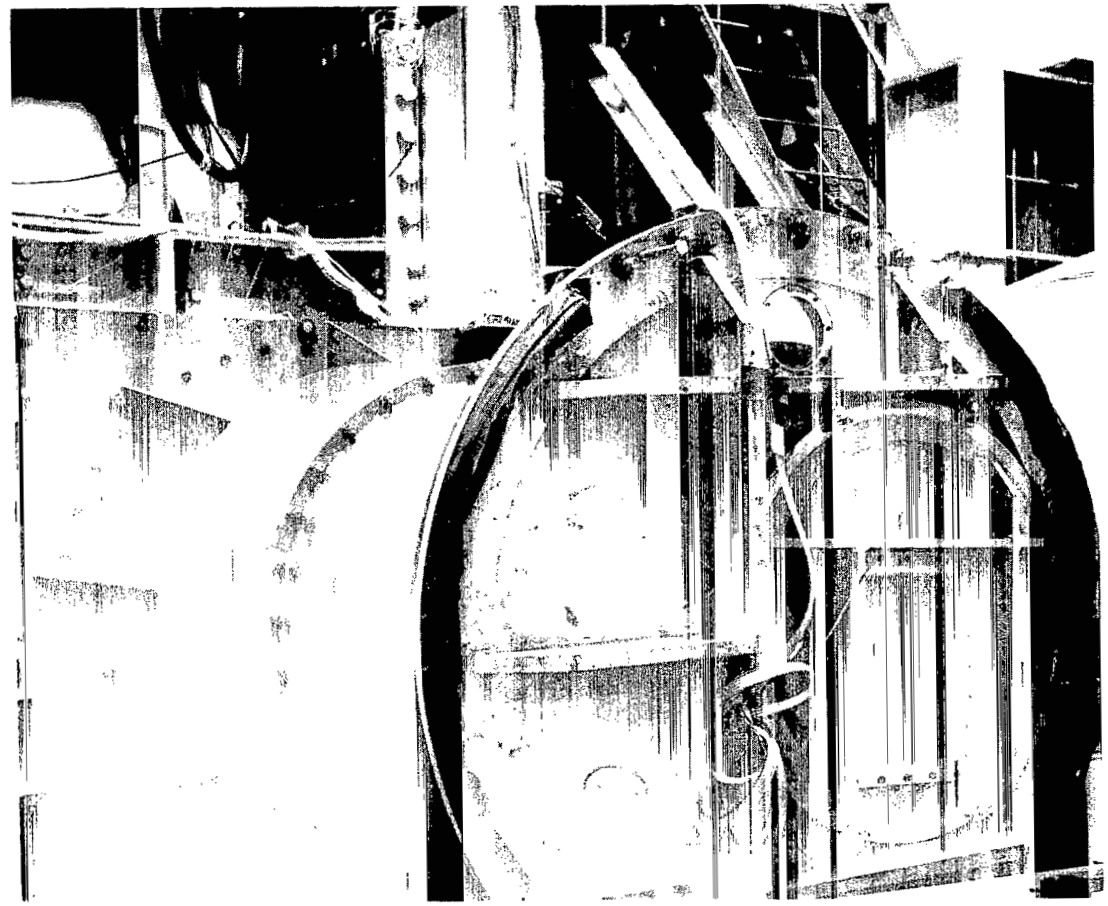

Figure 2.- External view of the deep-cavity structure on the side of the wind tunnel.

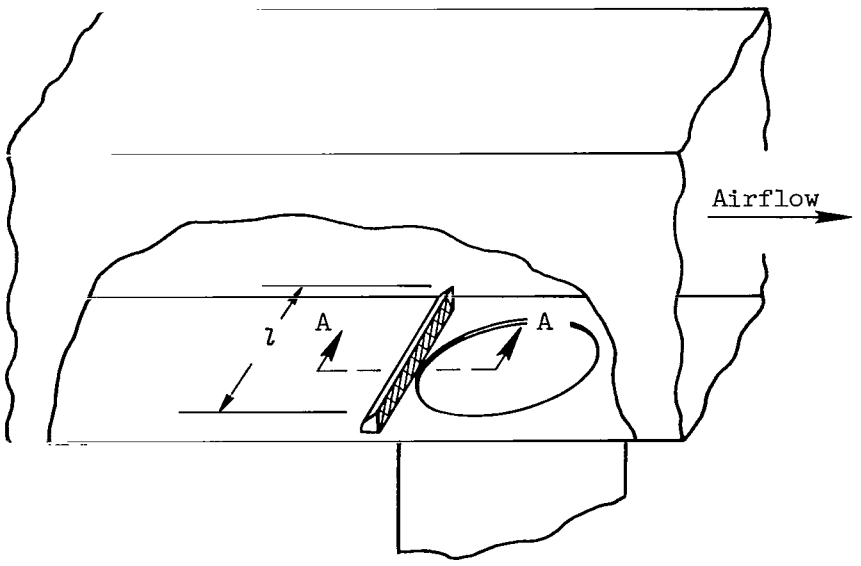

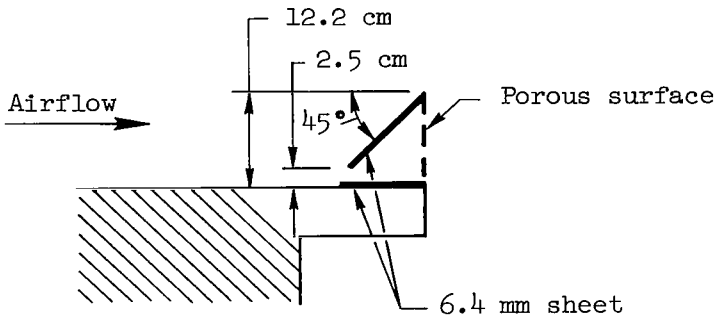

Section A-A, 45° diffuser

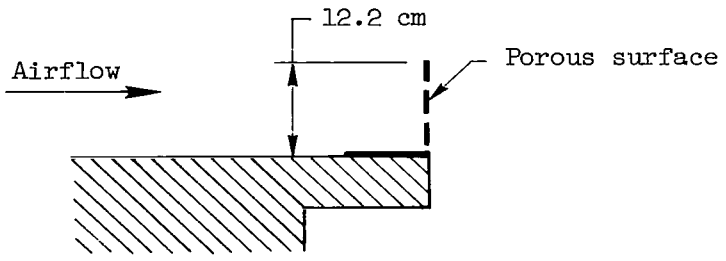

Section A-A, porous spoiler

Figure 3.- Details of the high-aspect-ratio diffuser and spoiler as antiresonance devices.

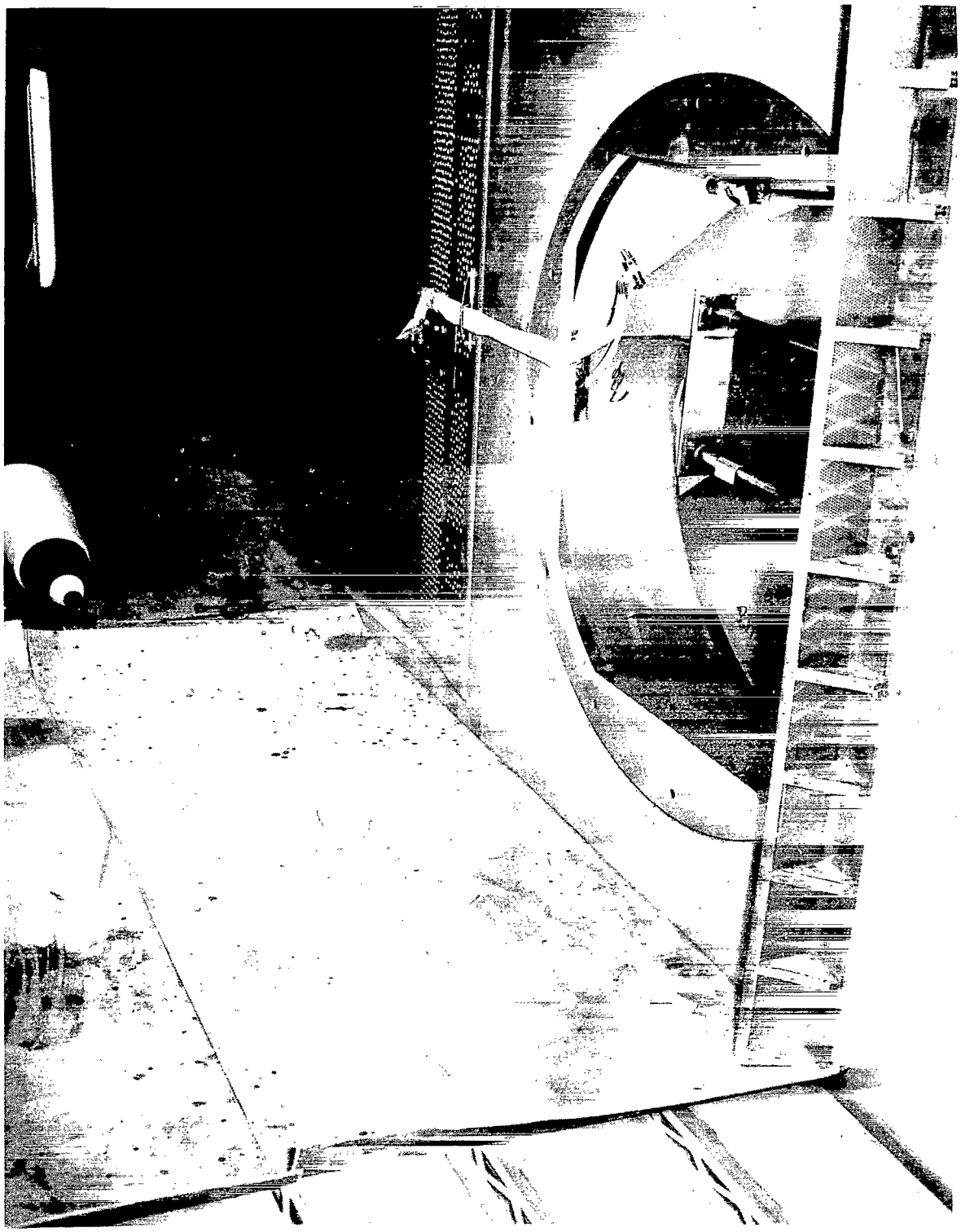

Figure 4.- The porous spoiler, the "square" opening, and wake rake as seen from inside the wind tunnel.

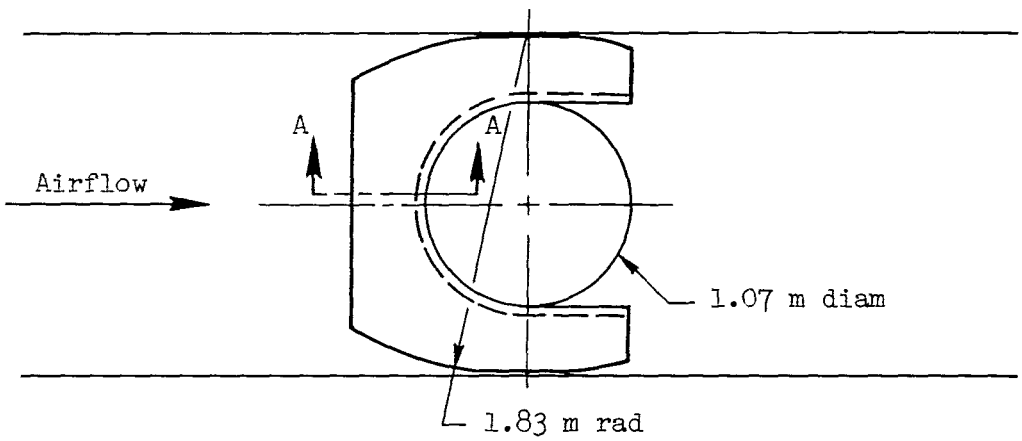

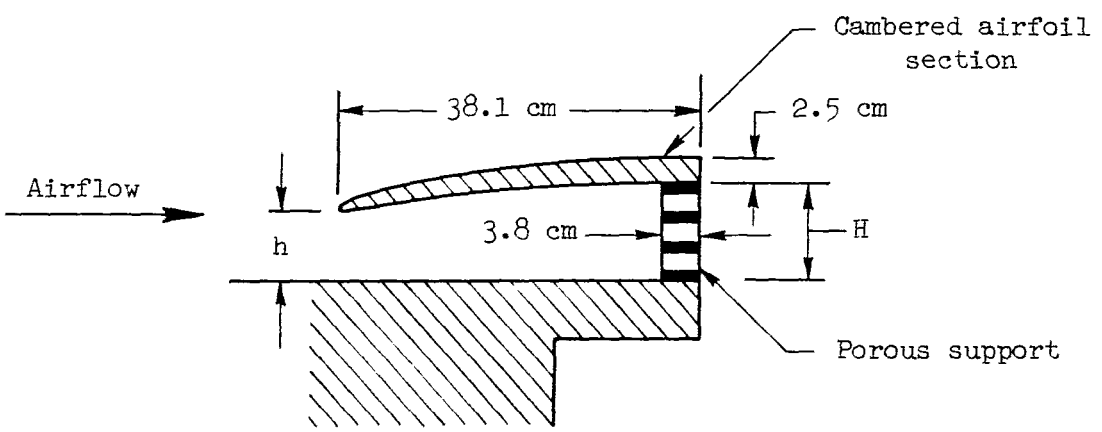

Section A-A

Figure 5.- Details of the cambered-plate diffuser.

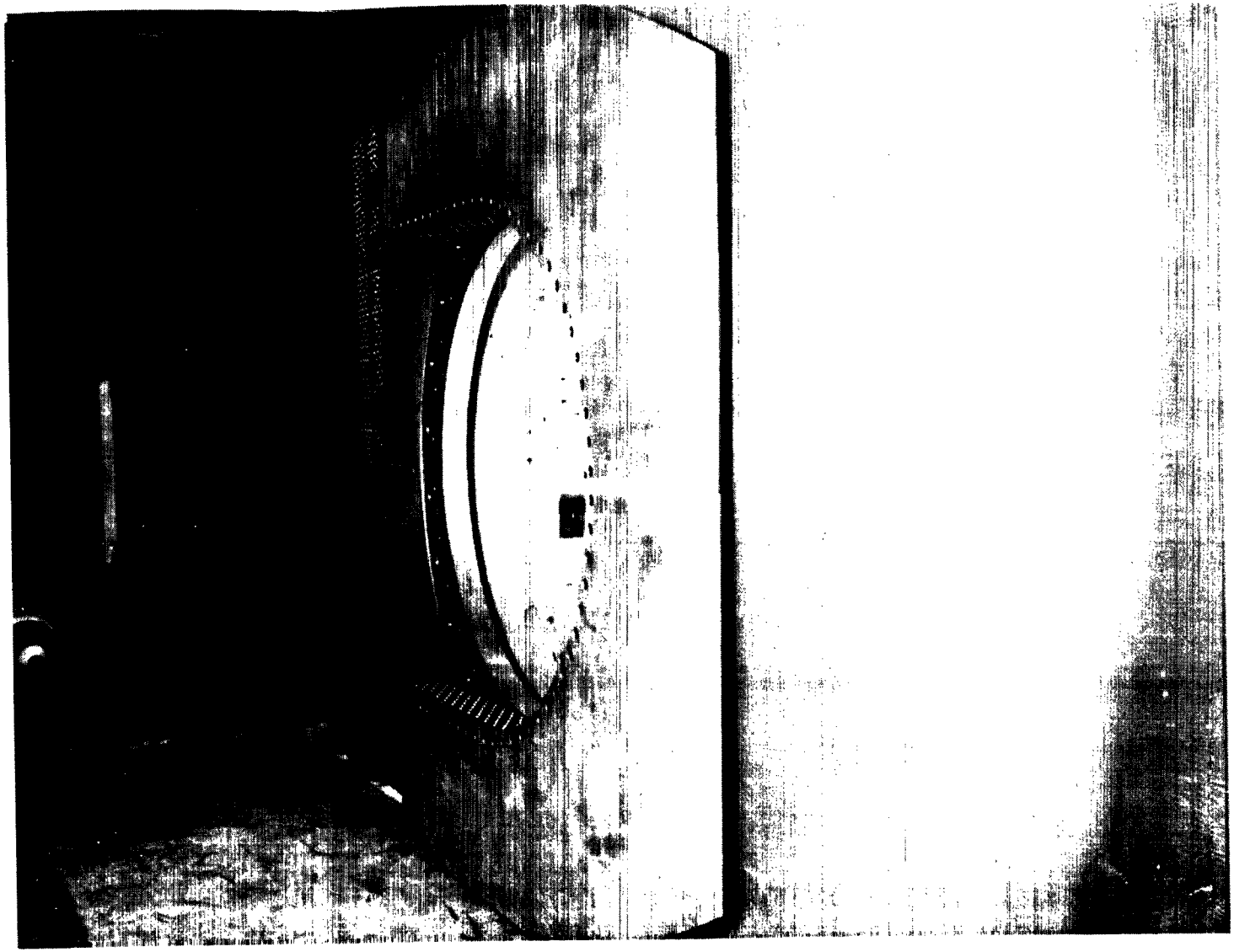

Figure 6.- The cambered-plate diffuser inside the wind tunnel.

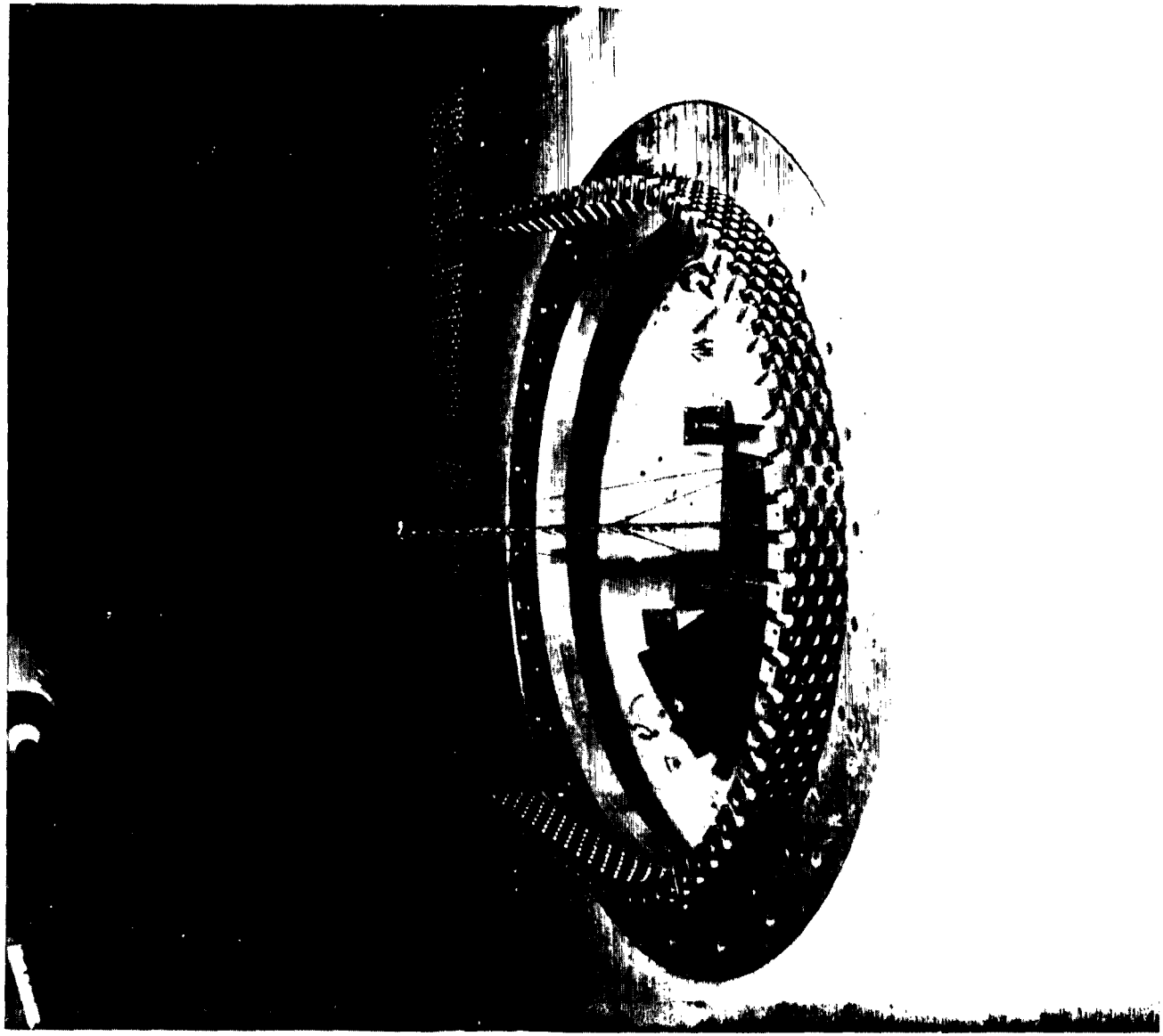

Figure 7.- The wraparound spoiler and the movable rake in the wind tunnel.

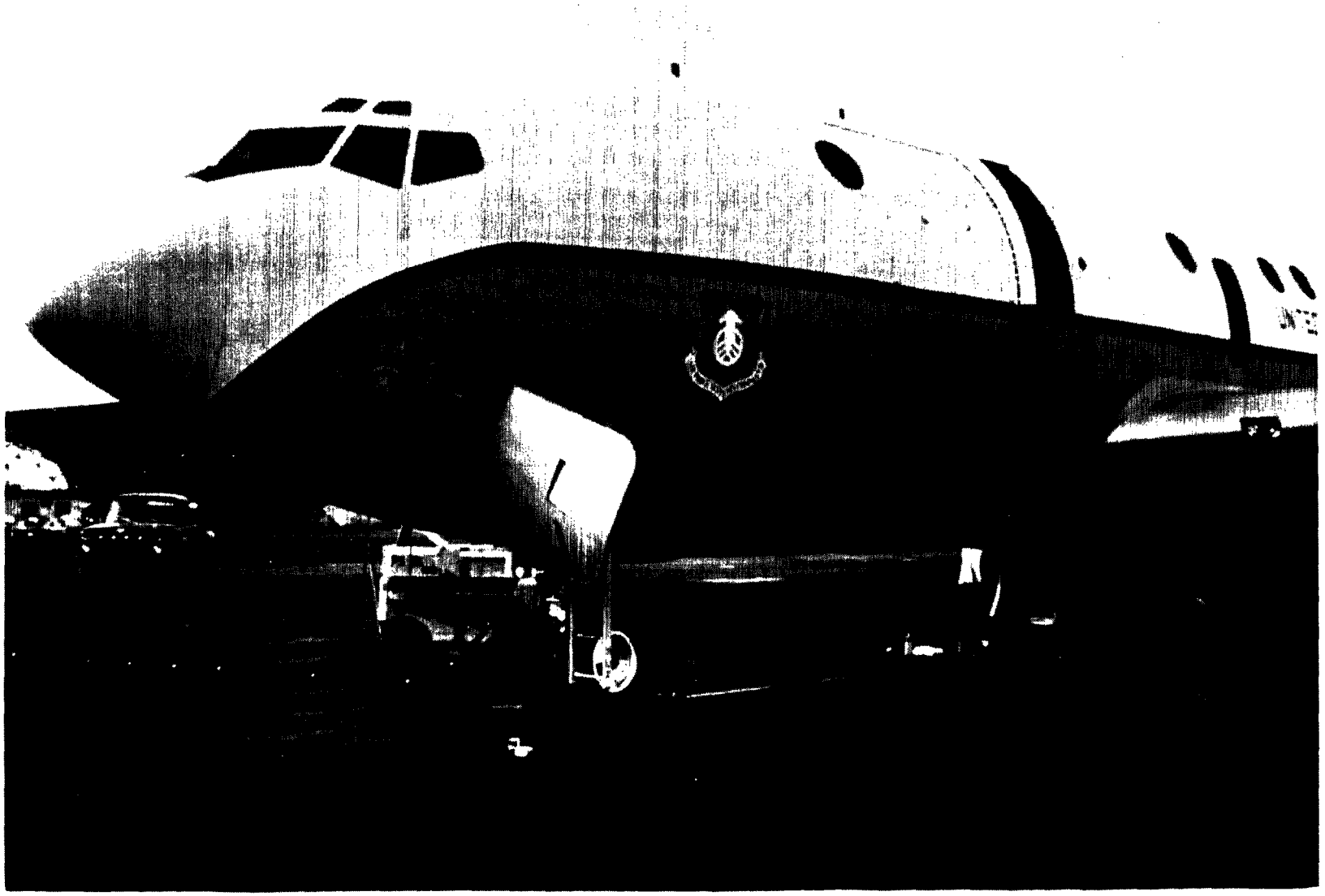

Figure 8.- Photograph of the airplane showing the cavity above and forward of the wing.

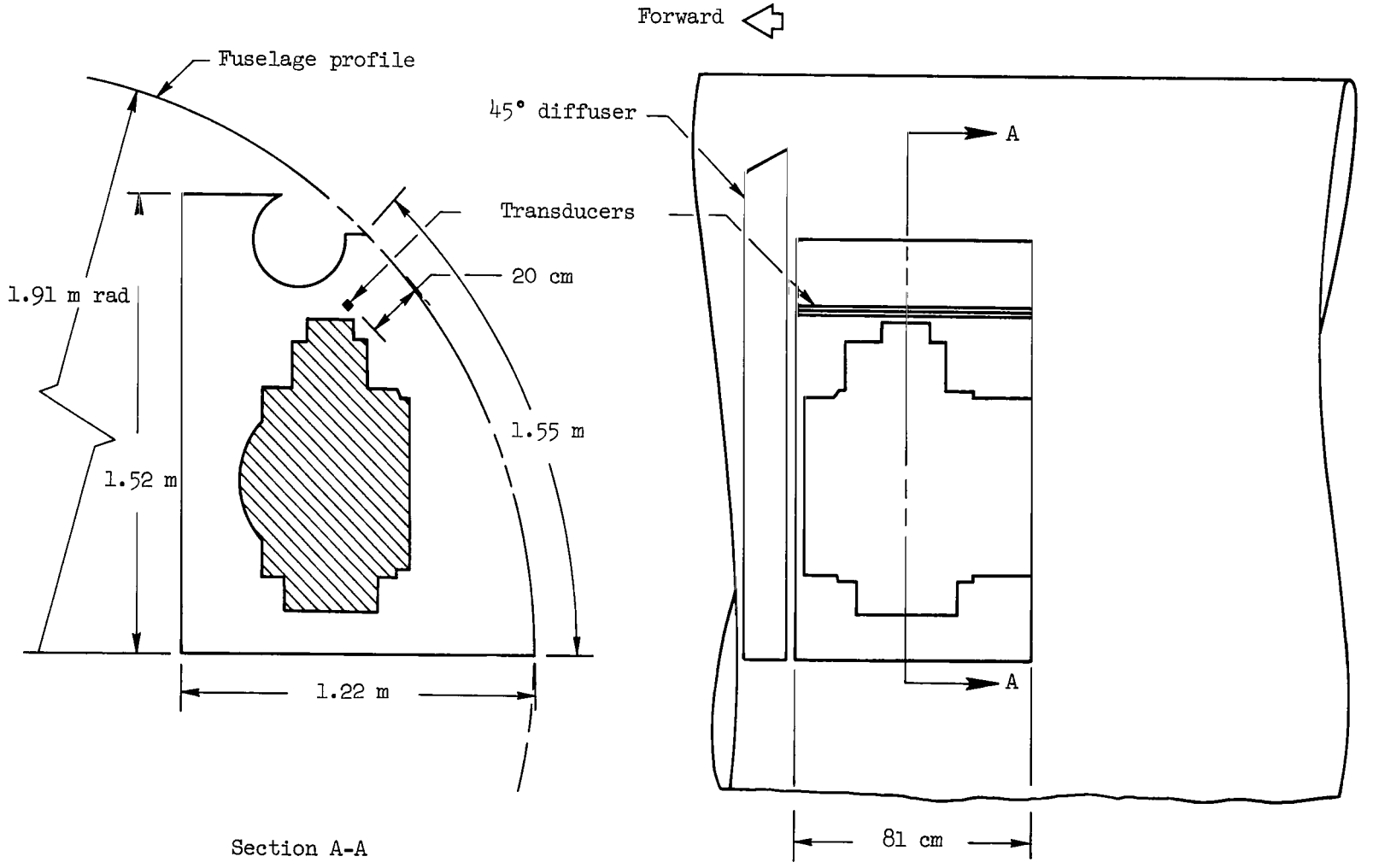

Figure 9.- Sketch of the airplane cavity.

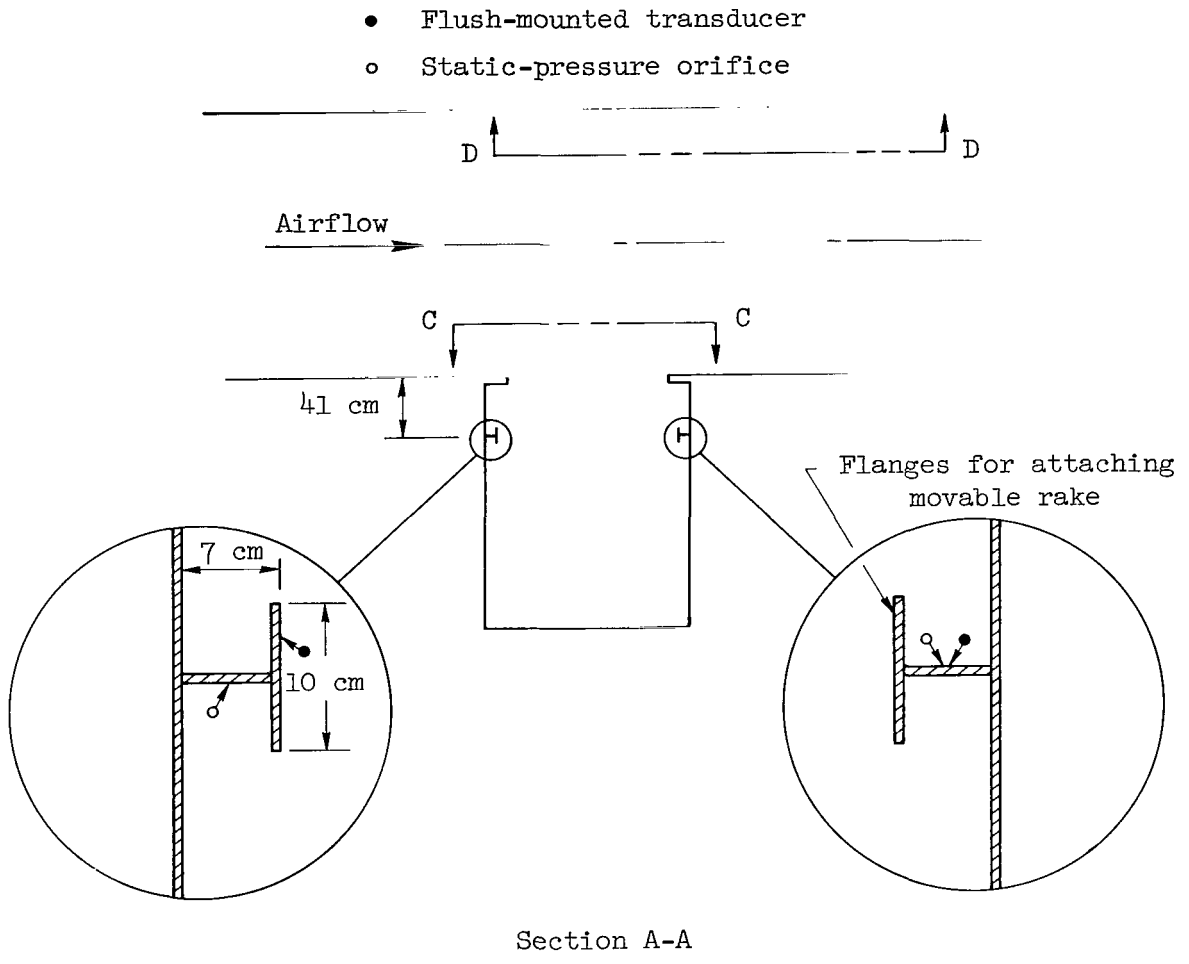

(a) Outside view and section A-A

Figure 10.- Locations of the pressure transducers and orifices in the wind tunnel and cavity.

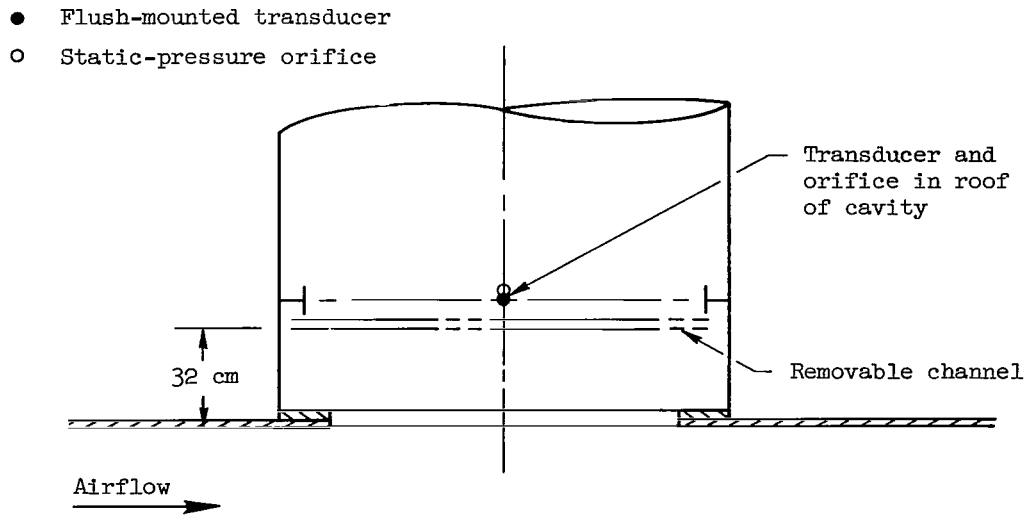

Sectional view B-B

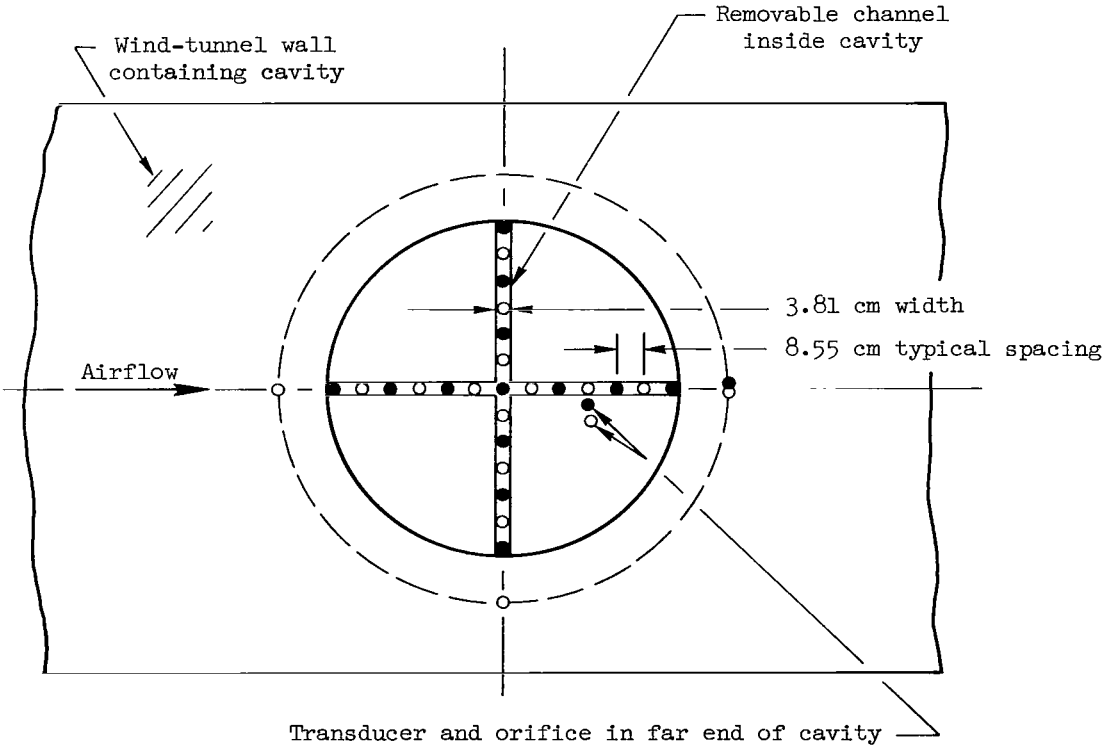

View C-C

(b) Views B-B and C-C

Figure 10.- Continued.

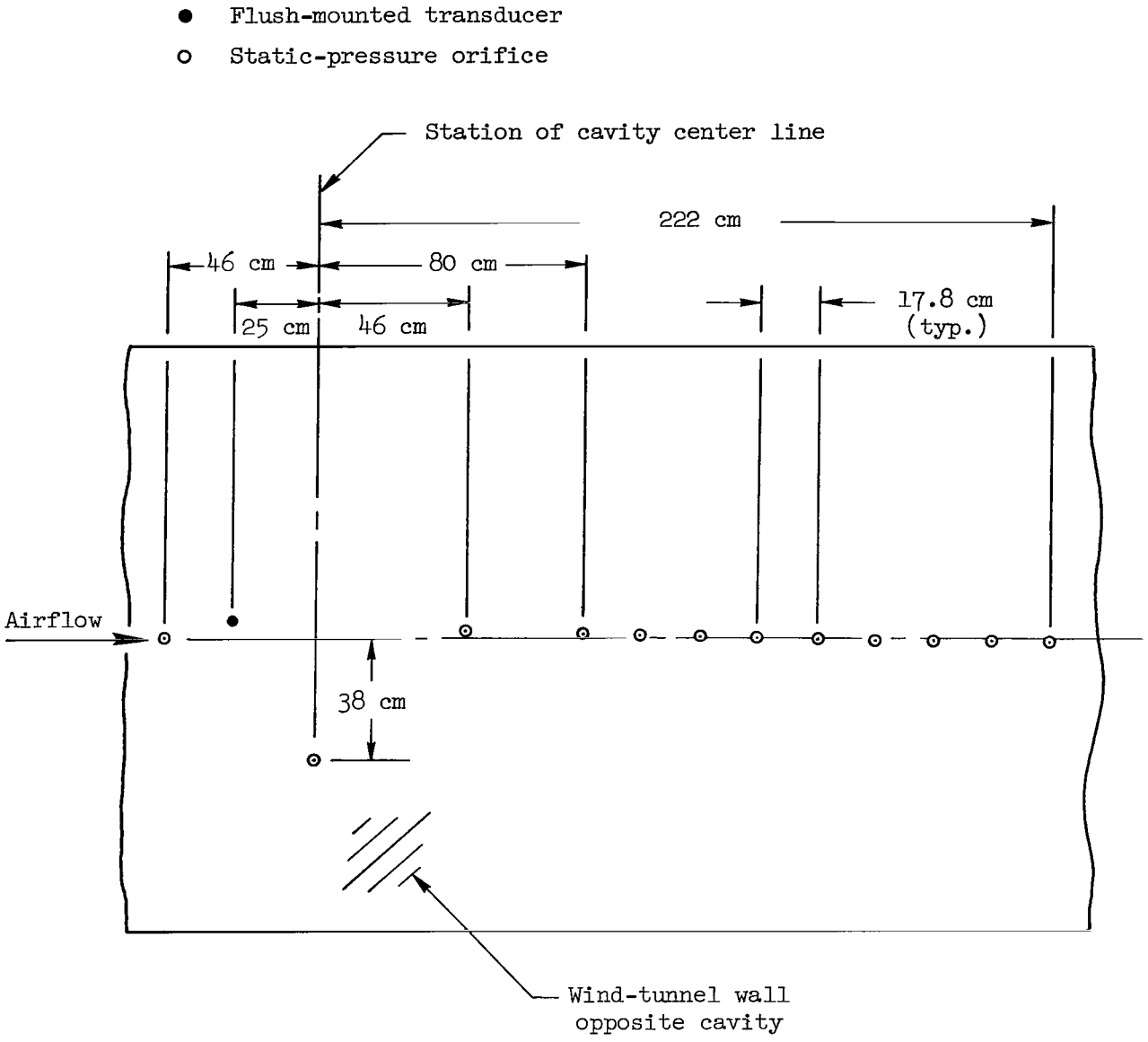

(c) View D-D

Figure 10.- Concluded.

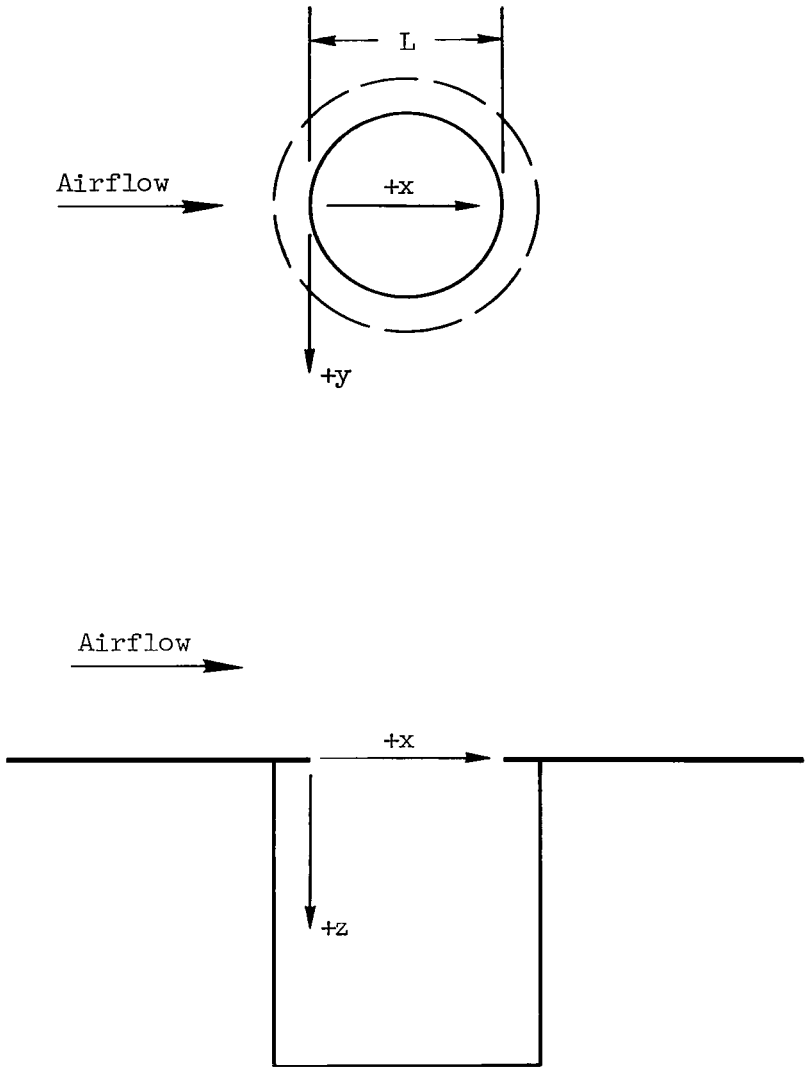

Figure 11.- The coordinate system.

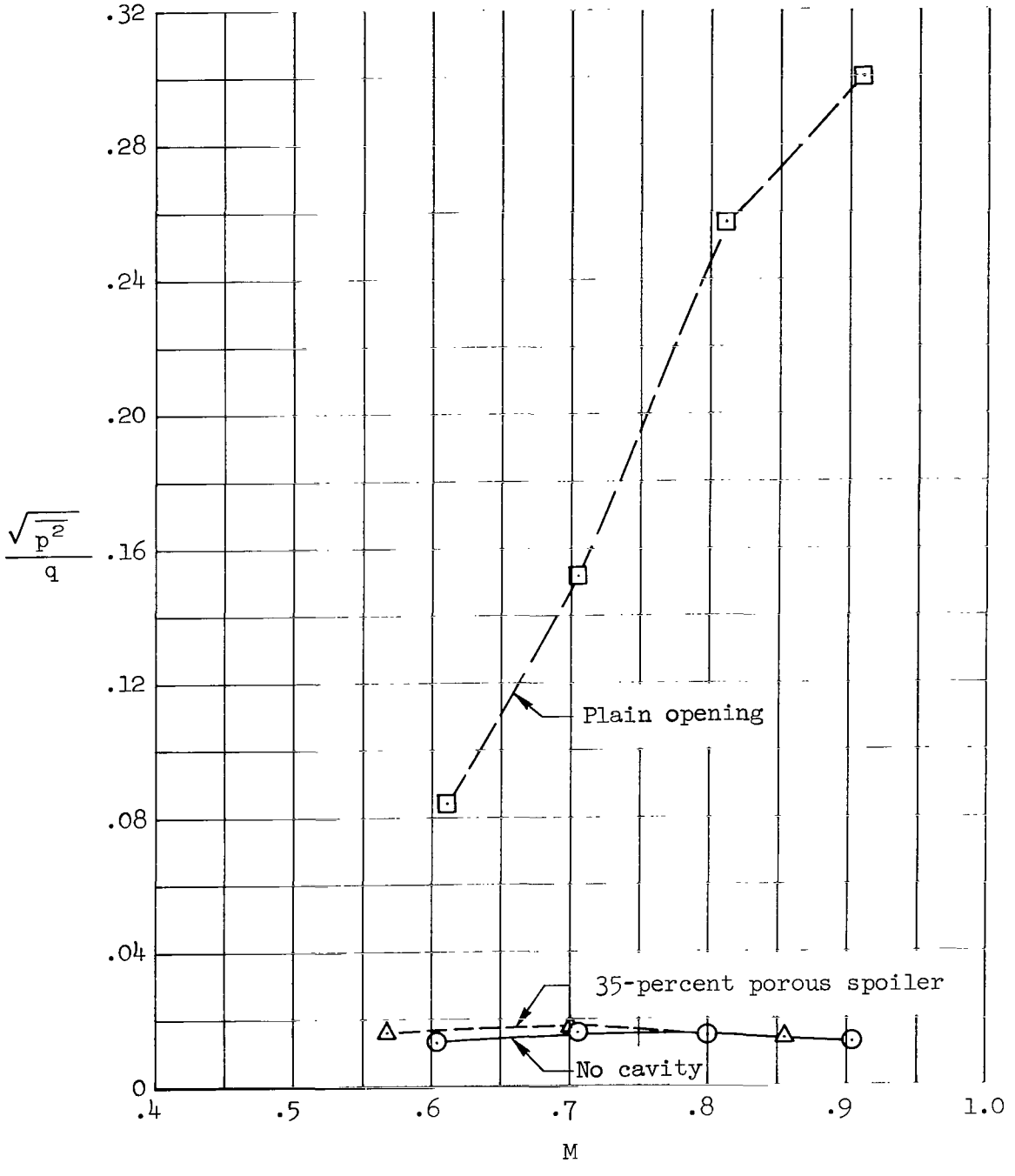

Figure 12.- The rms of the pressure fluctuations on the tunnel wall with no cavity, compared with that on the downstream wall of the cavity with and without the 35-percent porous spoiler; cavity depth = 1.6 L, round opening.

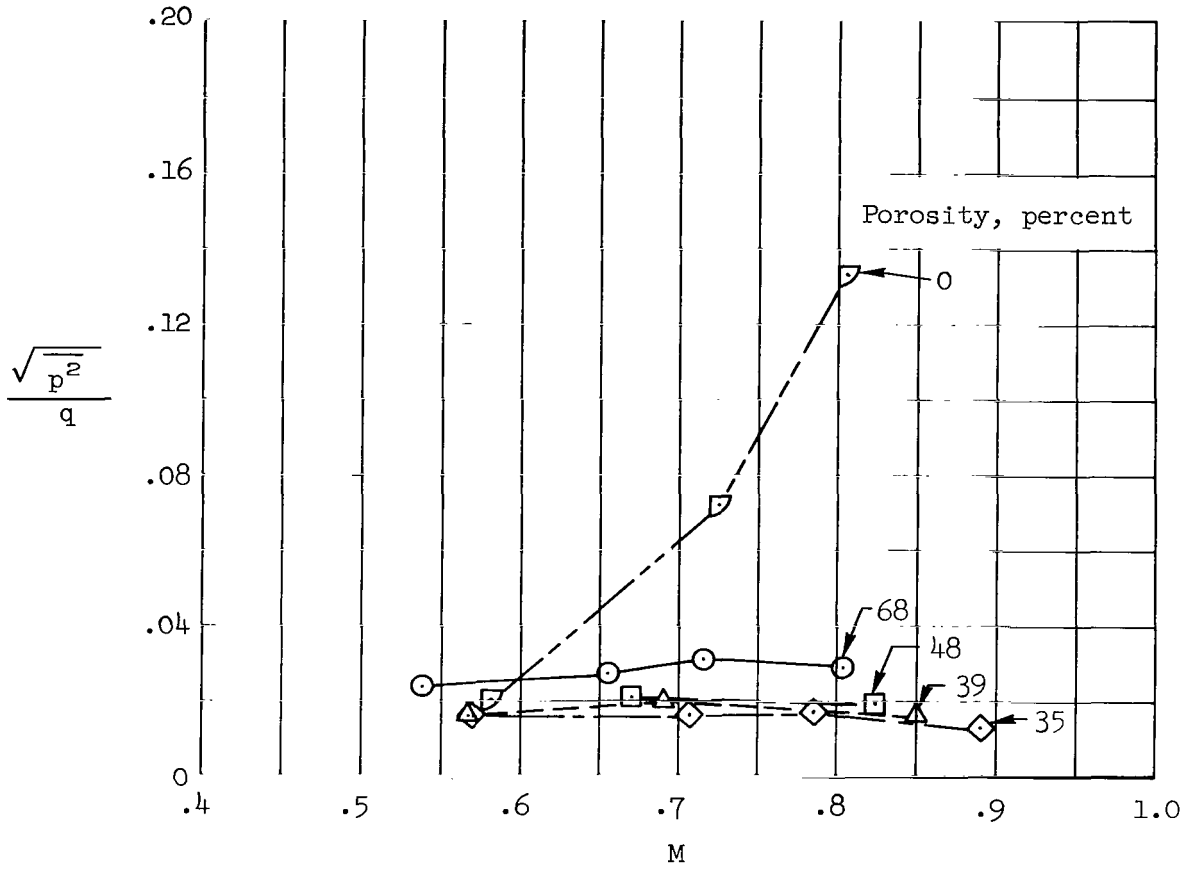

Figure 13.- The rms of the pressure fluctuations on the downstream wall of the cavity with the porous spoiler; cavity depth = 1.6 L, "square" opening.

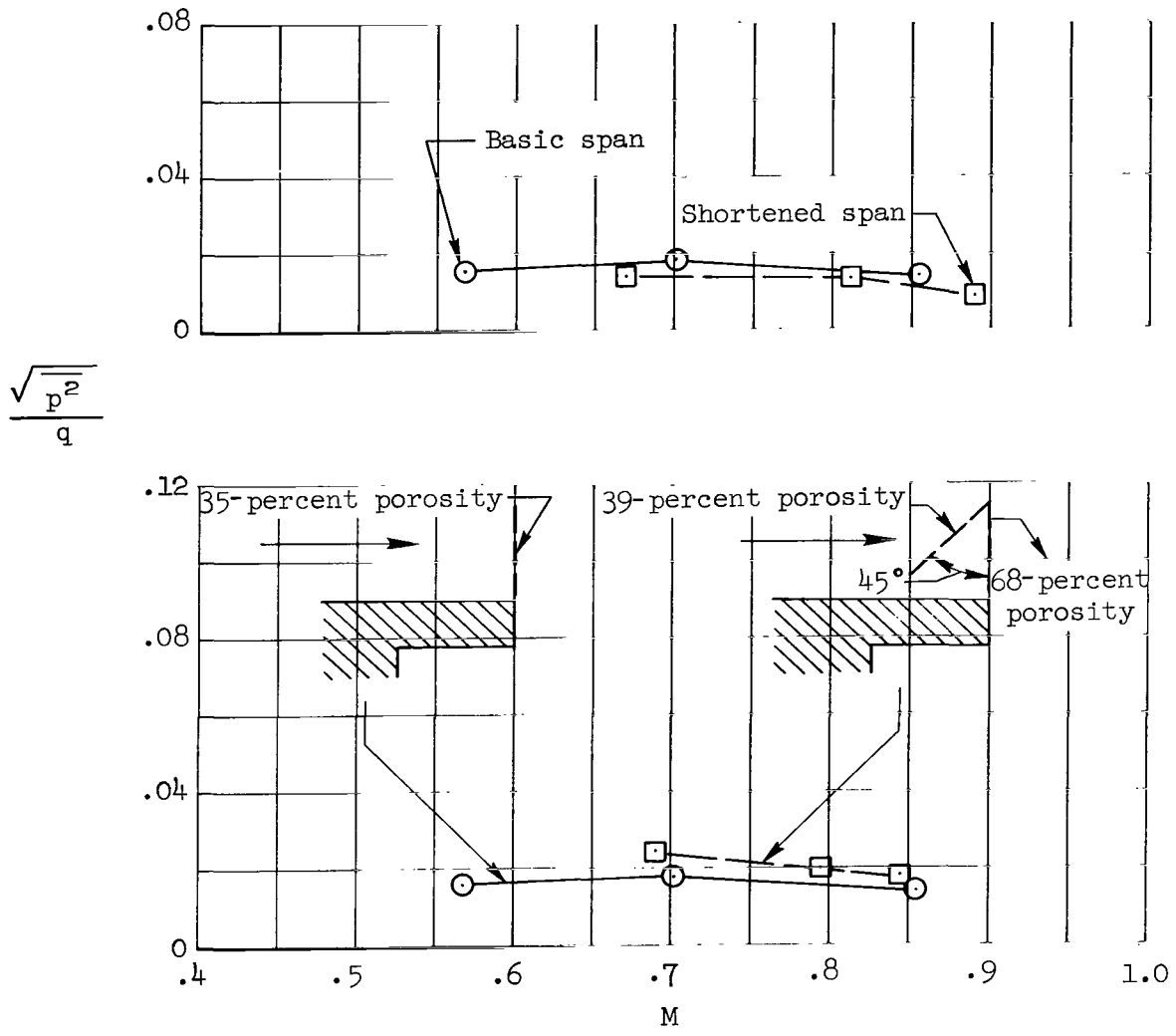

Figure 14.- The rms of the pressure fluctuations on the downstream wall of the cavity with the basic 35-percent porous spoiler compared with data for a shortened spoiler and for a porous ramp; cavity depth = 1.6 L, round opening.

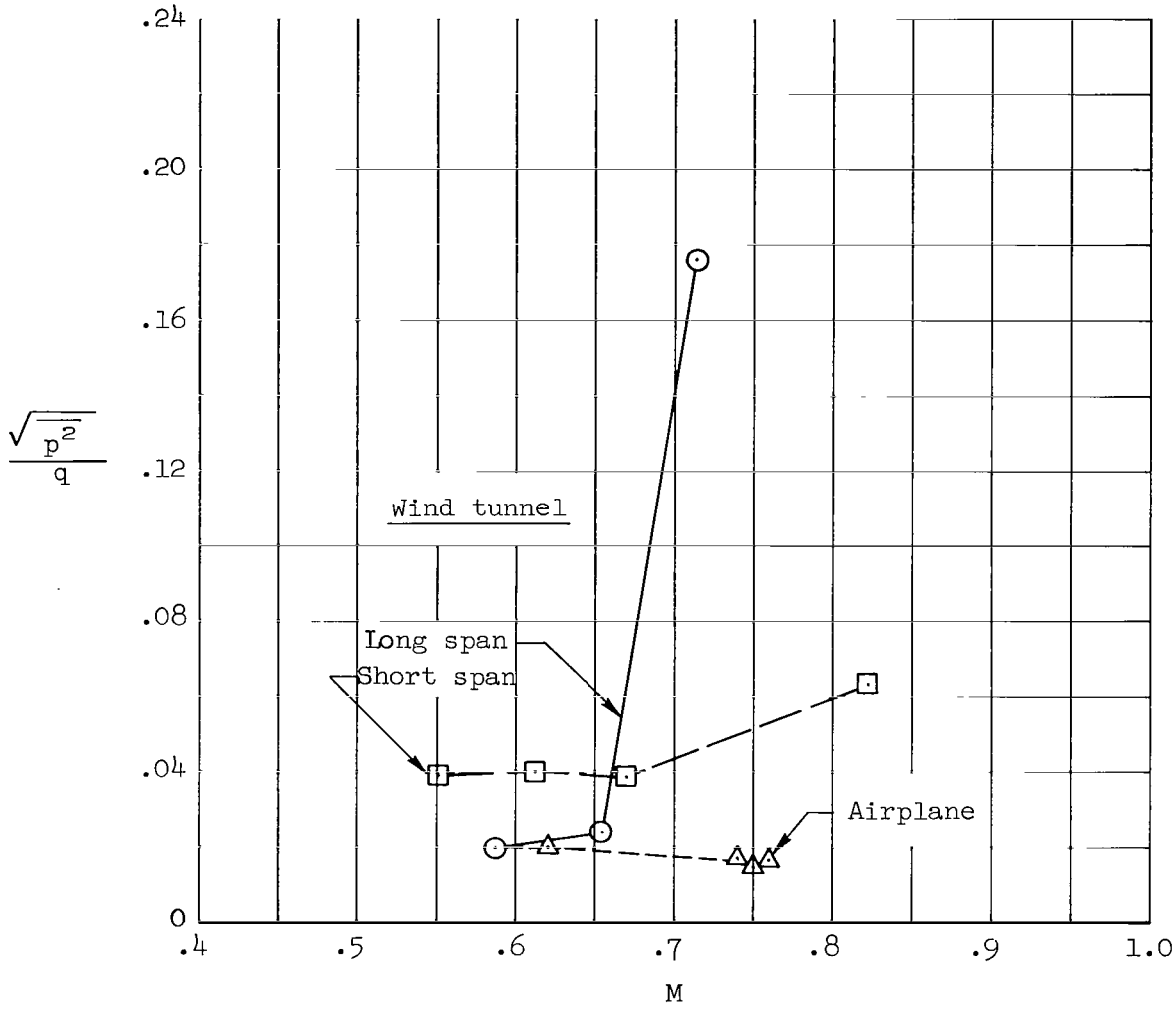

Figure 15.- A comparison between wind-tunnel and flight values of the rms of the pressure fluctuations near the downstream wall of the cavities with the 45° diffuser; wind-tunnel-cavity depth = 1.6 L, "square" opening.

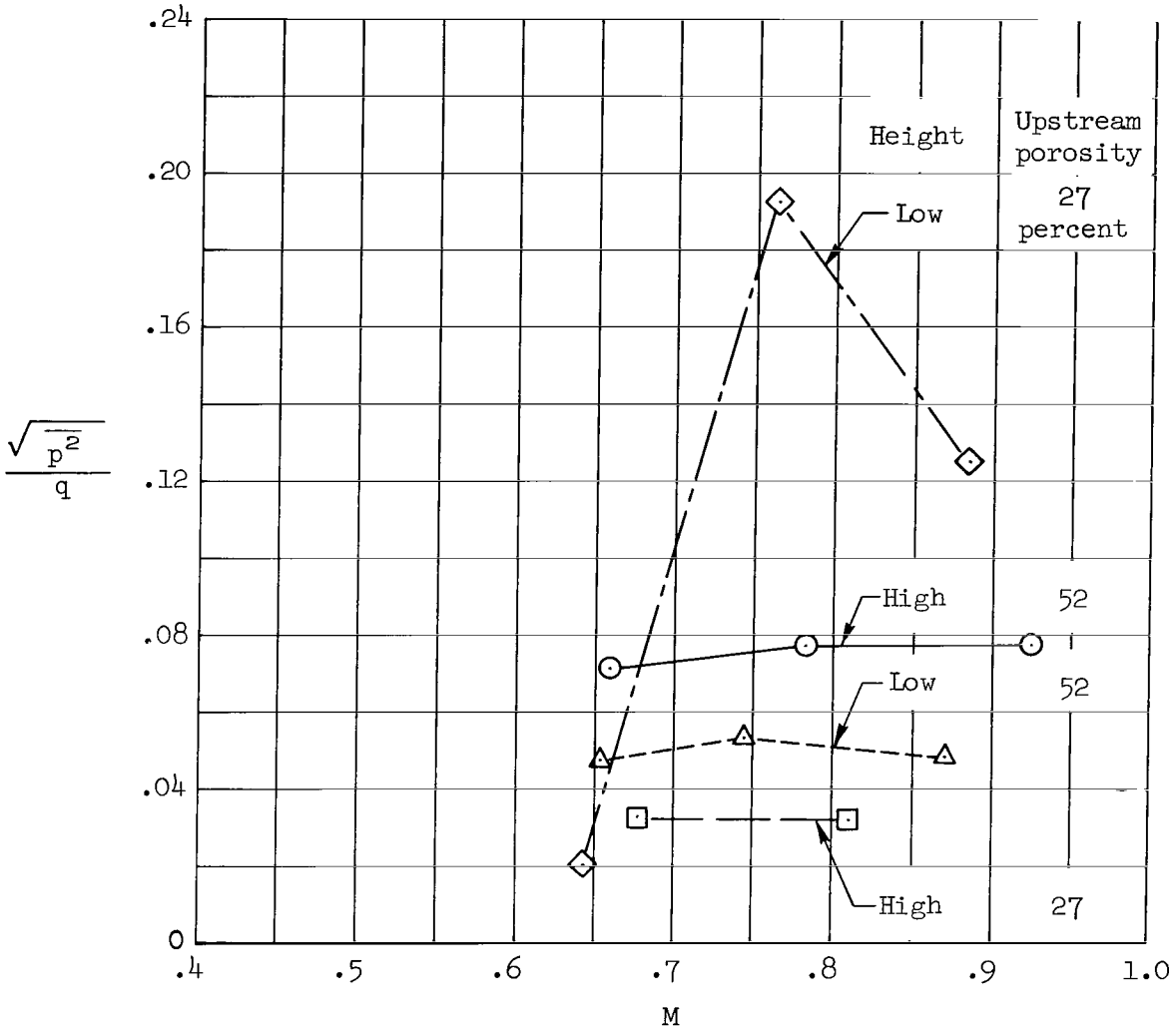

Figure 16.- The effect of spoiler height and porosity on the rms of the pressure fluctuations on the downstream wall of the cavity with the wraparound spoilers; cavity depth = 1.6 L, round opening.

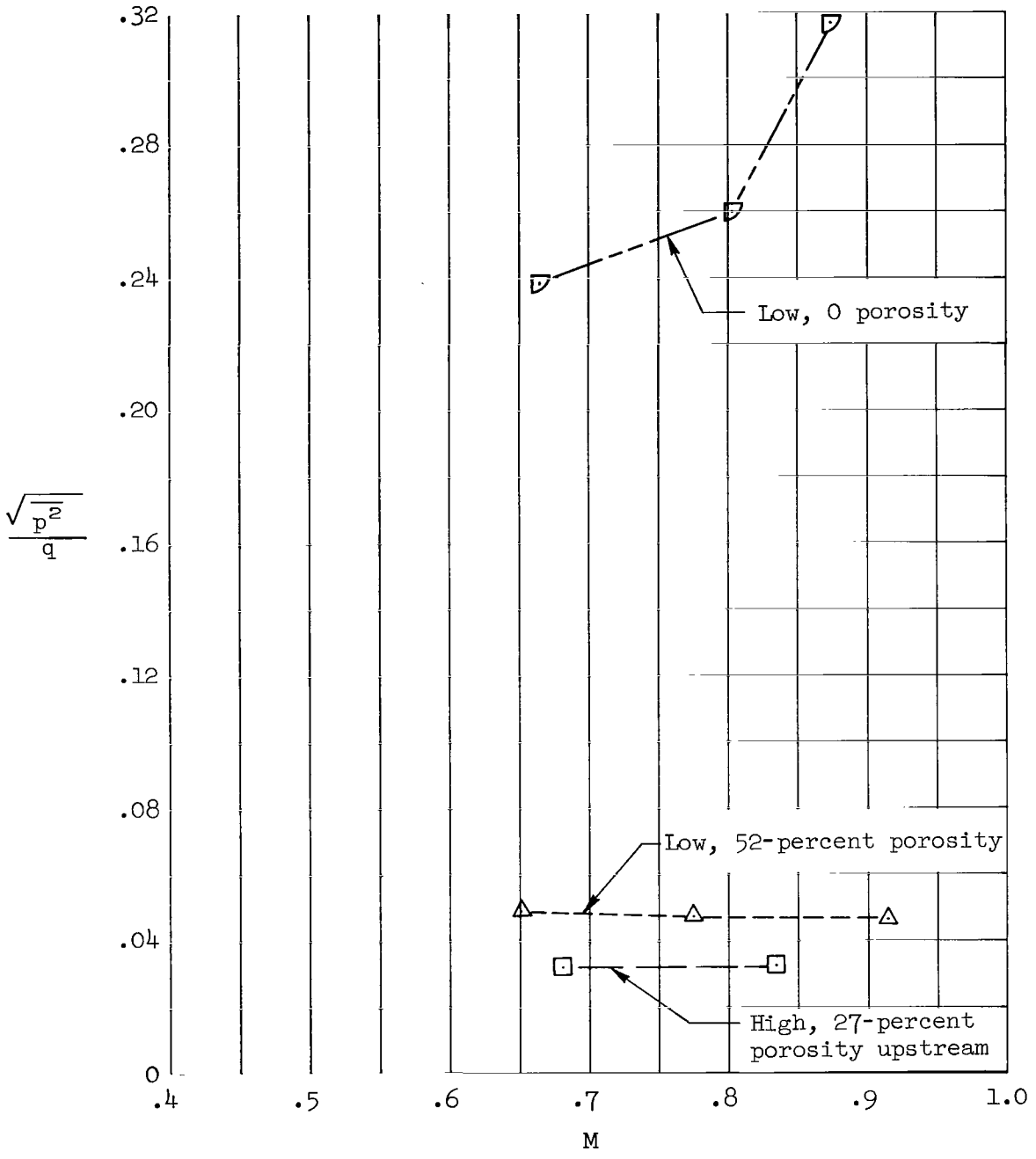

Figure 17.- The effect of diffuser height and porosity on the rms of the pressure fluctuations on the downstream wall of the cavity with the cambered-plate diffusers; cavity depth = 1.6 L, round opening.

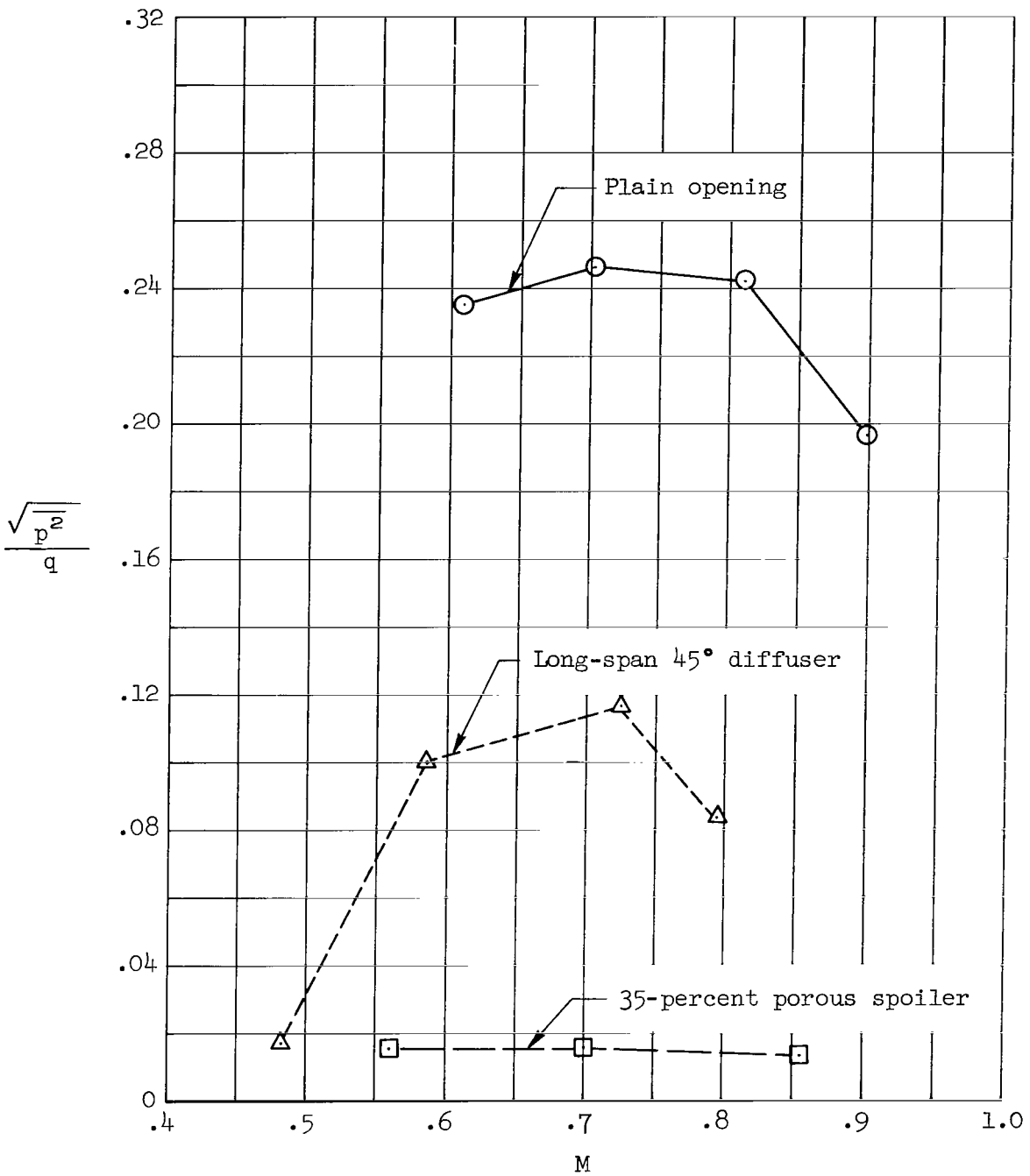

Figure 18.- The effect of the antiresonance devices on the rms of the pressure fluctuations on the downstream wall of the deep cavity; cavity depth = 4.0 L, round opening.

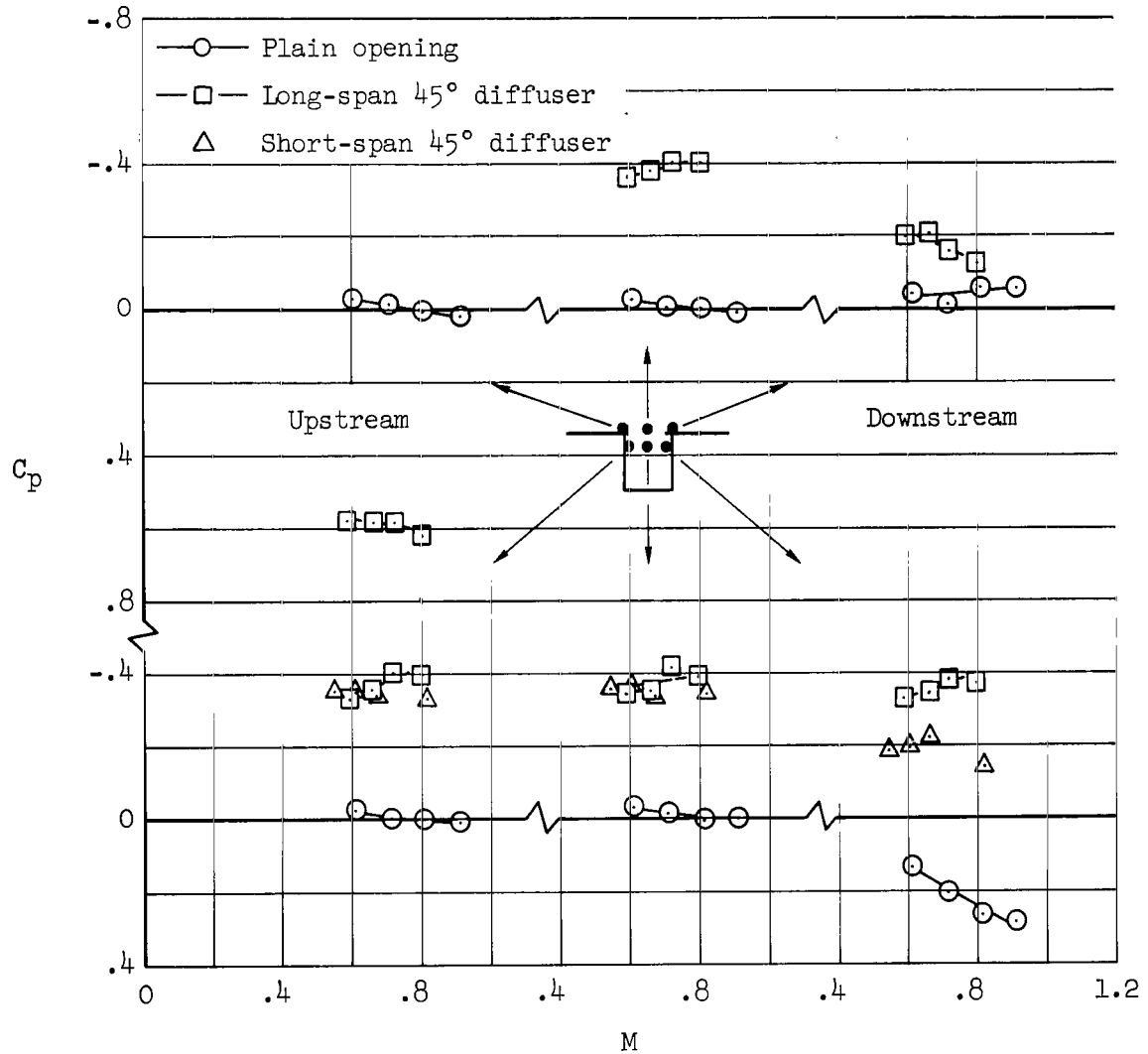

(a) Plain opening and 45° diffusers

Figure 19.- The static pressures in and near the cavity with and without the antiresonance devices; cavity depth = 1.6 L, x/L = -0.1, 0.5, and 1.1; z/L = 0 and 0.4.

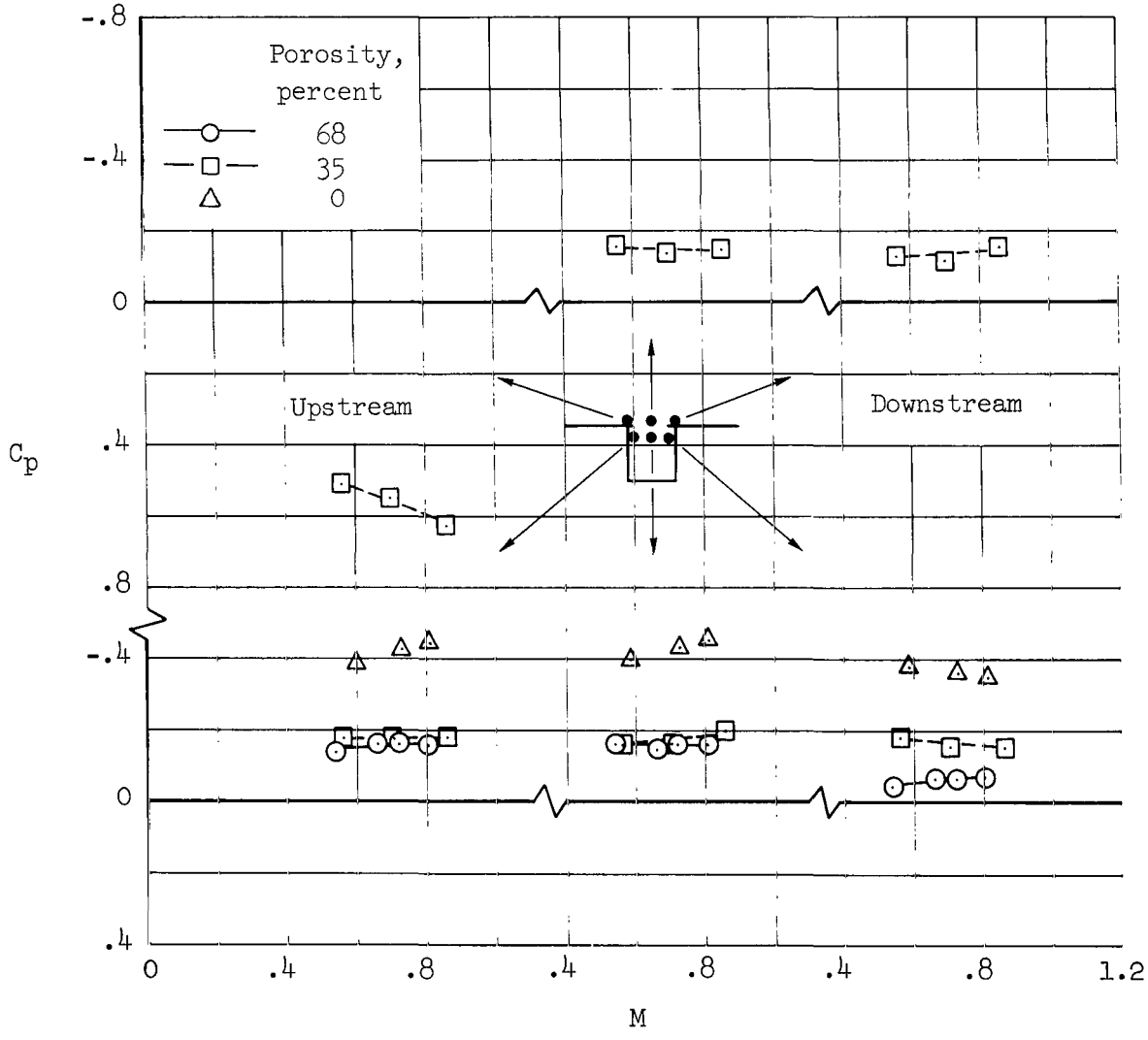

(b) Porous spoilers

Figure 19.- Continued.

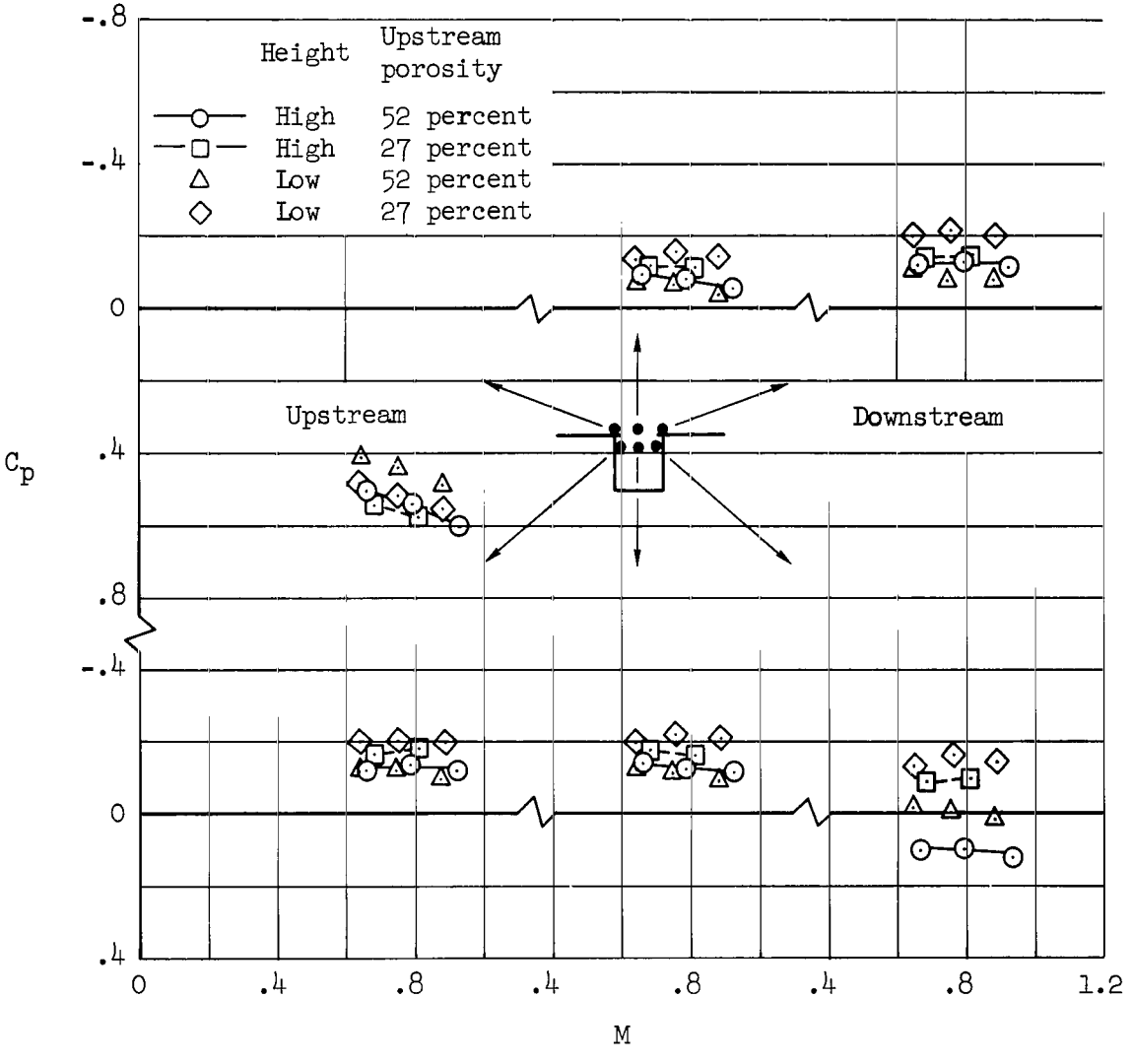

(c) Wraparound spoilers

Figure 19.- Continued.

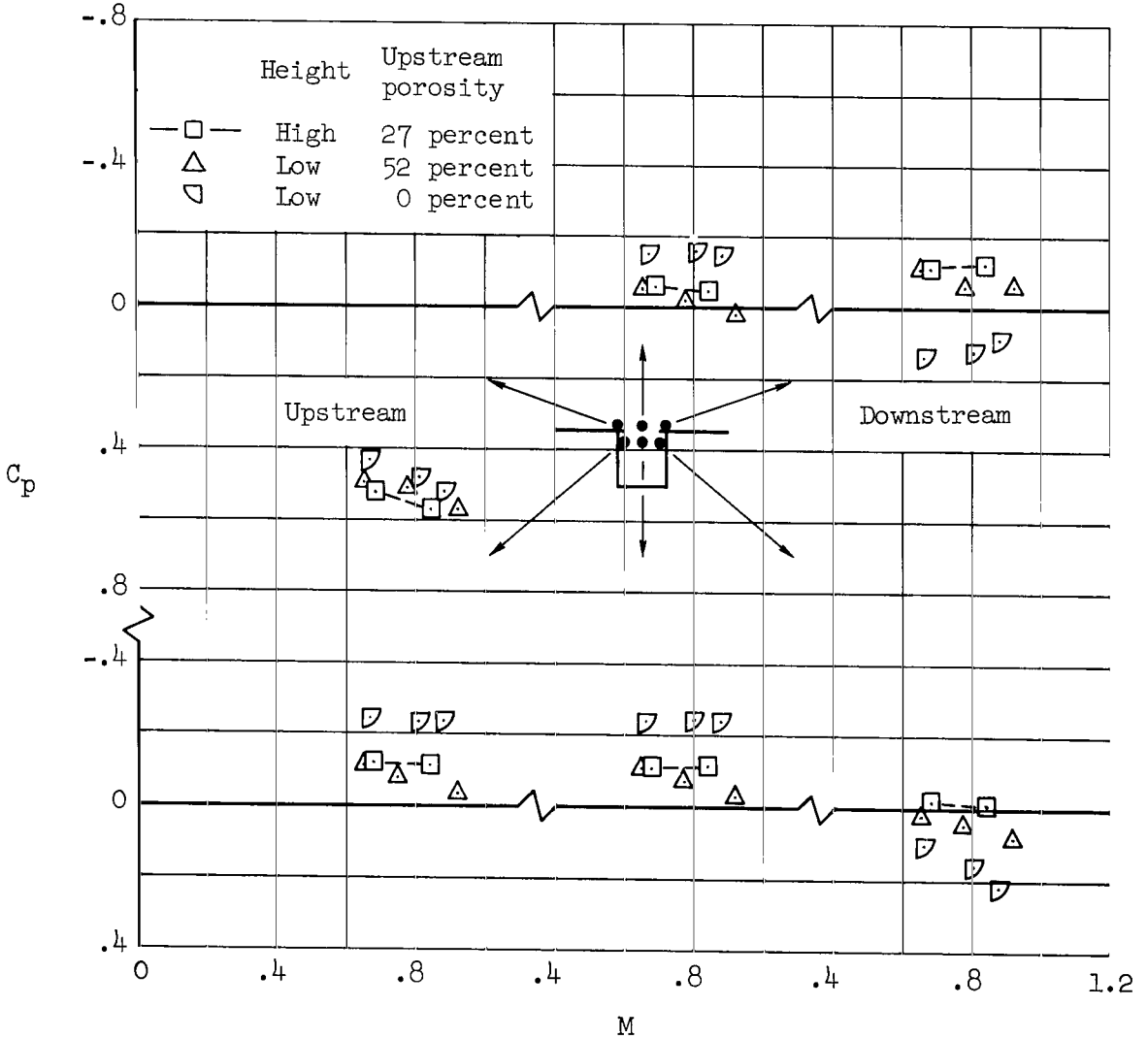

(d) Cambered-plate diffusers

Figure 19.- Concluded.

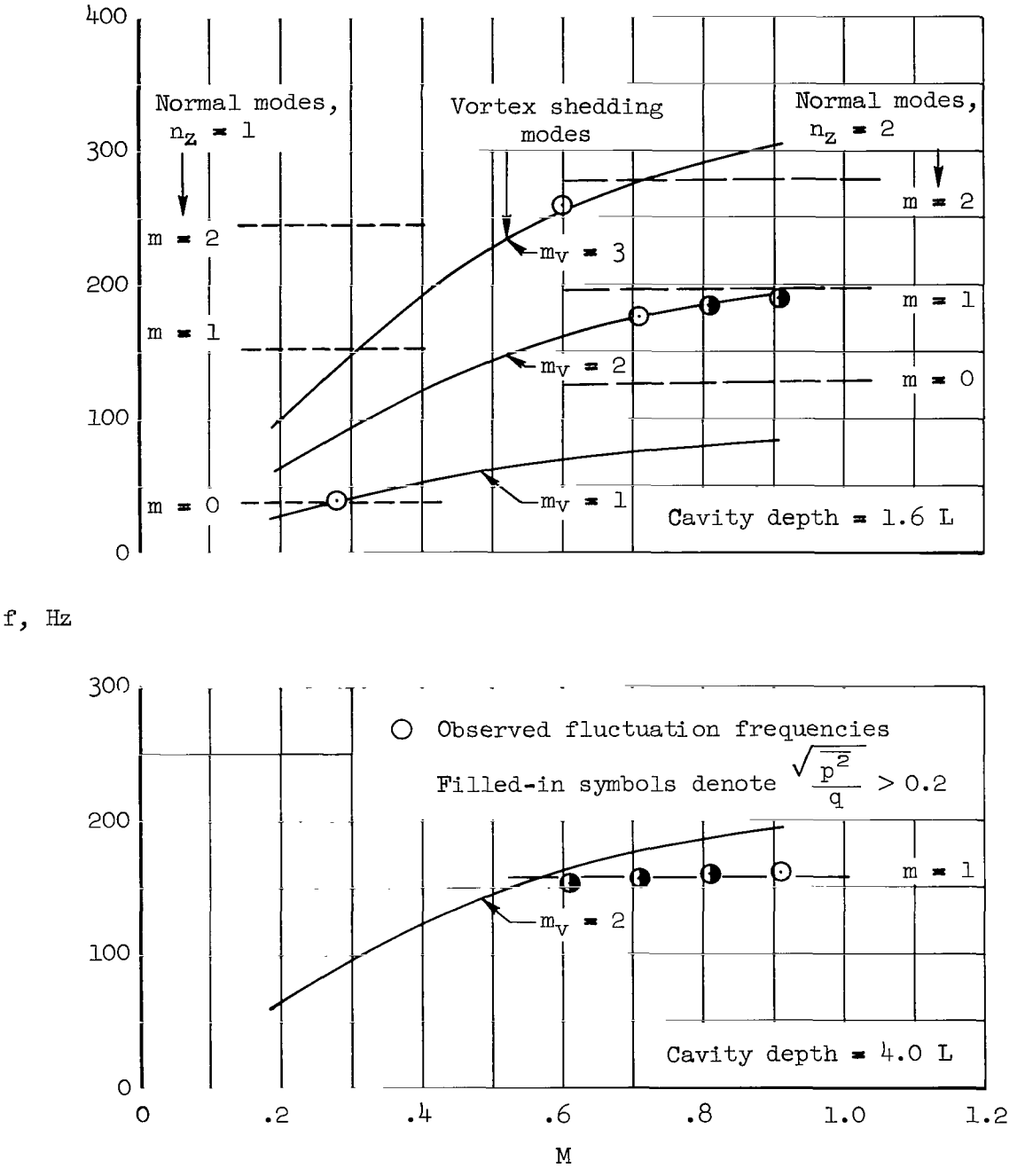

Figure 20.- Comparison of the vortex-shedding frequencies, acoustical normal-mode frequencies, and observed frequencies of the pressure fluctuations in the cavity with the plain opening.

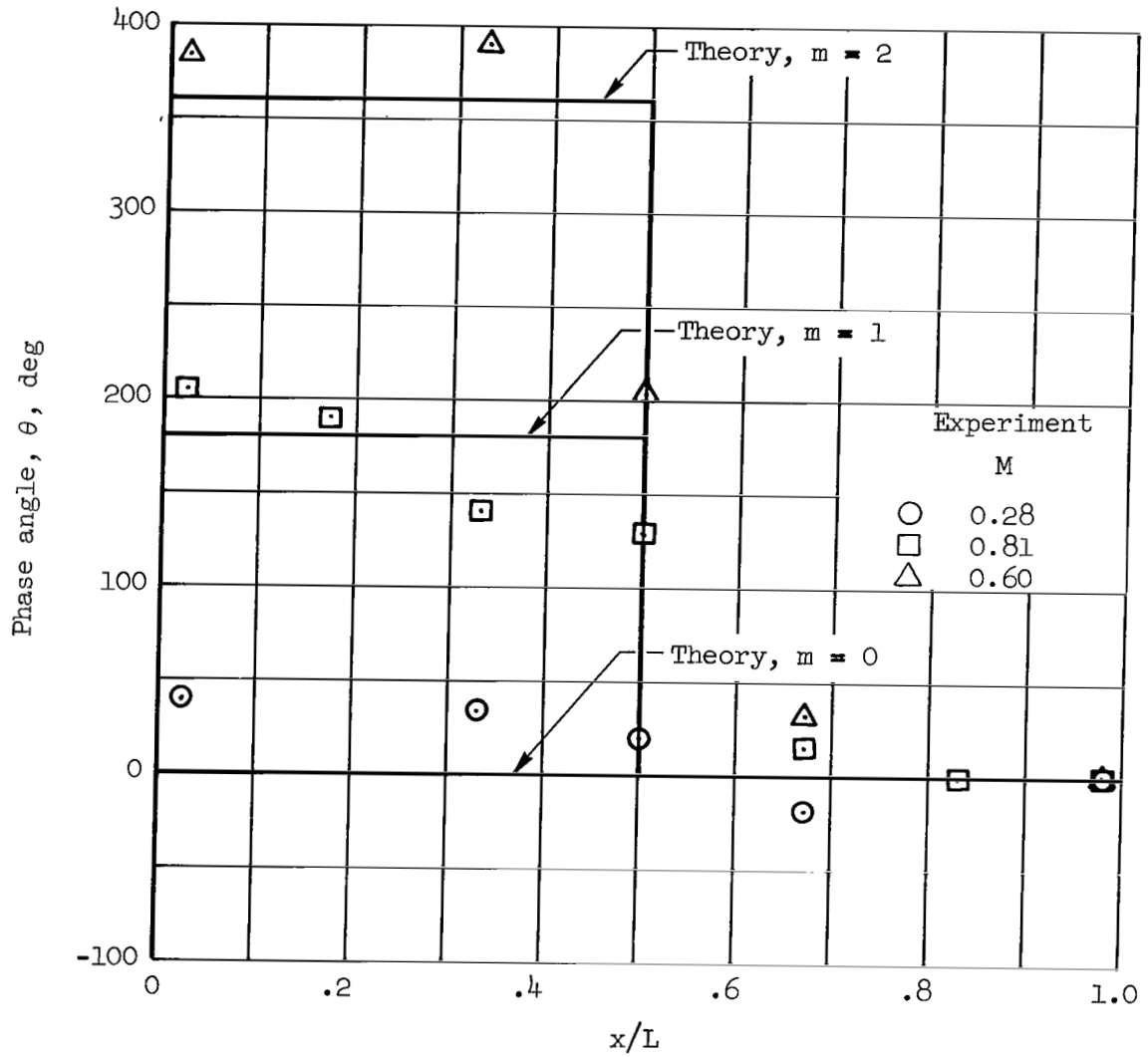

Figure 21.- A comparison of the measured and theoretical phase angles of the pressure fluctuations in the cavity with the plain opening; measuring locations 0.3 L from the airstream.

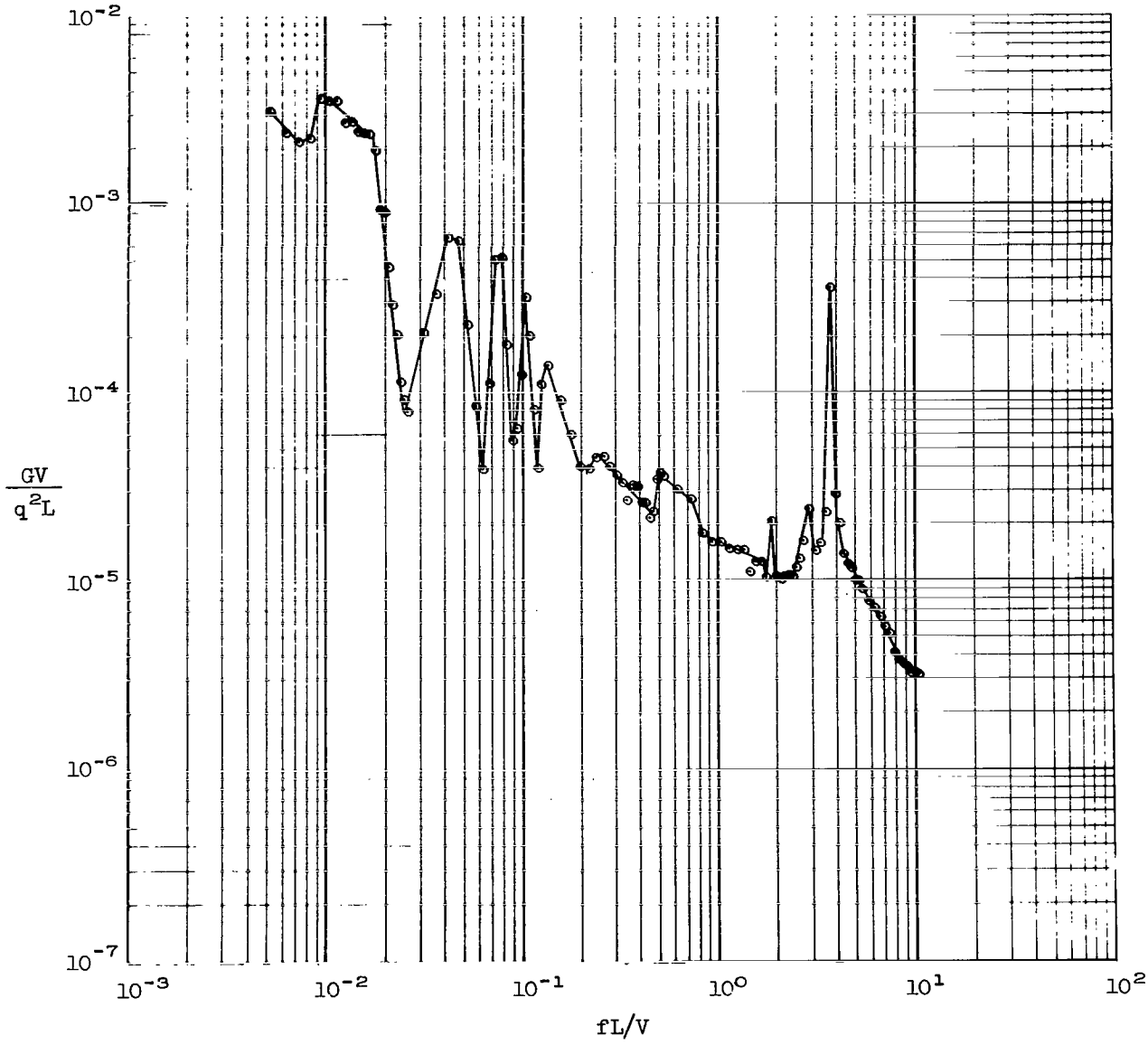

Figure 22.- Spectra of the pressure fluctuations on the wall of the wind tunnel without a cavity; M = 0.80.

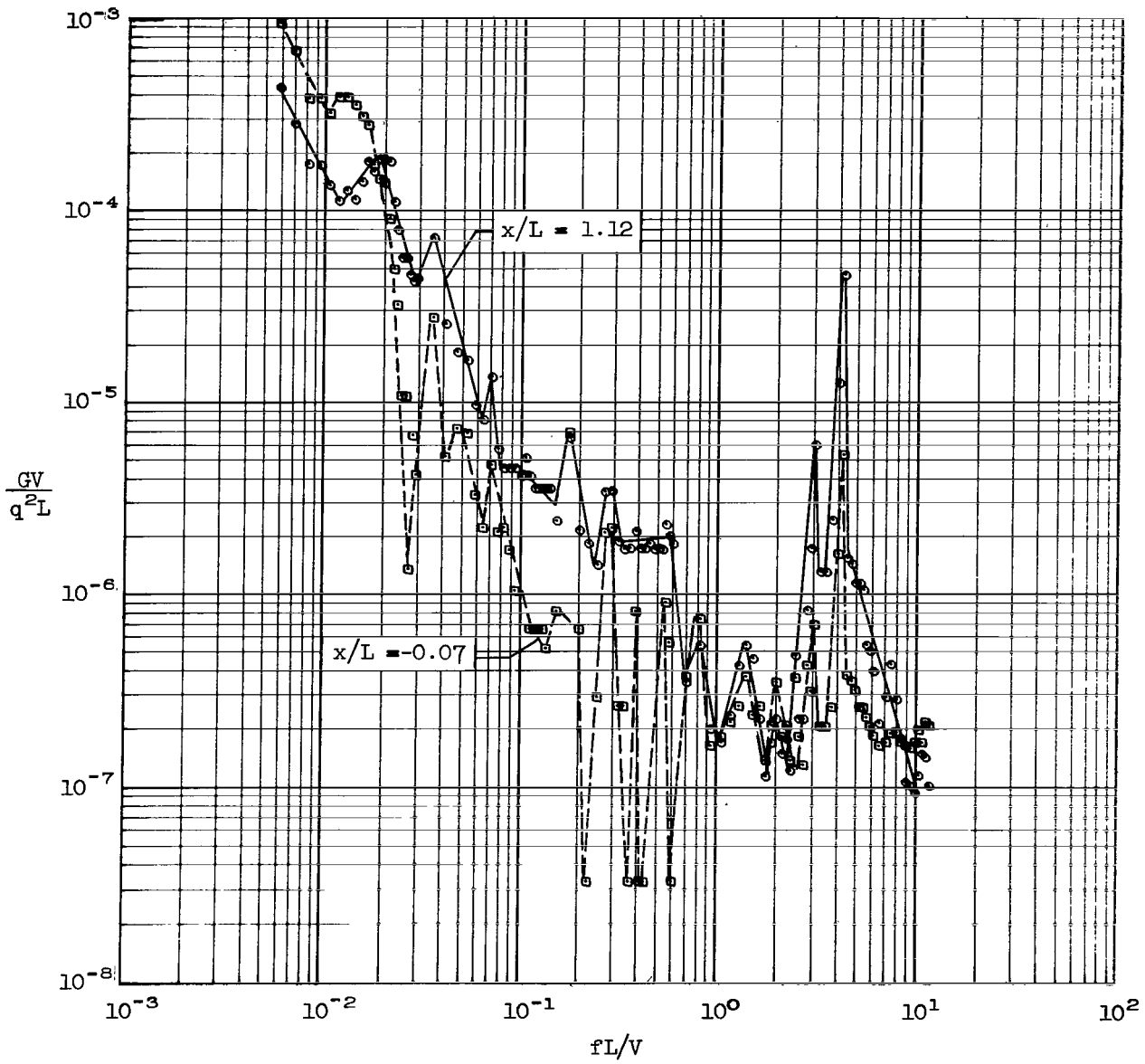

Figure 23.- Spectra of the pressure fluctuations in the wind-tunnel cavity with the opening covered; cavity depth = 1.6 L, z/L = 0.4, M = 0.70.

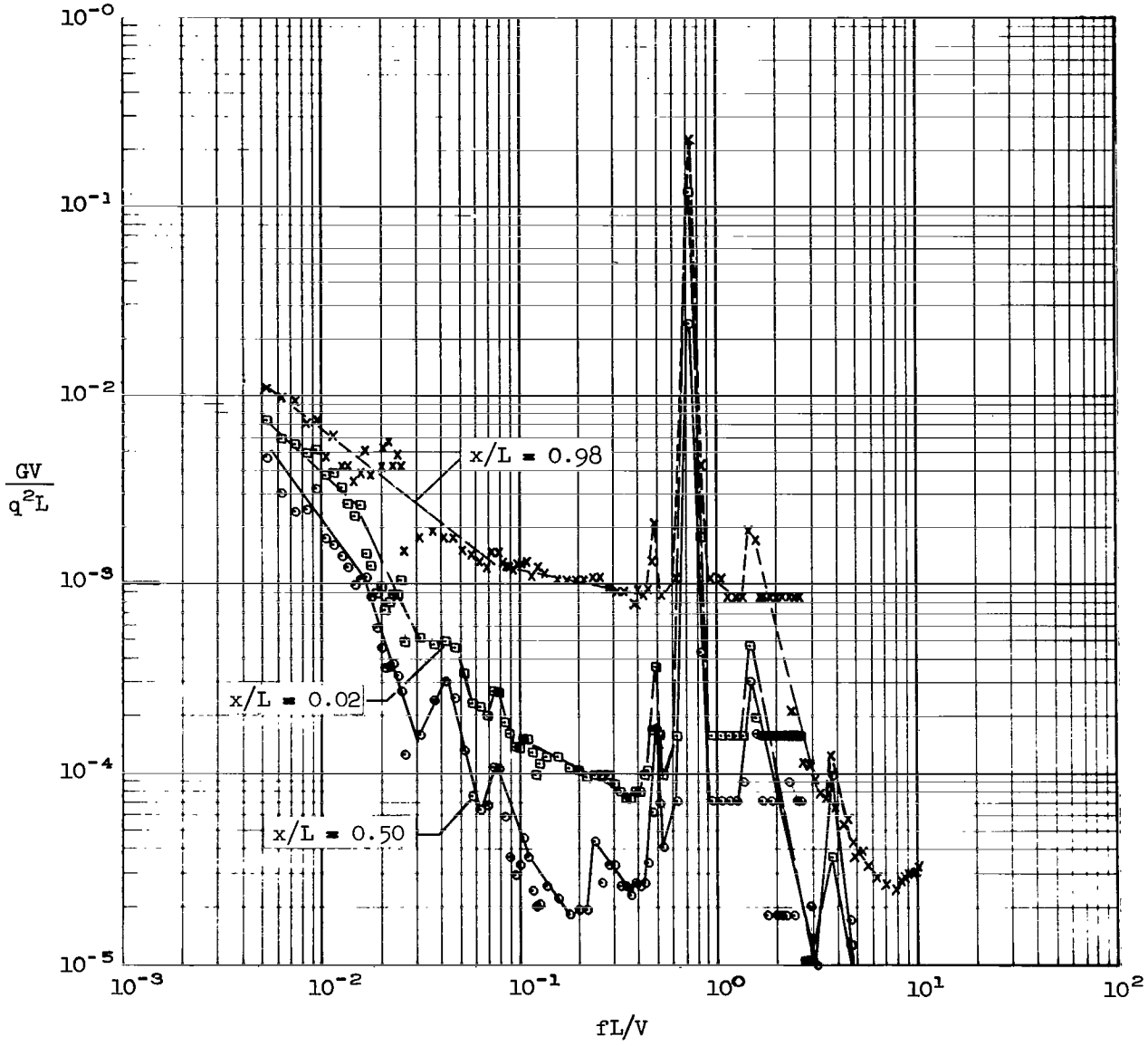

Figure 24.- Spectra of the pressure fluctuations in the wind-tunnel cavity with the plain opening; cavity depth = 1.6 L, round opening, z/L = 0.3, M = 0.80.

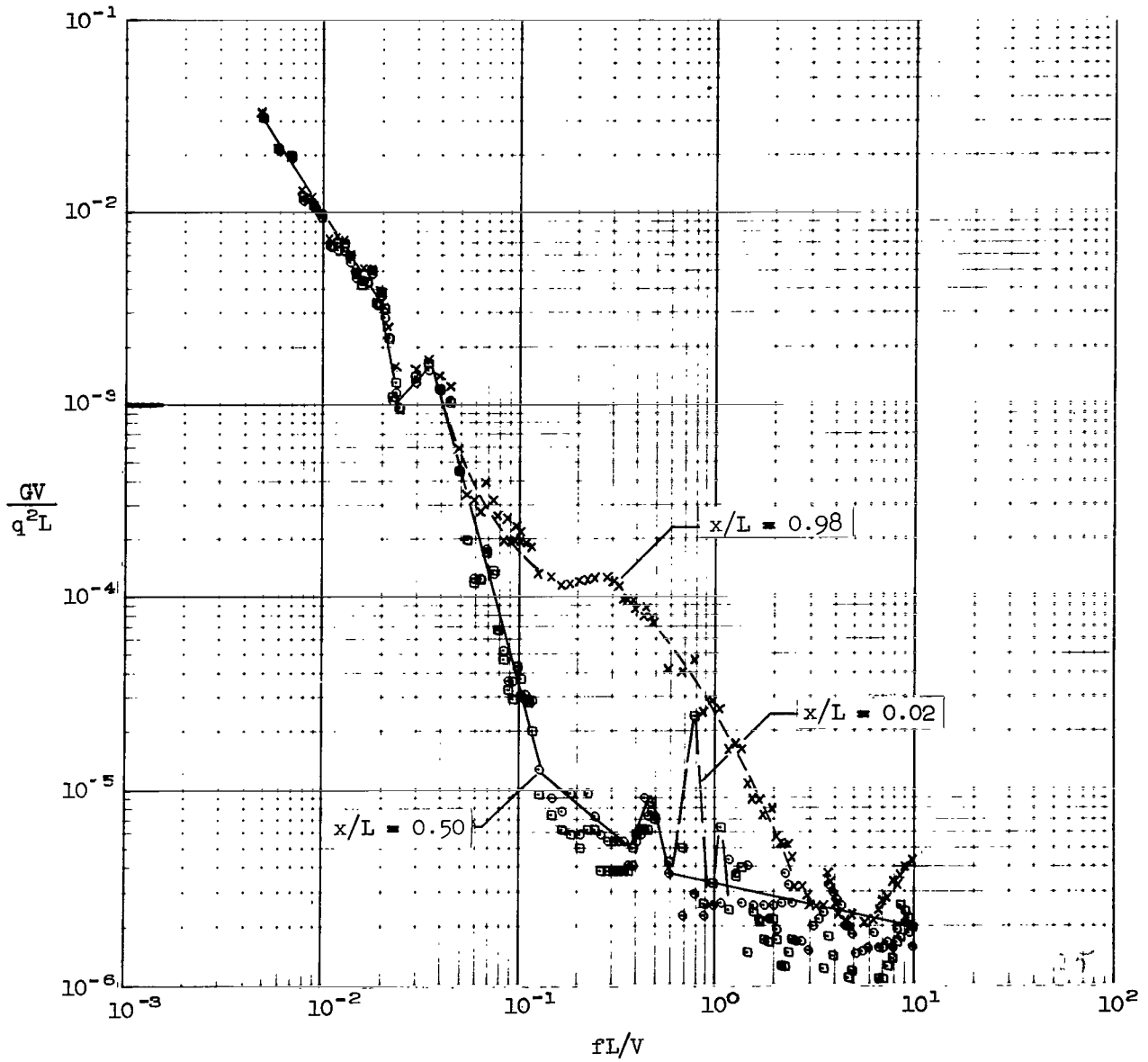

Figure 25.- Spectra of the pressure fluctuations in the wind-tunnel cavity with the 35-percent porous spoiler; cavity depth = 1.6 L, round opening, z/L = 0.3, M = 0.86

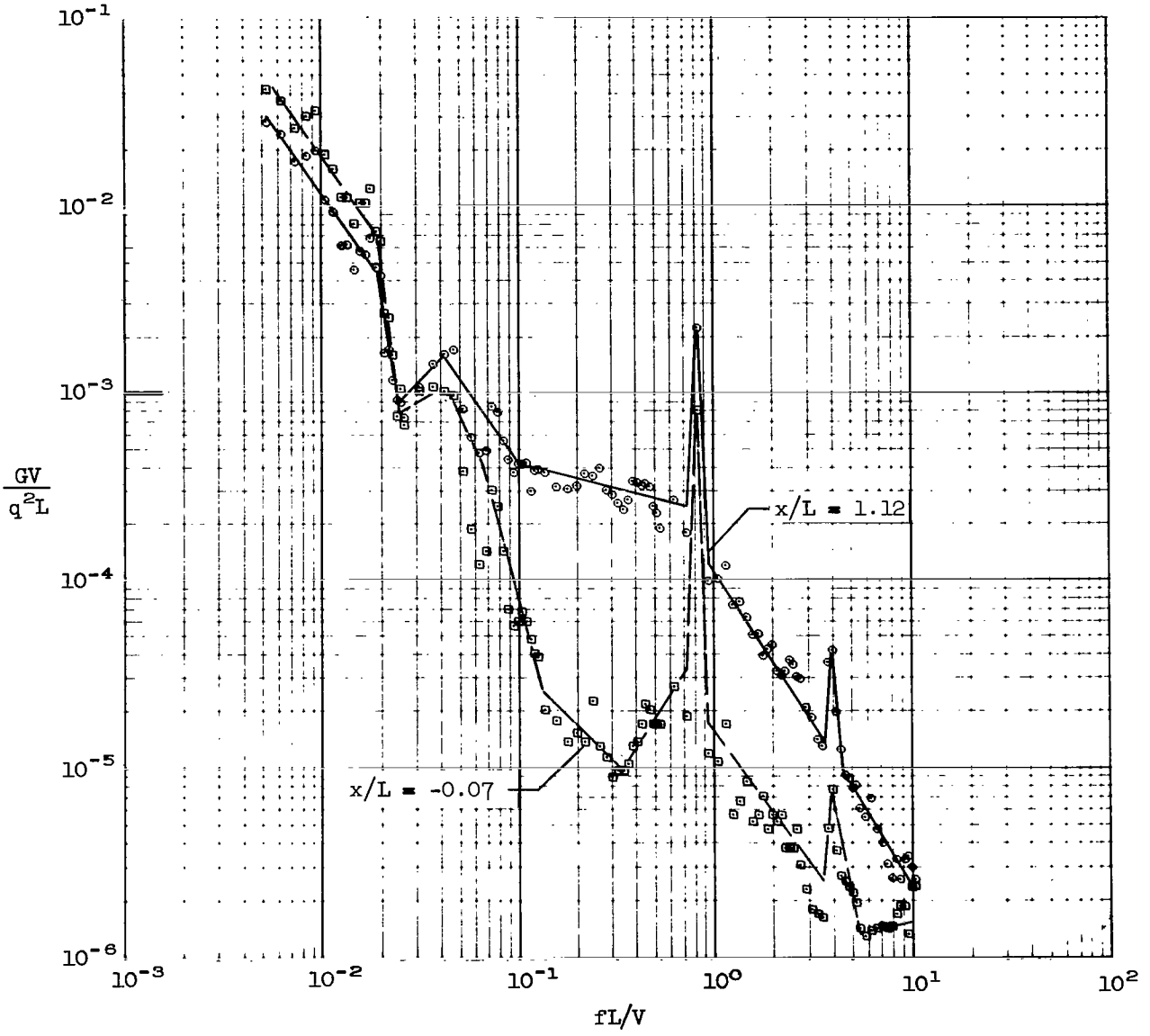

Figure 26.- Spectra of the pressure fluctuations in the wind-tunnel cavity with a high-porosity (68 percent) spoiler; cavity depth = 1.6 L, "square" opening, z/L = 0.4, M = 0.80.

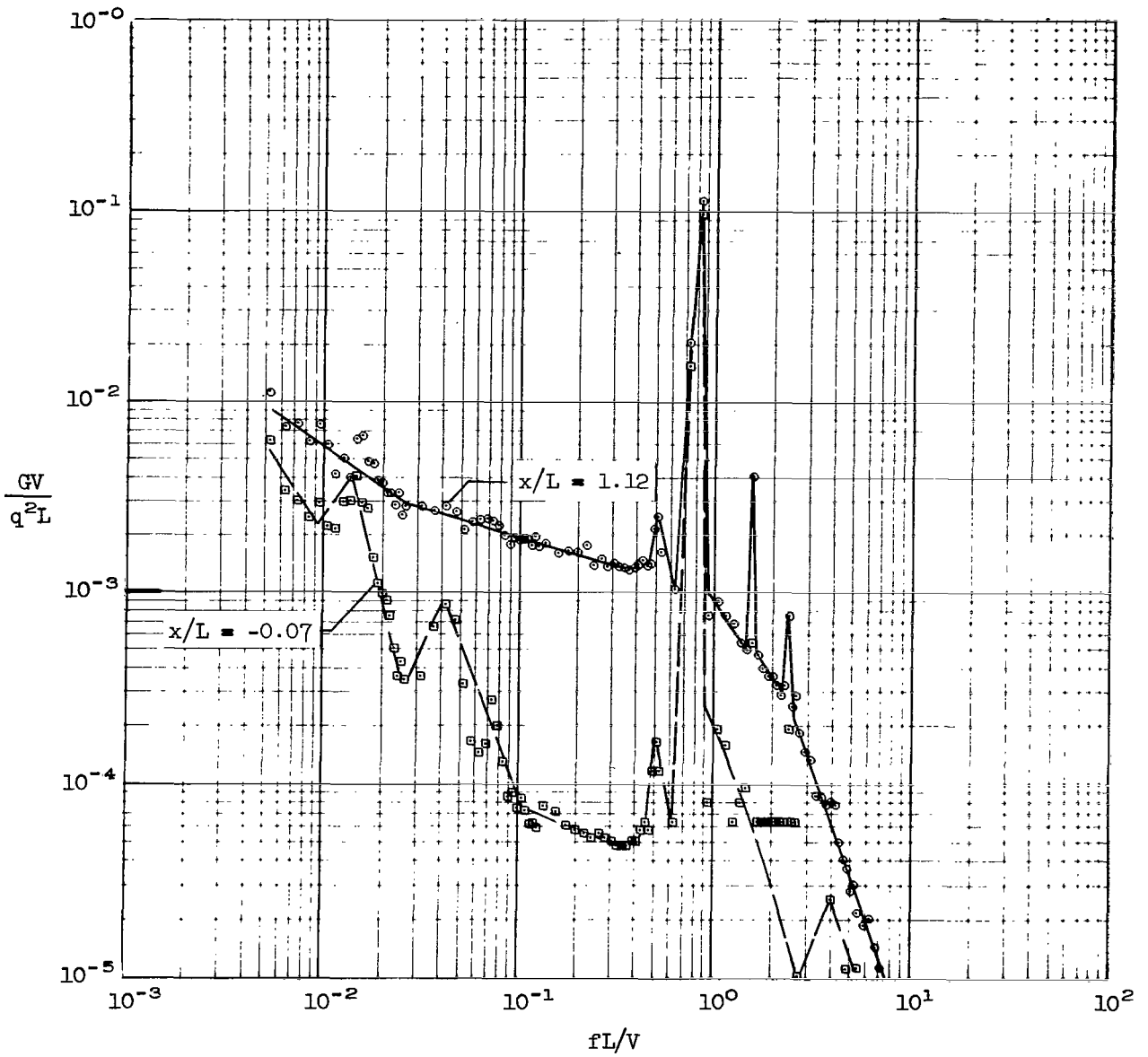

Figure 27.- Spectra of the pressure fluctuations in the wind-tunnel cavity with a zero-porosity spoiler; cavity depth = 1.6 L, "square" opening, z/L = 0.4, M = 0.80.

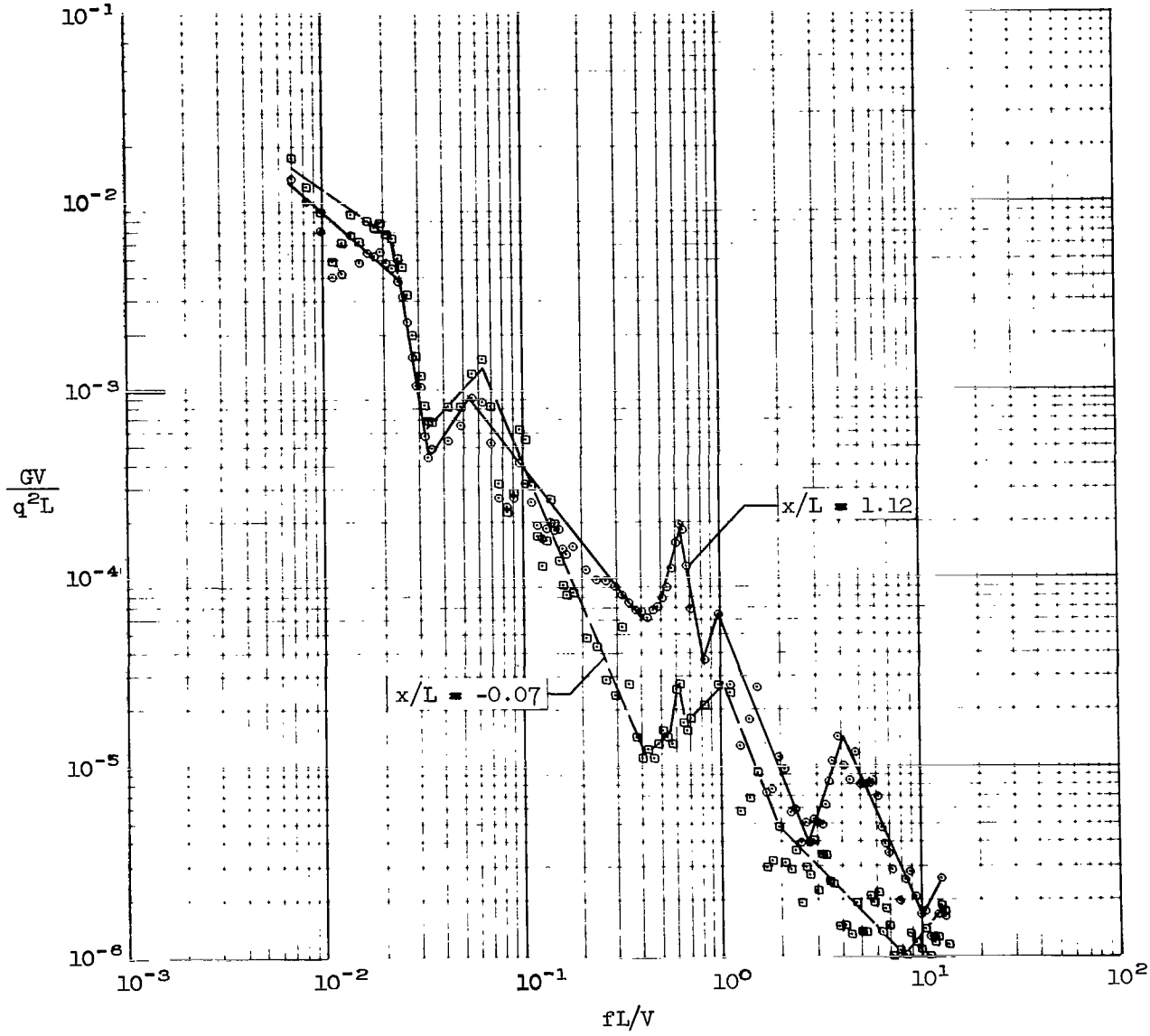

Figure 28.- Spectra of the pressure fluctuations in the wind-tunnel cavity with the long-span 45° diffuser; cavity depth = 1.6 L, "square" opening, z/L = 0.4, M = 0.59.

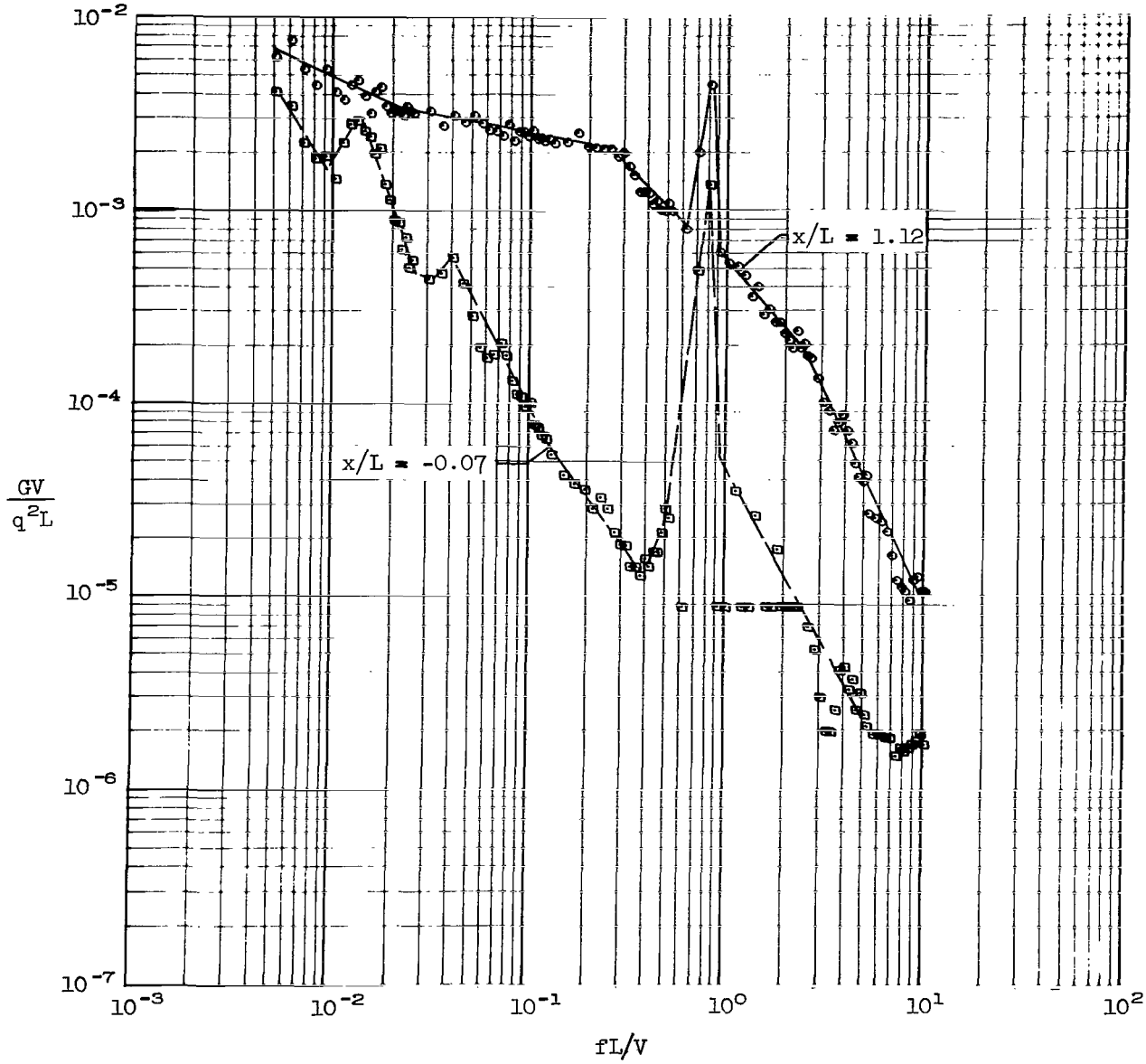

Figure 29.- Spectra of the pressure fluctuations in the wind-tunnel cavity with the short-span 45° diffuser; cavity depth = 1.6 L, "square" opening, z/L = 0.4, M = 0.82.

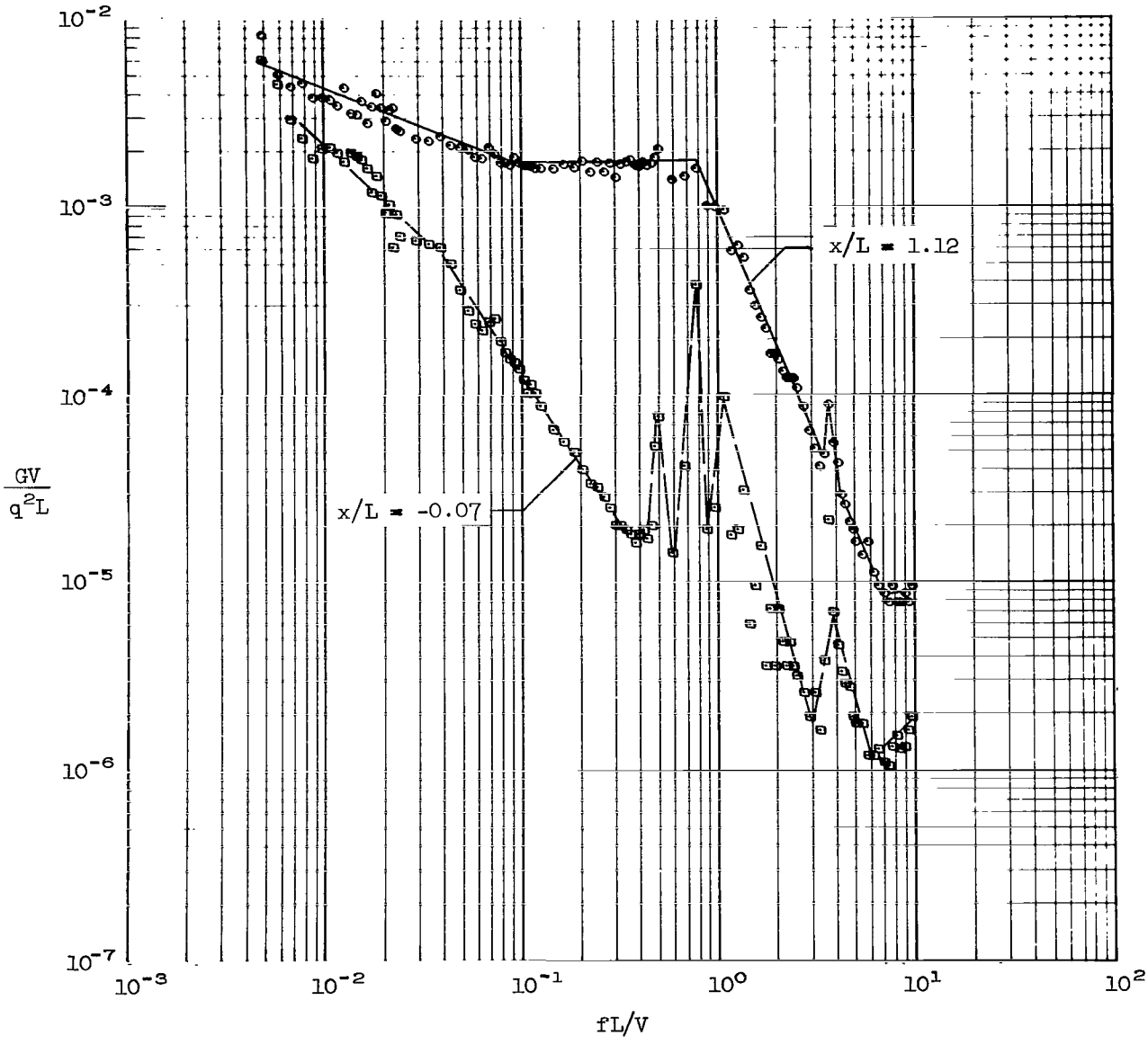

Figure 30.- Spectra of the pressure fluctuations in the wind-tunnel cavity with the low wraparound spoiler; cavity depth = 1.6 L, round opening, z/L = 0.4, M = 0.87.

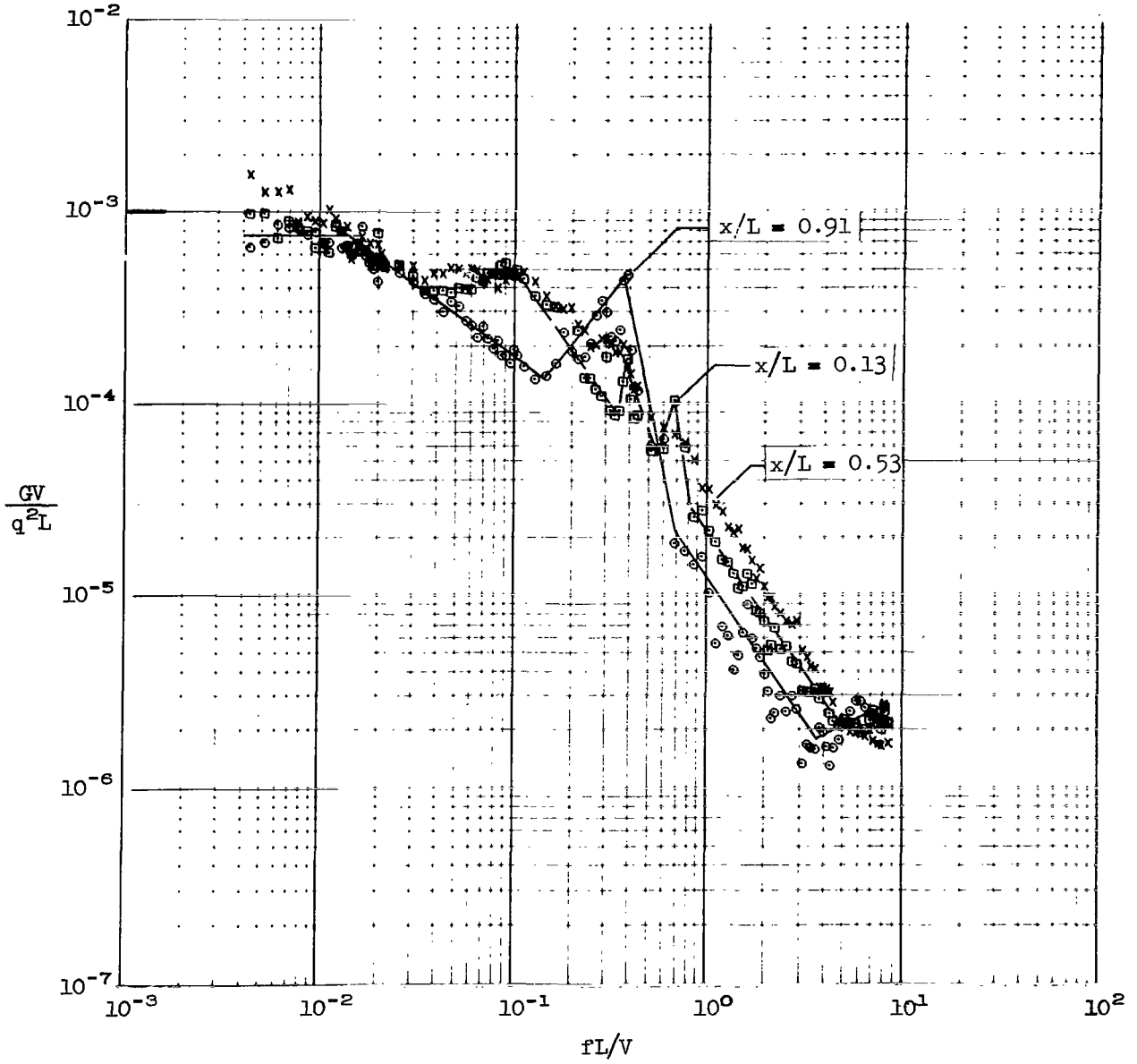

Figure 31.- Spectra of the pressure fluctuations in the airplane cavity; z/L = 0.3, M = 0.76.

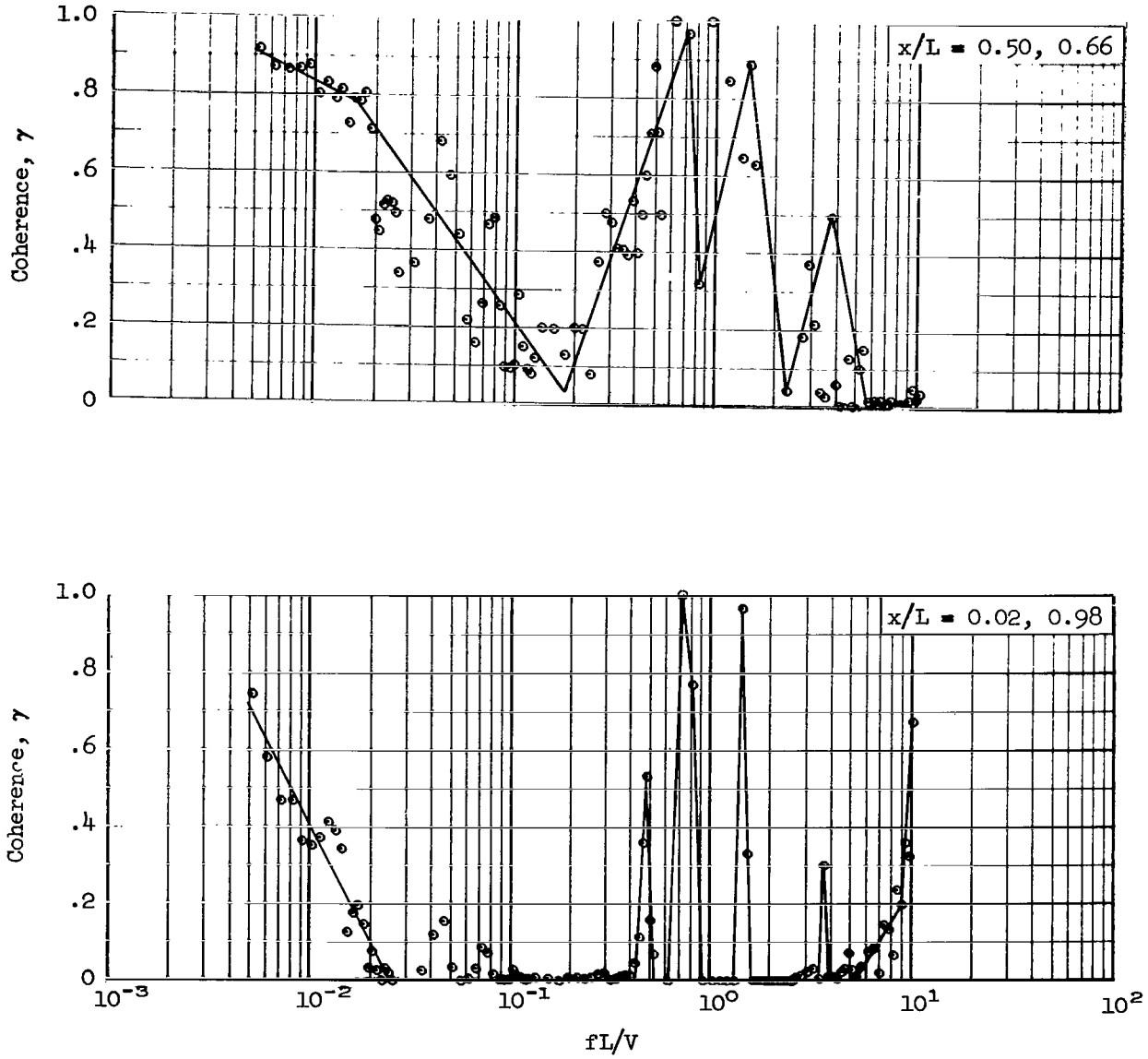

Figure 32.- Coherence of the pressure fluctuations in the wind-tunnel cavity with the plain round opening; cavity depth = 1.6 L, z/L = 0.3, M = 0.80.

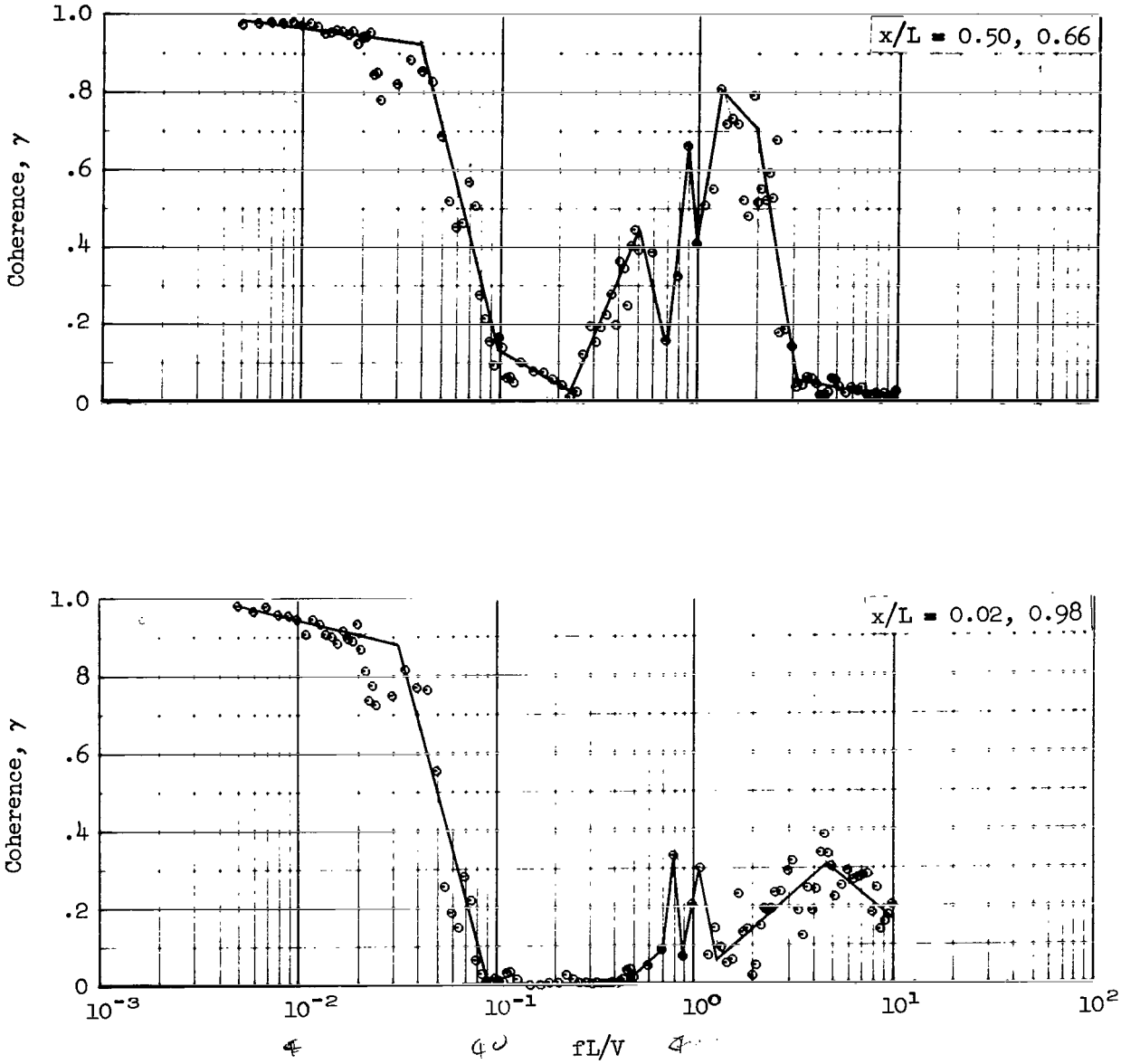

Figure 33.- Coherence of the pressure fluctuations in the wind-tunnel cavity with the 35-percent porous spoiler; cavity depth = 1.6 L, round opening, z/L = 0.3, M = 0.86.

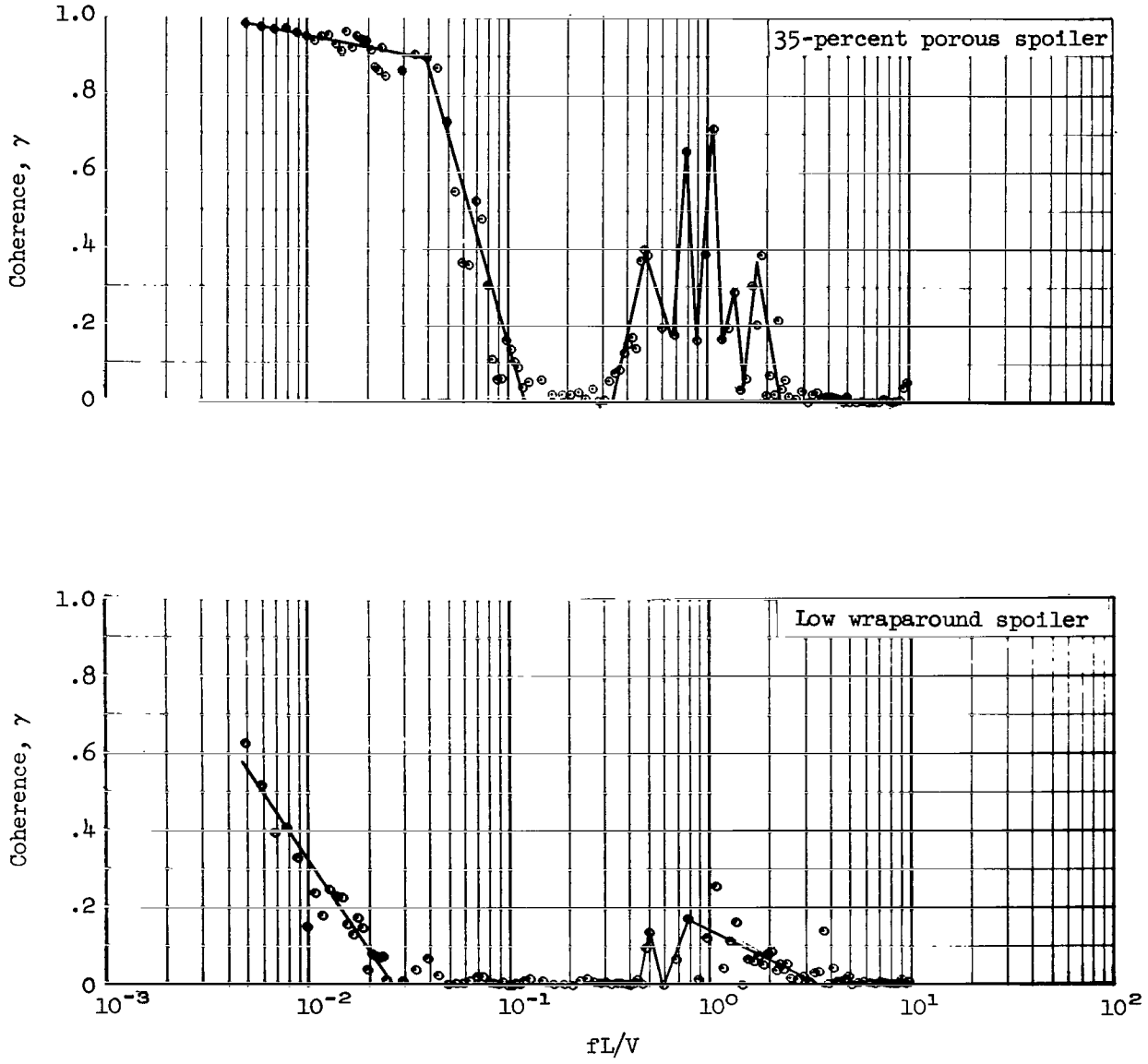

(a) Spoilers, round opening, M = 0.86

Figure 34.- Coherence of the pressure fluctuations in the wind-tunnel cavity at x/L = -0.07 and 1.12; cavity depth = 1.6 L, z/L = 0.4.

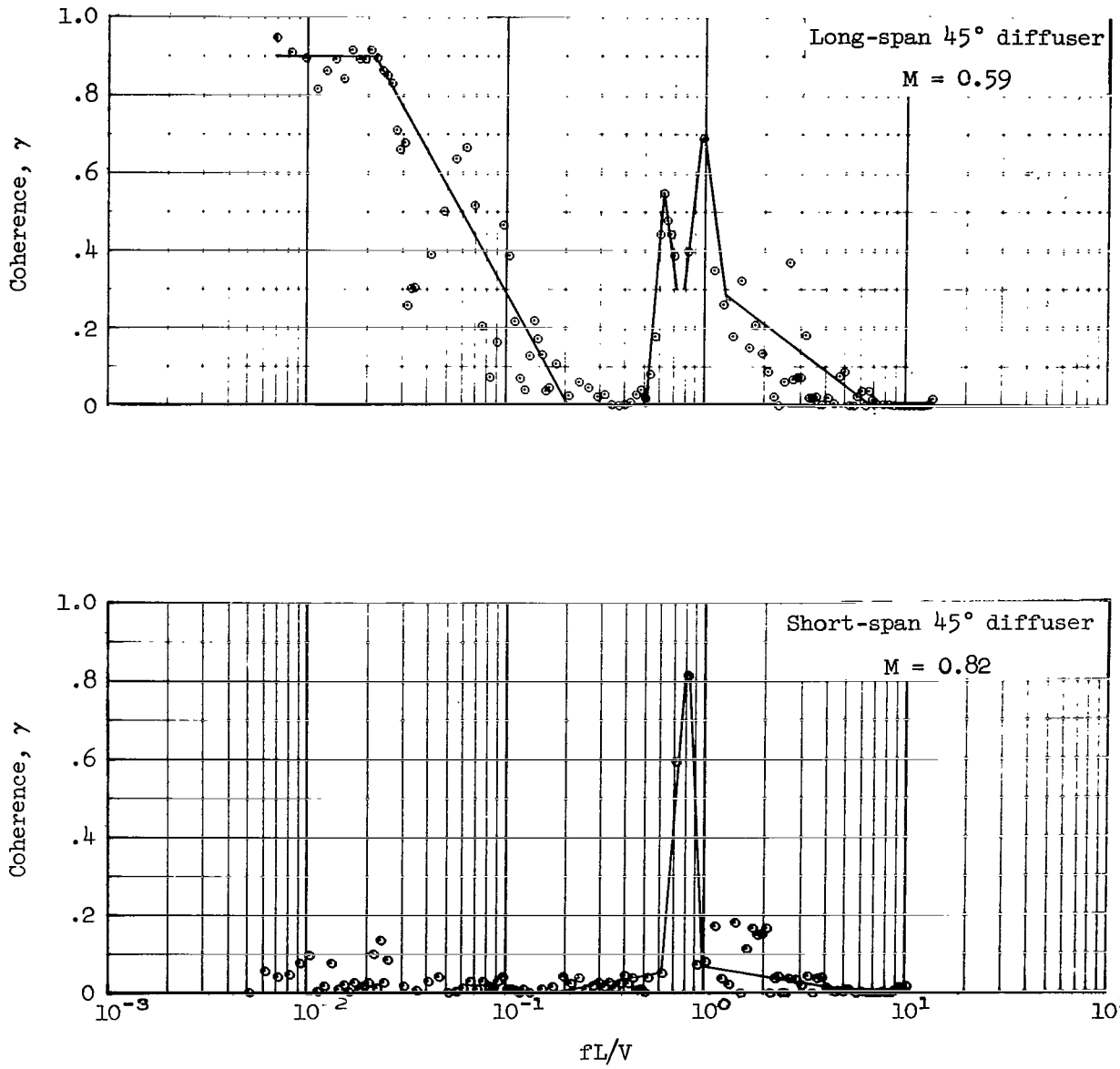

(b) Diffusers, "square" opening

Figure 34.- Concluded.

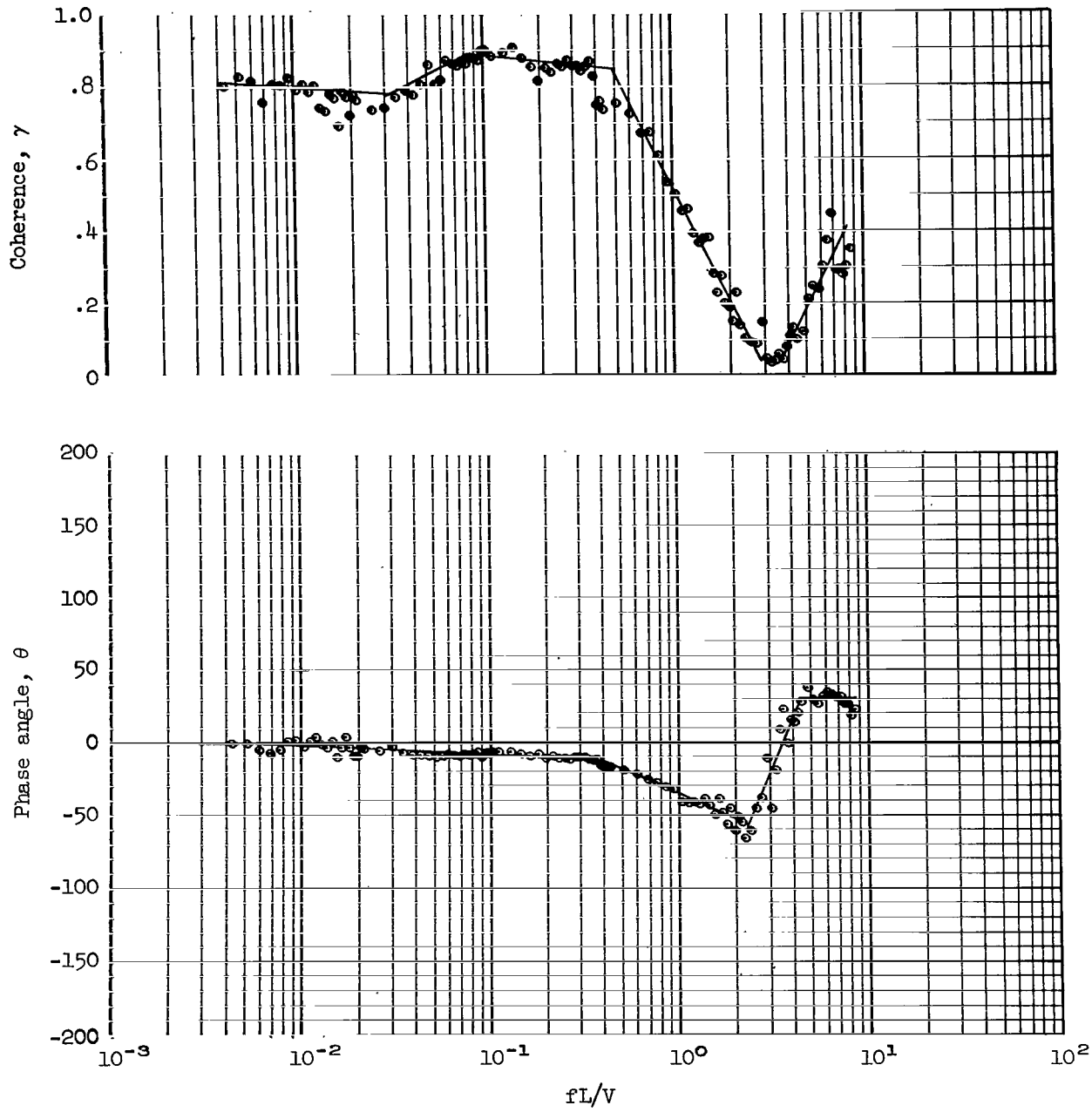

(a) x/L = 0.50 and 0.53

Figure 35.- Coherence and phase angle of the pressure fluctuations in the airplane cavity; z/L = 0.3, M = 0.76.

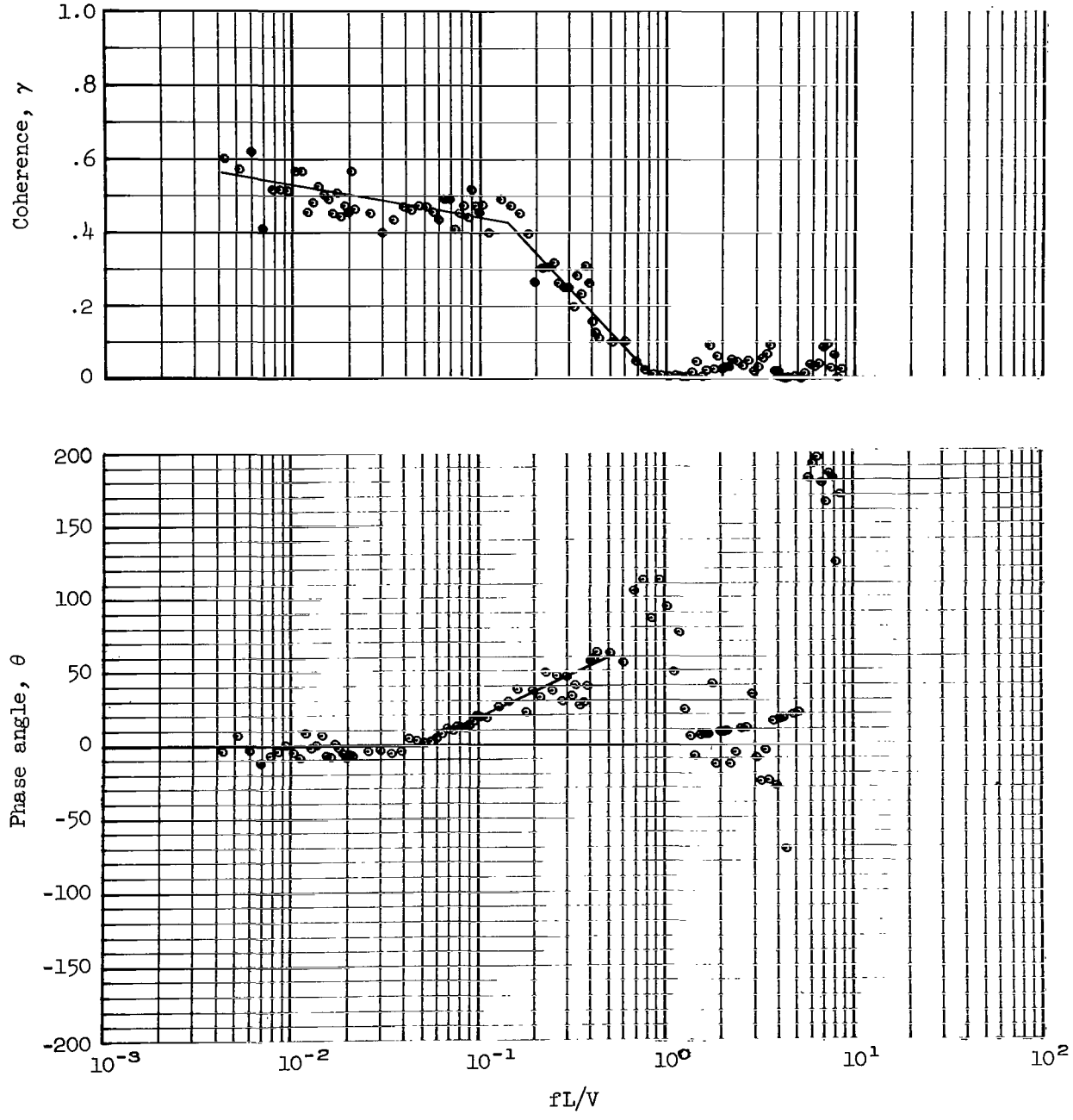

(b) x/L = 0.66 and 0.53

Figure 35.- Continued.

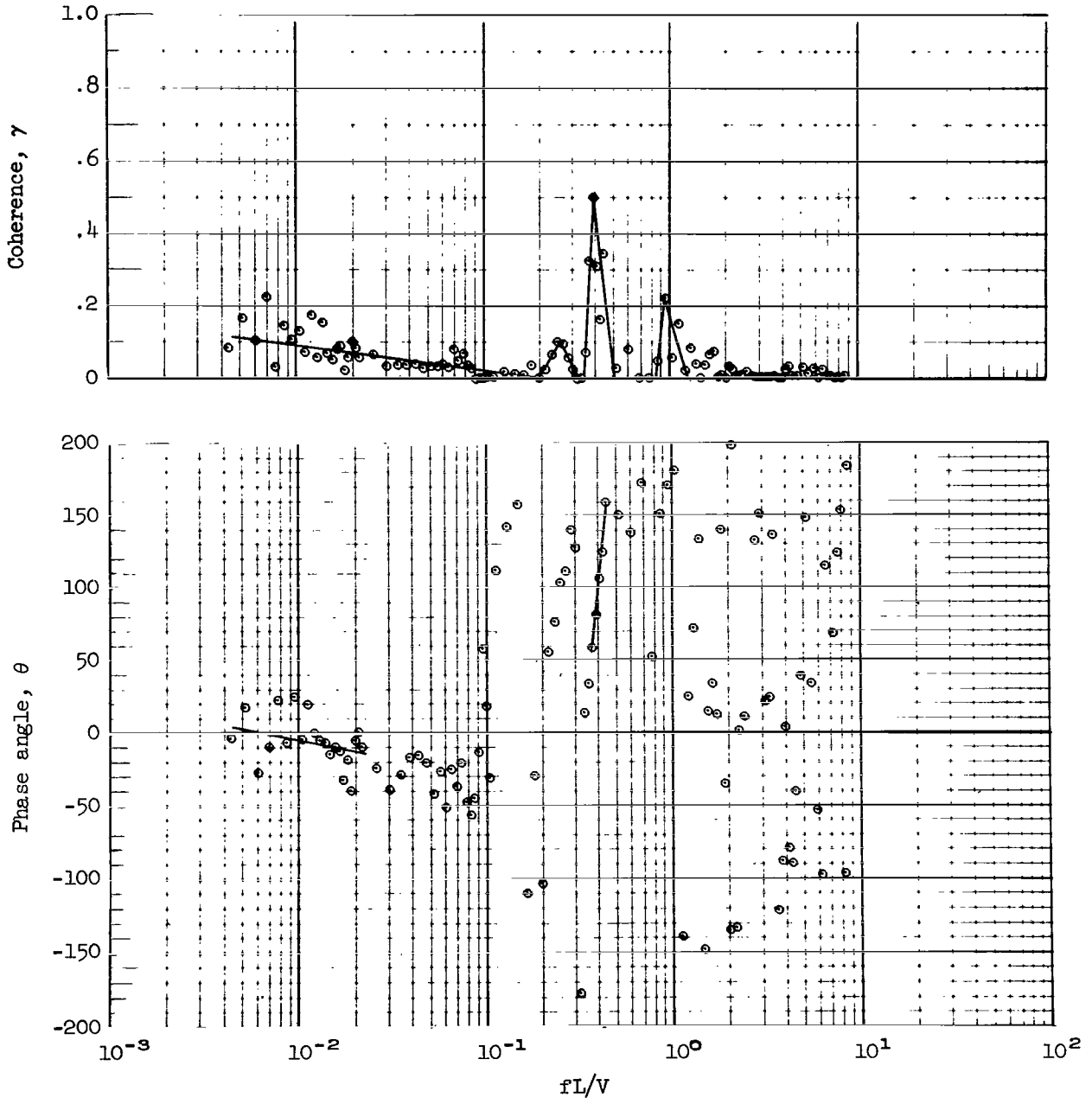

(c) x/L = 0.91 and 0.13

Figure 35.- Concluded.

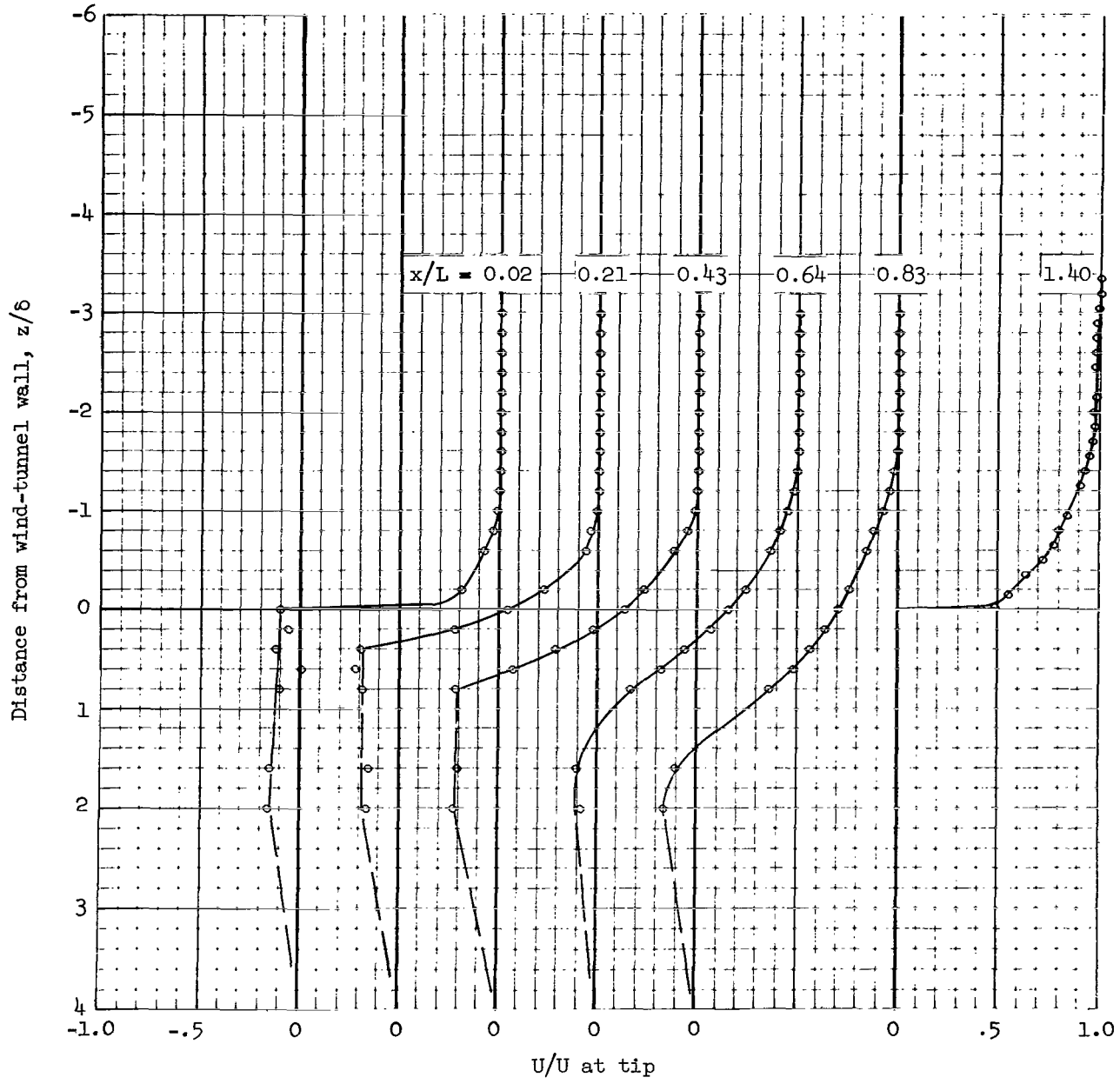

(a) Plain opening, M = 0.77

Figure 36.- Velocity profiles near the round cavity opening; cavity depth = 1.6 L.

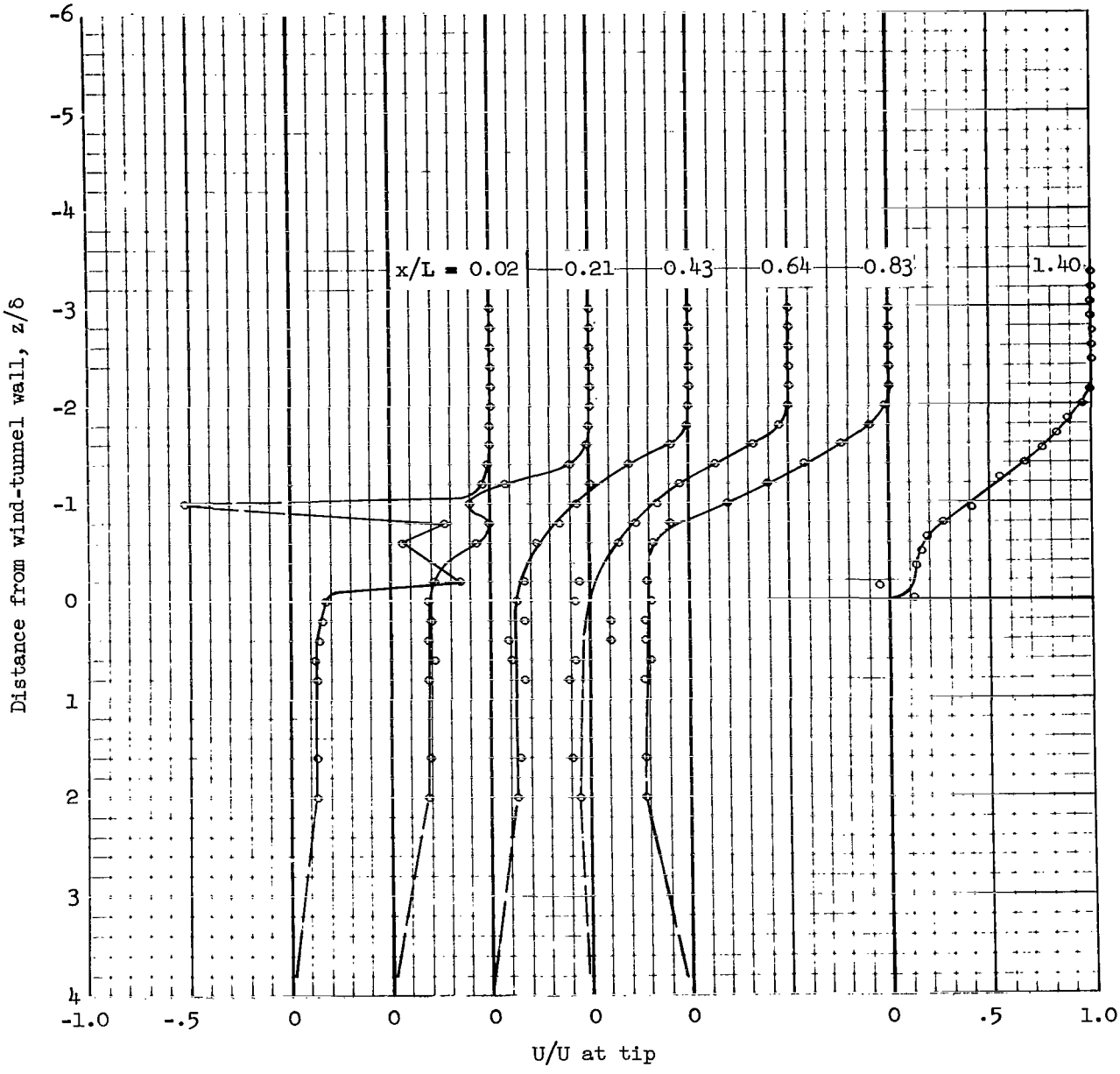

(b) 35-percent porous spoiler, M = 0.87

Figure 36.- Concluded.

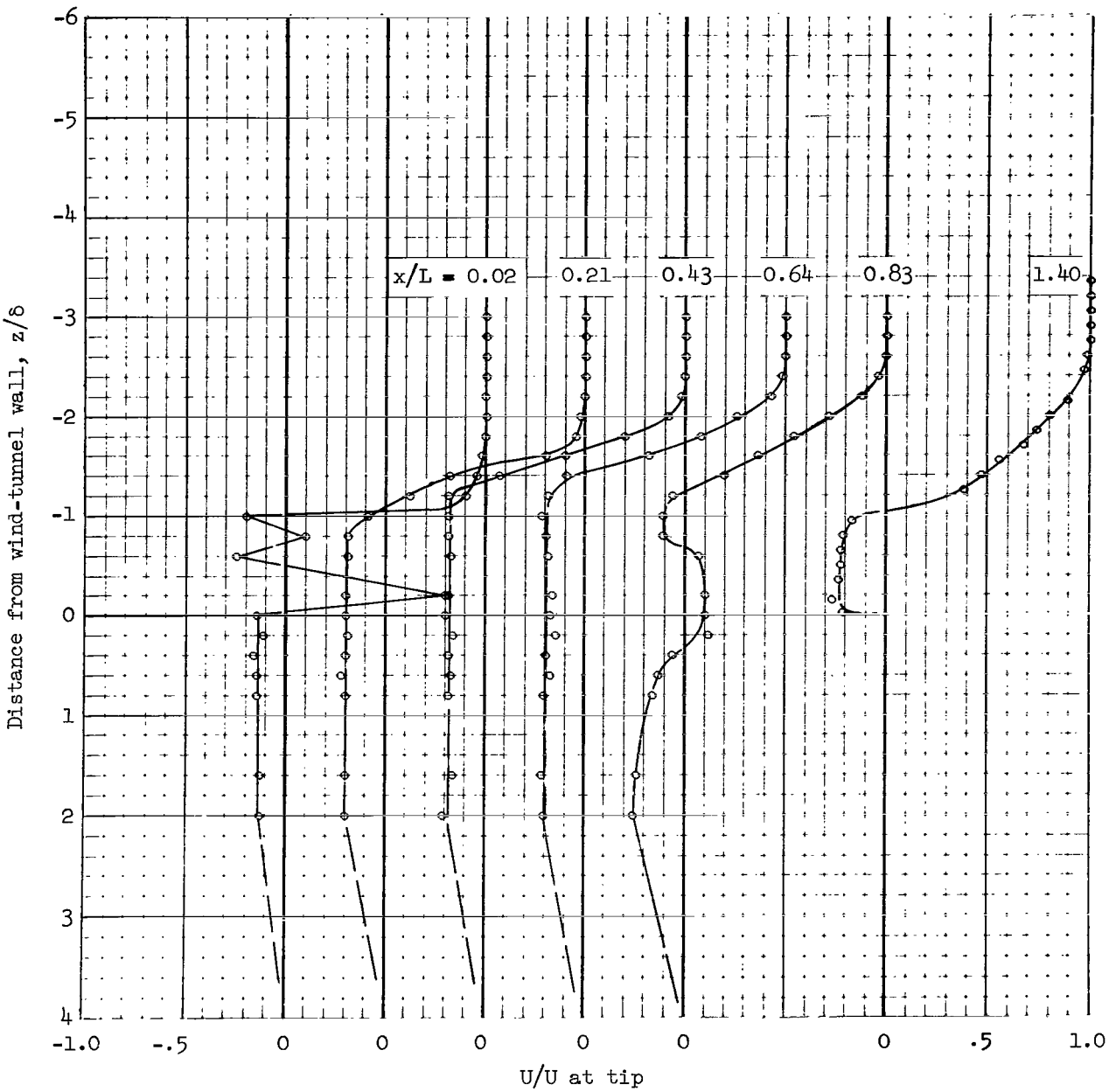

(a) M = 0.59

Figure 37.- Velocity profiles near the "square" opening with the long-span 45° diffuser; cavity depth = 1.6 L.

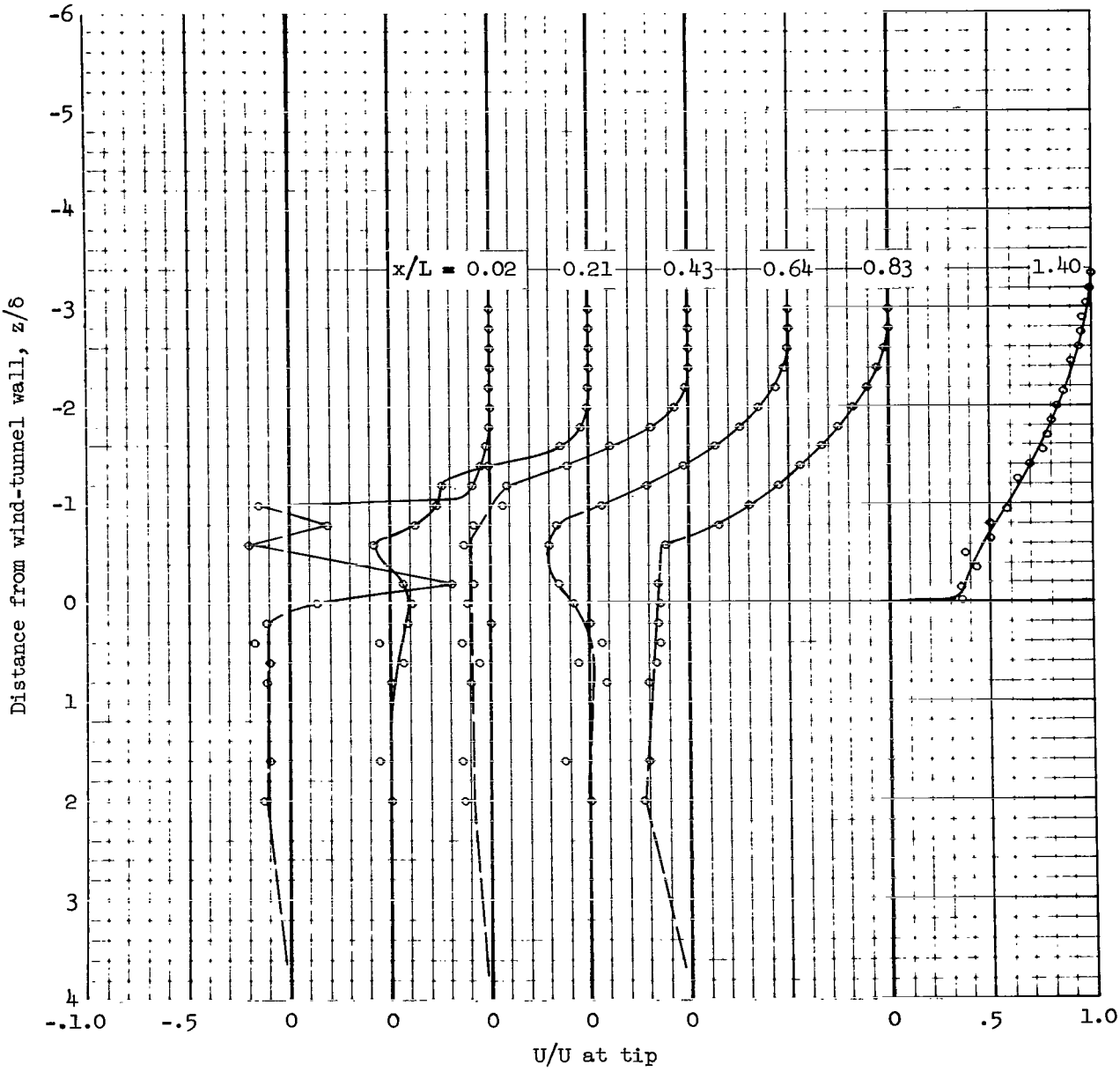

(b) M = 0.71

Figure 37.- Concluded.

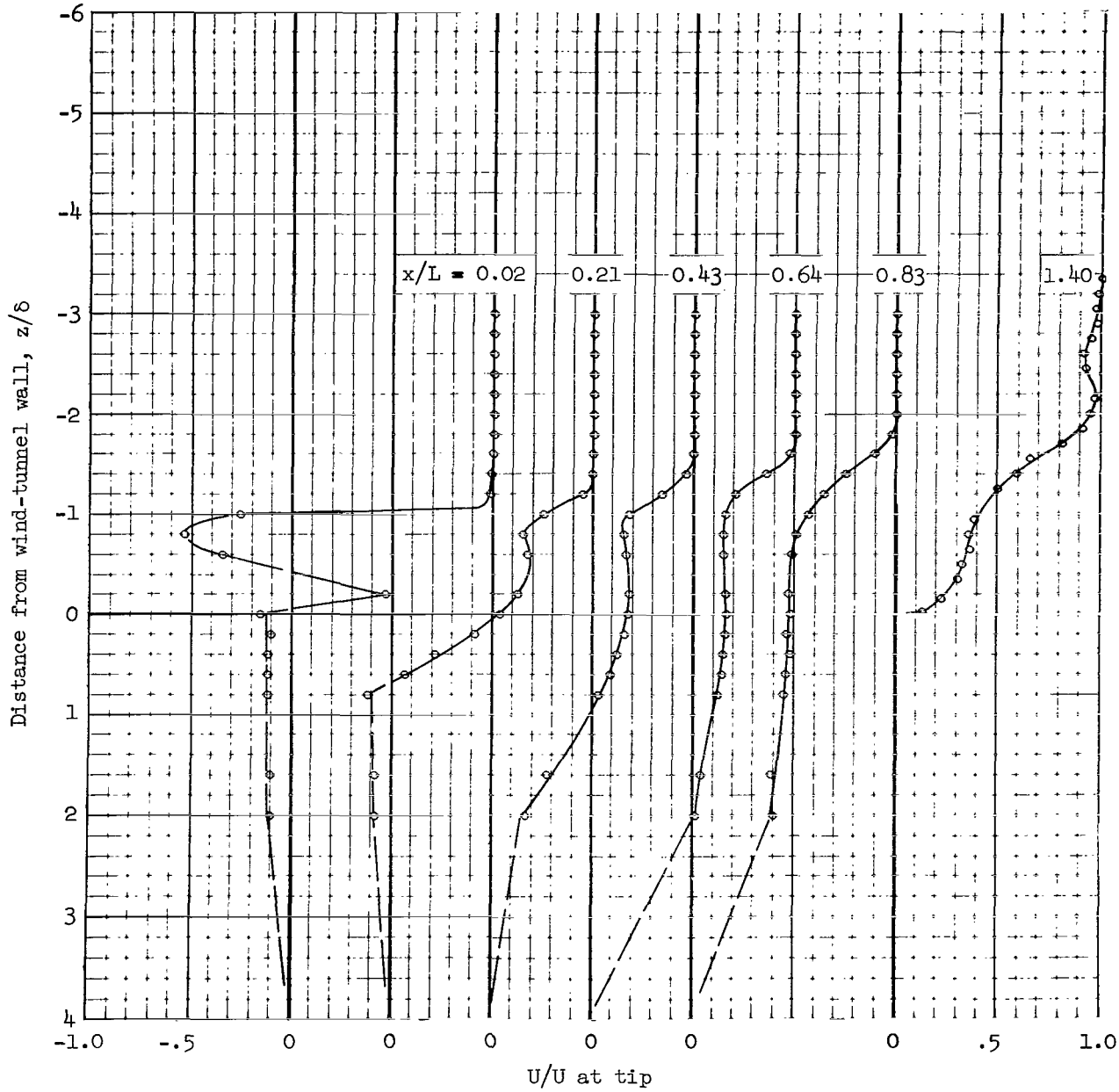

(a) Porosity = 52 percent

Figure 38.- Velocity profiles near the round opening with the low cambered-plate diffuser; cavity depth = 1.6 L, M = 0.80.

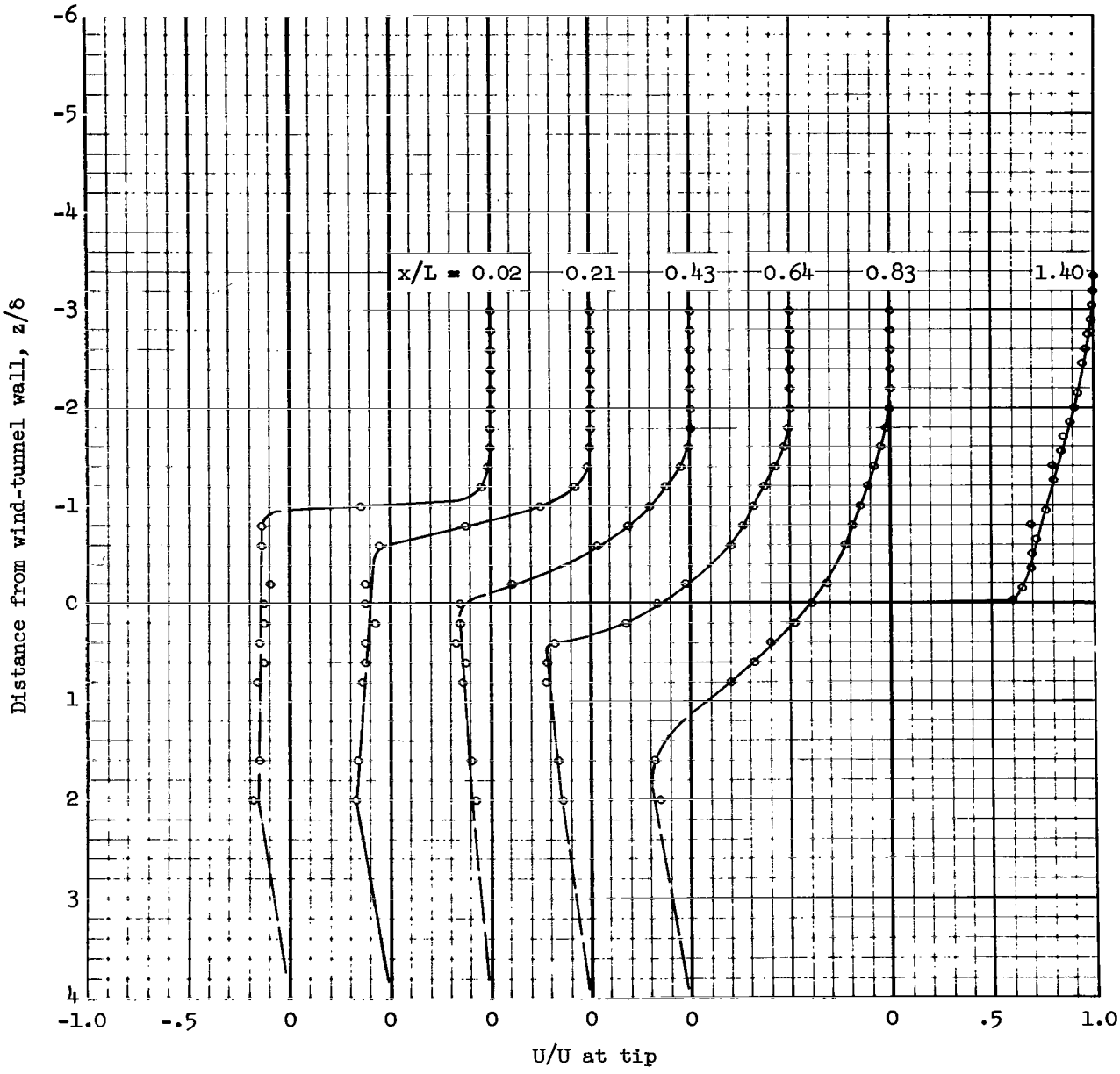

(b) Porosity = 0

Figure 38.- Concluded.